



저작자표시-비영리-변경금지 2.0 대한민국

이용자는 아래의 조건을 따르는 경우에 한하여 자유롭게

- 이 저작물을 복제, 배포, 전송, 전시, 공연 및 방송할 수 있습니다.

다음과 같은 조건을 따라야 합니다:



저작자표시. 귀하는 원저작자를 표시하여야 합니다.



비영리. 귀하는 이 저작물을 영리 목적으로 이용할 수 없습니다.



변경금지. 귀하는 이 저작물을 개작, 변형 또는 가공할 수 없습니다.

- 귀하는, 이 저작물의 재이용이나 배포의 경우, 이 저작물에 적용된 이용허락조건을 명확하게 나타내어야 합니다.
- 저작권자로부터 별도의 허가를 받으면 이러한 조건들은 적용되지 않습니다.

저작권법에 따른 이용자의 권리는 위의 내용에 의하여 영향을 받지 않습니다.

이것은 [이용허락규약\(Legal Code\)](#)을 이해하기 쉽게 요약한 것입니다.

[Disclaimer](#)

공학박사학위논문

**A Study on the Control for Decomposition of
Bis-(3-Sulfopropyl) Disulfide (SPS) and Polyethylene Glycol
(PEG) Additive in Copper Electrodeposition Bath**

구리 전해 도금 용액에 사용되는 첨가제인
비스-설퍼프로필 다이설파이드 및 폴리에틸렌 글라이콜의
분해 조절을 위한 연구

2021년 8월

서울대학교 대학원
화학생물공학부
김태영

**A Study on the Control for decomposition of
Bis-(3-Sulfopropyl) Disulfide (SPS) and Polyethylene Glycol (PEG)
Additive in Copper Electrodeposition bath**

구리 전해 도금 용액에 사용되는 첨가제인
비스-설퍼프로필 다이설파이드 및 폴리에틸렌 글라이콜의
분해 조절을 위한 연구

지도교수 김 재 정

이 논문을 공학박사 학위논문으로 제출함
2021 년 7 월

서울대학교 대학원
화학생물공학부
김 태 영

김태영의 공학박사 학위논문을 인준함
2021 년 8 월

위 원 장

부위원장

위 원

위 원

위 원

Abstract

Copper electrodeposition is one of the root-technology for 4th industrial revolution era in various industries: semiconductor, lithium ion 2nd battery, and catalyst, because of its high productivity and economic efficiency. In order to control the deposited Cu properties, organic additives are used a key role in the Cu electroplating. However, the organic additive is degradable under the Cu electrodeposition process, which gradually decompose through the degradation pathways. In this study, it was attempted to identify the bis-(3-sulfopropyl) disulfide (SPS) and polyethylene glycol (PEG) decomposition mechanism in each electrode, and the factor of additive decomposition was searched. Through this, for the purpose of controlling the additive decomposition, the method of suppressing for decomposition factor was proposed.

The mechanisms of cathodic and anodic SPS decomposition, which is plays as an accelerator in the Cu electrodeposition process, were examined via both electrochemical and spectroscopy analysis under three conditions; open- circuit, short-circuit, and electrolysis conditions. With an open circuit at catholyte, the SPS was finally oxidized to oxidation to 1,3-propane disulfonate (PDS) at the Cu plate via the chemical reaction by active radical ($\cdot\text{OH}$) formed by Cu^+ with dissolved O_2 . No chemical reactions took

place at the insoluble anode. With a short-circuit, SPS at the Cu plate (cathode) and the Ir/IrO_x plate (on Ti/TiO_x, insoluble anode) were simultaneously broken down at an equal rate because of the formation of Cu⁺ at the Ir/IrO_x bath by a galvanic disproportionation reaction. With current flowing in electrolysis condition, SPS in the catholyte was consumed via the reaction with active radical by Cu⁺ and dissolved O₂ as well as by incorporation, while that in the anolyte was decomposed faster via anodic electrochemical oxidation compared to chemical reactions.

Under the open-circuit conditions, PEG decomposition occurred only at the Cu plate, owing to the effect of the Cu⁺ ions. Under the short-circuit conditions, PEG degraded at both electrodes through the galvanic disproportionation reaction, owing to which Cu⁺ was also formed at the Ir/IrO_x plate. Under the electrolysis conditions, PEG also was degraded at both electrodes, but a difference in the average molecular weight of PEG (MW_{PEG}) between the two electrodes was observed after 48 h. The PEG breakdown at the Cu plate appeared to be related to the Cu⁺ ions, while that at the Ir/IrO_x plate was caused by the ·OH radicals formed by water splitting. In addition, direct Cu⁺ ion catalytic reaction was generated without dissolved O₂ in Cu electrodeposition bath. Therefore, it is concluded that PEG degradation did not proceed through a direct electrochemical reaction, but rather through an active radical-induced chemical and Cu⁺ directly catalytic

reaction.

The decomposition factors; active radical ($\cdot\text{OH}$), Cu^+ ion, and dissolved O_2 were identified through the investigation of the decomposition mechanism of SPS and PEG. Therefore, the effect of reducing agents to decrease the decomposition factors was investigated through SPS decomposition. In first, after reducing agents (hypophosphite, formaldehyde, glyoxylic acid, hydrazine, and oxalic acid) added into the Cu plating bath, their effects examined on the voltammetric response, bath performance, and stability of SPS. It was determined that only formaldehyde and glyoxylic acid could be used as reducing agents in Cu electrolytes. Formaldehyde reduced the rate of SPS decomposition more effectively. The bath performance with and without formaldehyde was evaluated by performing a via-fill test. Consequently, when formaldehyde was present, the filling performance was maintained for up to 9 h and SPS decomposition in the open-circuit condition rarely occurred. These results indicate that formaldehyde reduces the number of active radicals, thereby reducing the chemical oxidation of SPS.

Keywords: Cu, electrodeposition, decomposition, additive, SPS, PEG, Cu^+ ion, active radical, reducing agent, formaldehyde

Student number: 2015-22827

Content

Abstract	i
List of Tables	vii
List of Figures	viii
Chapter I. Introduction	1
1.1. Recent trends of Cu electrodeposition industry.....	1
1.2. Cu electrodeposition and organic additive.....	6
1.2.1. Cu electrodeposition.....	6
1.2.2. Properties of Cu bath and organic additive.....	8
1.3. Mechanism of additive behavior.....	13
1.4. Decomposition of organic additive.....	20
1.4.1. SPS decomposition.....	20
1.4.2. PEG decomposition.....	23
1.5. Measurement of organic additive.....	28
1.5.1. Cyclic voltammetry stripping (CVS) analysis.....	28
1.5.2. Spectroscopy (NMR, MALDI-TOF) analysis.....	30
1.6. Purpose of this study.....	36
Chapter 2. Experimental	38

2.1. Degradation experiment.....	38
2.1.1. Degradation of SPS.....	39
2.1.2. Degradation of PEG.....	40
2.1.3. Filling performance.....	41
2.2 Electrochemical analysis.....	43
2.2.1. LSV analysis.....	43
2.2.2. CVS analysis.....	44
2.2.2.1. Measurement of SPS concentration (C_{SPS}).....	44
2.2.2.2. Measurement of PEG average molecular weight (MW_{PEG}).....	46
2.3. Spectroscopy analysis.....	52
2.4. Filling performance.....	55
Chapter III. Results and Discussion.....	58
3.1. Mechanism of SPS decomposition.....	58
3.1.1. Measurement of C_{SPS} by CVS.....	58
3.1.2. Analyzing the SPS decomposition by spectroscopy analysis.....	62
3.1.3. Verification of SPS decomposition factor.....	63
3.2. Mechanism of PEG decomposition.....	78
3.2.1. Measurement of MW_{PEG} by CVS.....	78
3.2.2. Analyzing the PEG decomposition by spectroscopy analysis.....	80

3.2.3. Verification of PEG decomposition factor.....	83
3.3. Decrease of additive decomposition.....	100
3.3.1. The factor of additive decomposition.....	100
3.3.2. Selection of reducing agent in Cu electrodeposition bath.....	102
3.3.3. Effect of reducing agent (Formaldehyde).....	107
Chapter IV. Conclusion.....	120
References.....	124
국문 초록.....	135
Appendix.....	139

List of Tables

Table 1.1. The Representative Accelerators and Suppressor for Cu Electro- deposition.....	11
Table 3.1. Rate of SPS Breakdown under Electrolytic Conditions.....	68

List of Figures

Fig. 1.1.	The new ecosystem of the electronics' industry based on semi-conductor technologies. (Ref. 1).....	3
Fig. 1.2.	Global oxygen-free Cu market size and forecast. (Ref. 26).....	4
Fig. 1.3.	Trends of global electroplating market size. (Ref. 27).....	5
Fig. 1.4.	Schematic diagram of Cu electrodeposition.....	12
Fig. 1.5.	Competitive adsorption of PEG, Cl ⁻ and SPS. (Ref. 73).....	16
Fig. 1.6.	The CEAC simulation on feature filling of Cu electrodeposition with various diffusion coefficient. (Ref. 74).....	17
Fig. 1.7.	The CDA model of the synthesized leveler with rotating disk electrode; (a) Lev 1, (b) Lev 2, (c) Lev 3, and (d) Lev 4. (Ref. 77).....	18
Fig. 1.8.	The S-NDR voltammogram with Tetric. (Ref. 78).....	19
Fig. 1.9.	The failure of Cu electrodeposition in various process. (a) trench filling performance, (b) TSV filling performance, and (c) Cu deposited surface after CMP. (Ref. 87, 92, and 81).....	25
Fig. 1.10.	Schematic diagram of SPS decomposition pathways (a) sequential oxidation, (b) participation of electron on anode.....	26
Fig. 1.11.	Schematic diagram of PEG decomposition pathways (a) nucleophilic substitution reaction, (b) active radical decomposition.....	27

Fig. 1.12.	Schematic diagram of 2-step MLAT-CVS method. (Ref. 108).....	32
Fig. 1.13.	Method of the average molecular weight of PEG. (a) influence of PEG molecular weight in CV, (b) Relation between the hysteresis area and PEG concentration for various MW_{PEG} , and (c) Calibration curve with maximum hysteresis area. (Ref. 110).....	33
Fig. 1.14.	Schematic diagram of iodide concentration method. (Ref. 92).....	34
Fig. 1.15.	Selective determination of PEG-PPG concentration by iodide ion. (a) formation of CuI inhibition layer, (b) elimination of anti-suppression action of SPS with I^- ion, and (c) determination of PEG-PPG concentration with small error and high linearity. (Ref. 114).....	35
Fig. 2.1.	The aging experiments were carried out under (a) open-circuit, (b) short-circuit, (c) electrolysis, and (d) elimination of dissolve O_2 in open-circuit.....	42
Fig. 2.2.	Schematic diagram of electrochemical analysis (a) LSV, (b) CVS.....	49
Fig. 2.3.	Method of the C_{SPS} by CVS analysis. (a) cyclic voltammogram for the Cu stripping region with additions. (b) The calibration curve of the charge ratio (Q/Q_0) vs. additive concentration ($C_S \cdot V_S / (V_i + V_S)$).....	50
Fig. 2.4.	Method of the MW_{PEG} by CVS analysis. Cyclic voltammogram for the Cu plating bath between -0.45 V and 0.1 V for different (a) C_{PEG} and (b) MW_{PEG} . The differences in the charge density between forward (Q_f)	

	and backward (Q_b) scans for different C_{PEG} and MW_{PEG} are shown in	
	(c). Calibration curve of the maximum value of $(Q_f - Q_b)$ vs. a function	
	of MW_{PEG} is shown in (d).....	51
Fig. 2.5.	Pretreatment of sample for spectroscopy analysis (MALDI-TOF,	
	NMR).....	54
Fig. 2.6.	Schematic diagram of flow cell for Cu micro-via filling.....	57
Fig. 3.1.	Concentration of SPS measured by CVS during the aging experiment	
	under the open-circuit. The measurements were carried out twice, (a)	
	as sampled the aging experiment and (b) after 3 days later.....	69
Fig. 3.2.	Concentration of SPS measured by CVS during the aging experiment	
	under the short-circuit. The measurements were carried out twice, (a)	
	as sampled the aging experiment and (b) after 3 days	
	later.....	70
Fig. 3.3.	Measurement of current flow under the short-circuit by multi-meter	
	with two different addition sequences. Input the materials in the (a) Cu	
	plate to Ir/IrO _x plate, (b) Ir/IrO _x plate to Cu plate.....	71
Fig. 3.4.	Concentration of SPS measured by CVS during the aging experiment	
	under the electrolysis condition (20 mA/cm ²). The measurements were	
	carried out twice, (a) as sampled the aging experiment and (b) after 3	
	days later. The effect of the current density on the breakdown rate are	

	shown in (c) and (d), respectively.....	72
Fig. 3.5.	Fig. 3.5. (a) ¹ H-NMR spectrum of accelerator species obtained from electrolytes (a1) without aging, (a2) with aging for 5 h under the open-circuit, and (a3) 3 days later. Concentration of accelerator species analyzed are presented at (b) SPS and PDS concentration by ¹ H-NMR and (c) SPS concentration by ¹ H-NMR and CVS, respectively.....	73
Fig. 3.6.	Consumption rates of SPS at electrodes under various conditions measured (a) immediately and (b) 3 days later.....	74
Fig. 3.7.	The concentrations of SPS by CVS after aging for 3 days under open-circuit w/ and w/o N ₂ purging (a) raw data and (b) C _{SPS}	75
Fig. 3.8.	The concentrations of additives by NMR w/ and w/o Cu ²⁺ and H ₂ O ₂ after aging for 10 days.....	76
Fig. 3.9.	Schematic diagram of the SPS chemical decomposition reactions.....	77
Fig. 3.10.	Value of Q _b -Q _f as a function of the amount of the aged solution (1 mL/addition) at (a) the Cu plate and (b) Ir/IrO _x plate added into VMS (50 mL). The aged solution was obtained under open-circuit conditions in a membrane cell. The MW _{PEG} values in the aged solution measured by CVS is presented in (c).....	88
Fig. 3.11.	Value of Q _b -Q _f as a function of the amount of the aged solution (1	

	mL/addition) at (a) the Cu plate and (b) Ir/IrO _x plate added into VMS (50 mL). The aged solution was obtained under short-circuit conditions in a membrane cell. The MW _{PEG} values in the aged solution measured by CVS is presented in (c).....	89
Fig. 3.12.	Changes in MW _{PEG} during electrolysis at 30 mA/cm ² , 40 mA/cm ² , and 50 mA/cm ² in (a) Cu plate and (b) Ir/IrO _x plate.....	90
Fig. 3.13.	MW _{PEG} measured by MALDI-TOF during the degradation experiment under electrolysis conditions (30 mA/cm ²) at (a) the Cu plate, and (b) Ir/IrO _x plate.....	91
Fig. 3.14.	Comparison between the MW _{PEG} values obtained with MALDI-TOF and with CVS analysis at (a) the Cu plate and (b) Ir/IrO _x plate.....	92
Fig. 3.15.	¹ H-NMR spectra of PEG after aging for 48 h, (a) pristine PEG and PEG in the fresh bath; (b) PEG aged under open-circuit conditions; (c) PEG aged under short-circuit conditions; (d) PEG aged under electrolysis conditions with 30 mA/cm ²	93
Fig. 3.16.	MW _{PEG} after 48 h aging under various conditions (open-circuit, short-circuit, and electrolysis).....	94
Fig. 3.17.	Intensity ratio of -OH/-CH ₂ -O for PEGs aged for 48 h under various conditions. Intensity ratio was obtained by integrating peaks at 3.7 ppm (-CH ₂ -O) and 4.8 ppm (-OH).....	95

Fig. 3.18.	Value of Q_b-Q_f as a function of the amount of the aged solution (1 mL/addition) at the Cu plate added into VMS (50 mL). The aged solution was obtained under open-circuit aging with and without N_2 purging. The MW_{PEG} values in the aged solution measured by CVS is presented in (b).....	96
Fig. 3.19.	(a) 1H -NMR spectra of PEG; fresh PEG, aged PEG under open circuit condition with N_2 purging, and that aged without N_2 purging. (b) Intensity ratio of $-OH/-CH_2-O$ for various conditions.....	97
Fig. 3.20.	Q_b-Q_f as a function of the amount of Cl-free aged solution (1 mL/addition) at (a) the Cu plate and (b) Ir/IrO _x plate added into VMS (50 mL). The aged solution was obtained under electrolysis conditions with 30 mA/cm ² . The MW_{PEG} values in the aged solution measured via CVS is presented in (c).....	98
Fig. 3.21.	Schematic diagram of the PEG chemical decomposition reactions.....	99
Fig. 3.22.	The voltammograms of the Cu bath with a Cu RDE (VMS# 1, 50 μ M SPS, and 88 μ M PEG-3350), with and without the addition of 100 μ M of each reducing agent, with a rotating speed of (a) 0 rpm, (b) 300 rpm, and (c) 1000 rpm.....	111
Fig. 3.23.	(a) The concentrations of SPS in the Cu bath during open-circuit aging with and without the addition of 100 μ M of each reducing agent, and	

	(b) corresponding consumption rates.....	112
Fig. 3.24.	Photographic images of the Cu bath with 10 mM of each reducing agent over a 10 h period.....	113
Fig. 3.25.	The voltammograms of the Cu bath (VMS#1, 50 μ M SPS, and 88 μ M PEG-3350) with 10 mM of each reducing agent on the Cu RDE ((a) 0 rpm, (b) 300 rpm, (c) 1000 rpm), and on the Pt RDE ((d) 0 rpm, (e) 300 rpm, (f) 1000 rpm).....	114
Fig. 3.26.	(a) The concentrations of SPS in the Cu bath (VMS#1, 50 μ M SPS) during open-circuit aging with and without 10 mM of each reducing agent, and (b) corresponding consumption rates.....	115
Fig. 3.27.	(a) SPS concentration during open-circuit aging, and (b) corresponding consumption rates. The Cu bath initially consisted of VMS#1, 50 μ M SPS, and 10 mM of each reducing agent was added to the electrolyte, which was sampled every 2 h.....	116
Fig. 3.28.	(a) Optical microscopy (OM) images of the PCB surface and micro-via after electrodeposition for 90 min using fresh and aged baths without the addition of formaldehyde (initial concentration= VMS#2 and 24 μ M SPS; supplement after aging= 100 μ M PEG-1500 and 100 μ M NH_4Br) (b) SPS concentration measured by CVS analysis.....	117
Fig. 3.29.	(a) Optical microscopy (OM) images of the PCB surface and micro-via	

after electrodeposition for 90 min using fresh and aged baths with the addition of formaldehyde (initial concentration = VMS#2 and 24 μM SPS, 10 mM formaldehyde; supplement after aging = 100 μM PEG-1500 and 100 μM NH_4Br) (b) SPS concentration measured by CVS analysis..... **118**

Fig. 3.30. Schematic diagram of the reduction of formaldehyde by active radicals..... **119**

CHAPTER I

Introduction

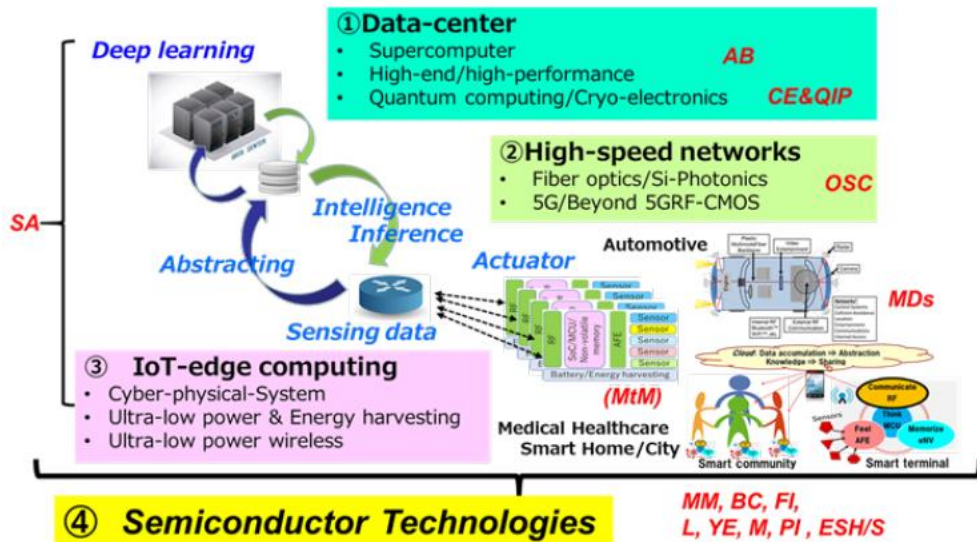
1.1. Recent trends of Cu electrodeposition industry

As the importance of convergence technology is emphasized in the era of the 4th industrial revolution, the amount and processing speed of data increase explosively. Especially, the semiconductor industry paradigm is changed the new ecosystem of electronics^{1,2} in **Fig. 1.1**. In addition, as science and technology advance in the direction of decreasing the environmental pollution, new and renewable energy has emerged.

Copper electrodeposition technology has been applied for a long time, but it is the root-technology that is the basis of the 4th industrial revolution. In particular, it has been used in many industries, such as the printed circuit board (PCB) process, which is the basis of electronic products, the interconnect process of semi-conductors called wire in the information era. It is also utilized in the energy industry, such as the current collector of Li secondary batteries that serve as engines of electric vehicle (EV) that replace internal combustion engine, and the electro-catalyst of CO₂ reduction.³⁻²¹ In recent semiconductor technology, as front end of line (FEOL) have reached their physical limitation,

the importance of the back end of line (BEOL), like package process (through silicon via (TSV), Redistribution layer (RDL), packaging on packaging (PoP)), has emerged. In the field of secondary battery technology, various studies are also underway to increase the energy density to correspond the 5G-technology, minimize the size and thickness of current collector and increase the roughness of the surface. At this time, a Cu electroplating method with industrial competitiveness is used.²²⁻²⁵

The market size of the global oxygen-free Cu metal industry is close to about USD 30 billion in 2019, and is expected to reach 5.5% annual growth rate from 2020 to 2026 in **Fig. 1.2**. The market value of the global electroplating industry also exceeded USD 12.8 billion in 2018, and recorded a compound annual growth rate (CAGR) of about 2.84% during the forecast period from 2019 to 2026 in **Fig. 1.3**. These Cu and electroplating industries are growing rapidly, and could be conclude that an important technology industry as a root-technology for 4th industrial revolution.^{26, 27}



AB: Applications Benchmarking, **SA:** Systems and Architecture, **OSC:** Outside system Connectivity, **MM:** More Moore, **BC:** Beyond CMOS, **CE&QIP:** Cryogenics Electronics and Quantum Information Processing, **PI:** Packaging Integration, **FI:** Factory Integration, **L:** Lithography, **YE:** Yield Enhancement, **M:** Metrology, **ESH/S:** Environment, Safety, Health, and Sustainability, **M&M:** More than Moore, **MDs:** Market drivers (automobile, medical devices).

Fig. 1.1. The new ecosystem of the electronics' industry based on semiconductor technologies. (Ref. 1)

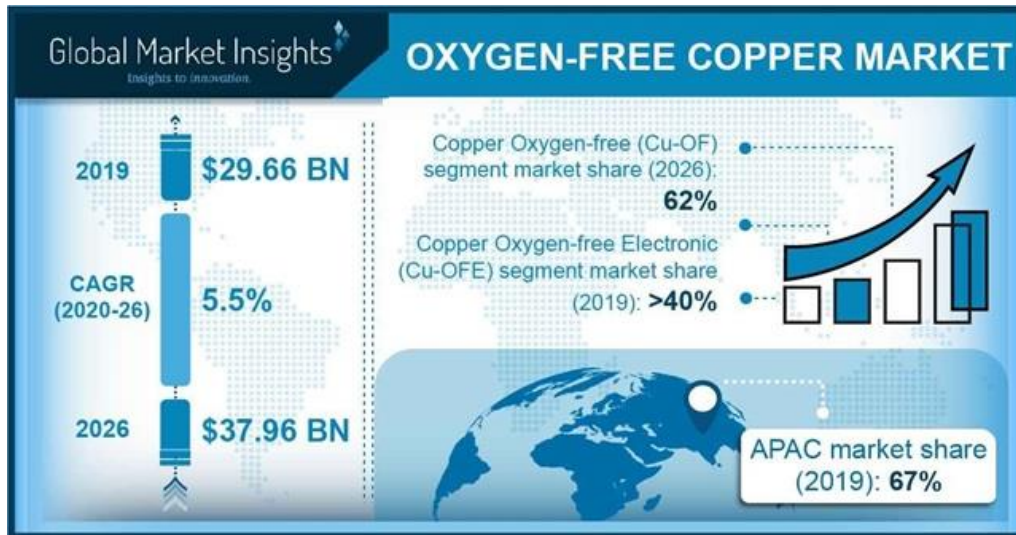


Fig. 1.2. Global oxygen-free Cu market size and forecast. (Ref. 26)



Fig. 1.3. Trends of global electroplating market size. (Ref. 27)

1.2. Cu electrodeposition and organic additive

Electrodeposition is the one of metal plating techniques in various industry, using the externally supplied electrons to reduce the metal ions in the electrolyte. In particular, in recent years, Cu electroplating is proceeding to enable in difficult conditions through an appropriate combination and synthesis of organic additives.

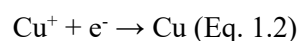
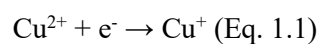
1.2.1. Cu electrodeposition

Metal plating includes various methods such as chemical vapor deposition (CVD), physical vapor deposition (PVD), atom layer deposition (ALD), eletrodeposition (ED), and electroless-deposition (ELD). Vapor deposition makes the material to be deposited in a gaseous state and deposits it in a high vacuum chamber, which applies high-level plating through precise metal plating. However, the process cost is high and productivity is low because the limitation of the chamber size and uniform plating is difficult depending on the features of the electrode. On the other hand, the electrodeposition method is very economical and easy to control in the industry. In this process, metal ions and elements are reduced by supplying electrons, and the desired electroplating is

performed by controlling various variables like current/potential, mass transfer, and electrical technique.

The copper possesses metallic properties that are easy to use in a variety of industries. Cu is the second lowest-resistance ($1.67 \mu\Omega\cdot\text{cm}$) material after silver among metals with high resistance to electro-migration in Cu interconnect, which has high deformation capacity. It has been widely applied in electronic products, because Cu is an economical metal compared to precious metals. In particular, in the case of Cu ions, since the standard reduction potential has more positive value than H^+ ion, it is convenient to control the Cu ion in electroplating industry.²⁸⁻³¹

Cu electrodeposition is shown in **Fig. 1.4**. Cu ions receive electron and are reduced by the following reactions. Cu^{2+} ion moves from the bulk solution to the electrode surface by electrical energy (voltage/current), which is affected by mass transfer. Afterward, 2-step reaction is proceeded in the electrode surface. The Cu^{2+} ion arriving at the electrode surface is reduced to Cu^+ by Eq. 1.1, which is known as the rate determining step (RDS), and Cu^+ ion is reduced to metallic Cu by Eq. 1.2.



In order to obtain the deposited Cu in electrodeposition process, the electrochemical parameters are controlled, the size of current/potential, the shape control such as pulse-reverse/step, the composition of the electrolyte, and the applying of additives that has a large effect with a small amount are used through optimization of the conditions.³²⁻³⁴ In recent years, as the electroplating conditions have become more difficult, there has been a limit to the method of controlling electrochemical parameters. Therefore, basic studies on additives have been continued, and a lot of research has been conducted on the synthesis of additives to obtain desired Cu performance.³⁵⁻³⁷

1.2.2. Properties of Cu bath and organic additive

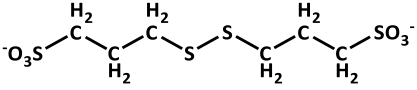
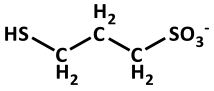
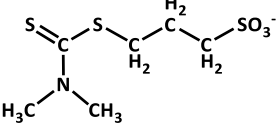
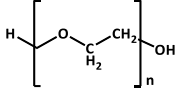
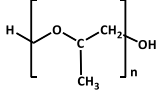
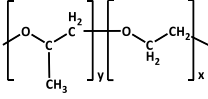
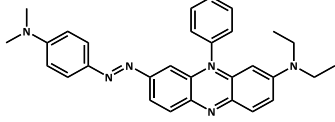
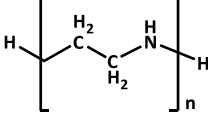
The Cu electrodeposition cell is composed of an electrode, an electrolyte, and an external power supply. In the case of electrode, 2-, or 3-electrode system is usually applied, a working electrode (WE), a counter electrode (CE), and reference electrode. The electrolyte is composed of metal ion source, a supporting electrolyte, and organic additives. In the case of a Cu ion source, CuSO₄, CuCN, CuCl etc., which are common materials in the Cu electrodeposition. Especially, CuSO₄, less harmful to the human body

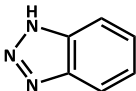
and polluting the environment, is mainly utilized in the industry. In addition, a supporting electrolyte is applied to decrease the solution resistance, where acid is typically taken because H^+ ion has high mobility (u_j). Therefore, the solution resistance is lowered by using H_2SO_4 to match the SO_4^{2-} ion, which is the counter ion of Cu^{2+} ion in $CuSO_4$. A small amount of organic additives contained in the electrolyte controls the property of Cu in electrode structure and components of Cu surface.

Organic additives are divided into three-types, which as shown in **Table 1.1**, according to application: an accelerator that increases the Cu electrodeposition rate, a suppressor which decreases the Cu electrodeposition rate, and a leveler that make the flat surface. The accelerator is an additive including S-S and S-H functional groups, typically bis-(3-sulfopropyl) disulfide (SPS), 3-mercapto-1-propanesulfonic acid (MPS), and 3-N,N-dimethylaminodithiocarbamoyl-1-propanesulfonic acid (DPS) is used. In particular, SPS, is the most common accelerator, increases the deposition rate through a substitution reaction with a suppressor.^{38, 39} On the other hand, surfactants such as polyethylene glycol (PEG), polypropylene glycol (PPG), and block copolymer (PEG-PPG-PEG) are mainly used as suppressor. The electrodeposition rate decreases by increasing the energy required for deposition by physically adsorption to the electrode surface. At this time, the suppressor is applied together with halide ions.⁴⁰⁻⁶² The leveler, usually containing

NH_4^+ groups, plays a role in reducing the topographic variation by chemically strong adsorption on the edge of the electrode surface where the current is focused through an adsorption mechanism dependent on mass transfer. Therefore, in order to make strong adsorption with leveler, various functional groups containing nitrogen are being controlled and developed. The desired Cu property or structure have been obtained using by controlling the combination and concentration of these organic additives.⁶³⁻⁶⁵

Table 1.1. The Representative Accelerators and Suppressor for Cu Electrodeposition

	Chemical name	Molecular structure
Accelerator (Acc)	Bis(3-sulfopropyl) disulfide (SPS)	
	3-Mercapto-1-propanesulfonic acid (MPS)	
	3-N,N-Dimethyleneamino dithiocarbonyl-1-propanesulfonic acid (DPS)	
Suppressor (Sup)	Poly ethylene glycol (PEG)	
	Poly propylene glycol (PPG)	
	PEG-PPG co-polymer	
Leveler (Lev)	Janus Green B (JGB)	
	Polyethyleneimine (PEI)	

	Benzotriazole (BTA)	
--	---------------------	---

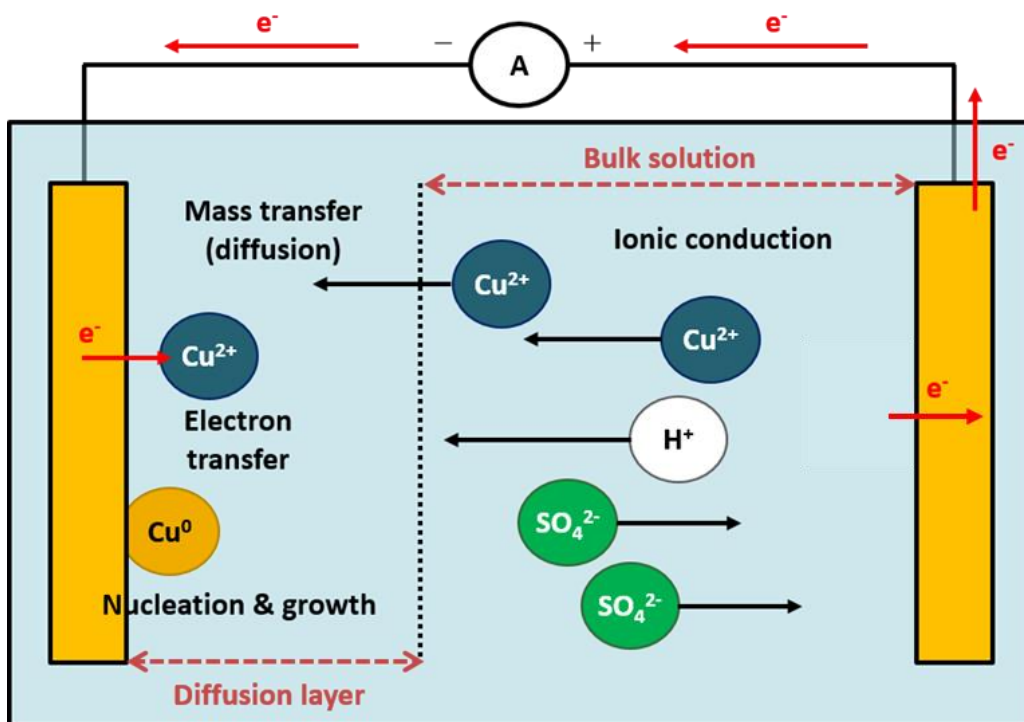


Fig. 1.4. Schematic diagram of Cu electrodeposition.

1.3. Mechanism of additive behavior

The organic additives SPS and PEG, which are representatively utilized in the industry, have undergone a lot of research on the additive reaction mechanism. It is explained by solution chemistry, competitive adsorption, curvature enhanced accelerator coverage (CEAC), S-shape negative differential resistance (S-NDR), convection dependent adsorption (CDA)

First, SPS chemically reacts in a Cu electrolyte to form a catalytic complex, which is the theory of solution chemistry. SPS acts as a catalyst by forming a Cu(I)thiolate complex that acts as a mediator of electron flow along with Cu^+ ions formed in the solution.⁶⁶⁻⁶⁸ Second, as shown in the **Fig. 1.5**, it is a competitive adsorption theory that appears when adsorbing competitively on the electrode surface with PEG. Usually, the relatively large amount of suppressor rapidly adsorbs than other additives on the surface. After that, PEG first forms PEG-Cu²⁺-Cl⁻ inhibition layer on the electrode surface with Cl⁻ ions, which is desorbed by SPS more strong adsorption with applied potential. As it is displaced, the deceleration effect of PEG inhibition layer decreases and the current increases, resulting in an acceleration effect.^{18, 69-73} As shown below Eqs. 1.3 and 1.4, the surface coverage change of adsorbed accelerator is described.

$$\theta_{\text{SPS}} + \theta_{\text{PEG}} = 1 \text{ (Eq. 1.3)}$$

$$d\theta_{\text{SPS}}/dt = k_{\text{ads}}(1-\theta_{\text{SPS}})C_{\text{SPS}} - k_{\text{inc}}(\theta_{\text{SPS}})^q \text{ (Eq. 1.4)}$$

Here in, θ_{SPS} is the adsorbed surface coverage of SPS, C_{SPS} is the concentration of SPS in bulk solution, k_{ads} is the adsorption rate constant of SPS, k_{inc} is the constant at which SPS is incorporated in the electrode, and q is the power-law consumption exponent.

In addition, structural electrodes such as trench or via follow the CEAC model, CDA model, and S-NDR model. In the CEAC model, since additives are structurally accumulated on the bottom region, the bottom up filling proceeds while having a relatively high speed deposition rate than the top region because the concentration of the accelerator raises at the bottom region. The simulation results is shown in **Fig. 1.6**.^{74, 75} In the CDA model, the adsorbed leveler makes decrease of the electrodeposition rate of Cu as the inhibition function increases due to high forced convection in the electrolyte in **Fig. 1.7**.^{76, 77} And in the S-NDR model, the leveler inhibits Cu electrodeposition with strong adsorption until the applied potential reaches a certain level, then quickly detaches from the electrode surface after this point, desorption the suppression layer. Therefore, as shown in **Fig. 1.8**, bifurcation of leveler on the surface with potential distribution

makes into active and passive regions according to the critical potential.^{78, 79}

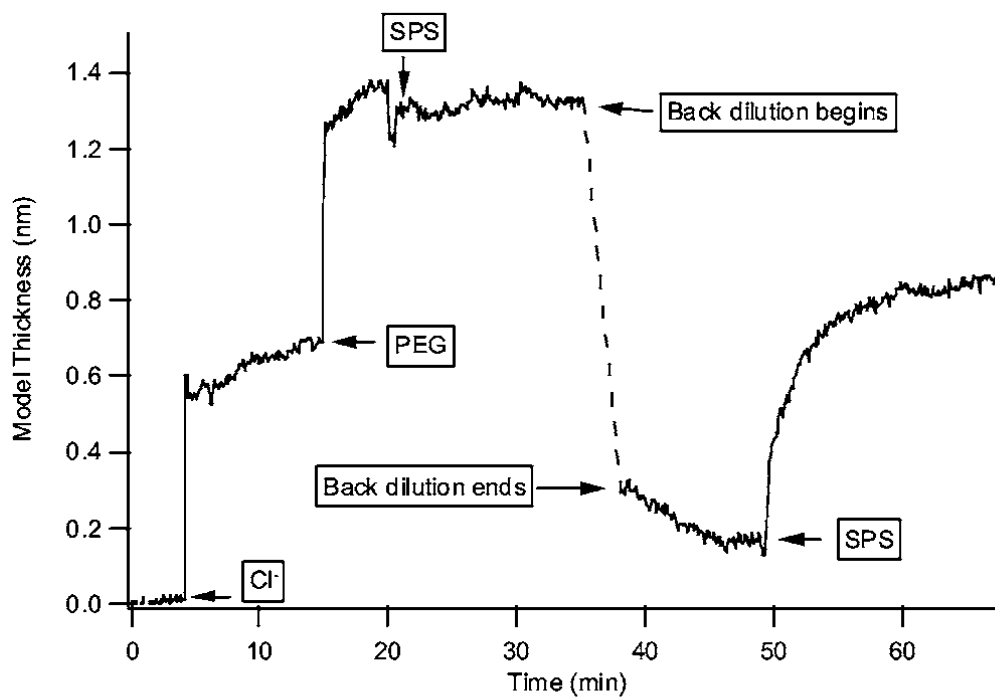


Fig. 1.5. Competitive adsorption of PEG, Cl⁻, and SPS. (Ref. 73)

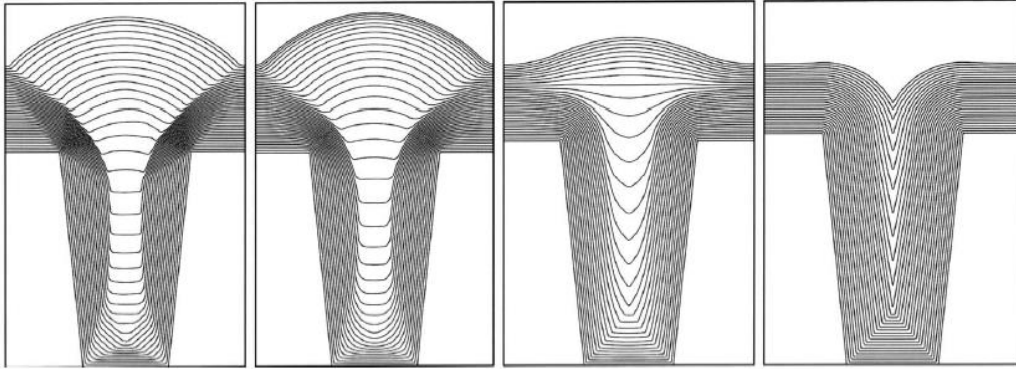


Fig. 1.6. The CEAC simulation on feature filling of Cu electrodeposition with various diffusion coefficient. (Ref. 74)

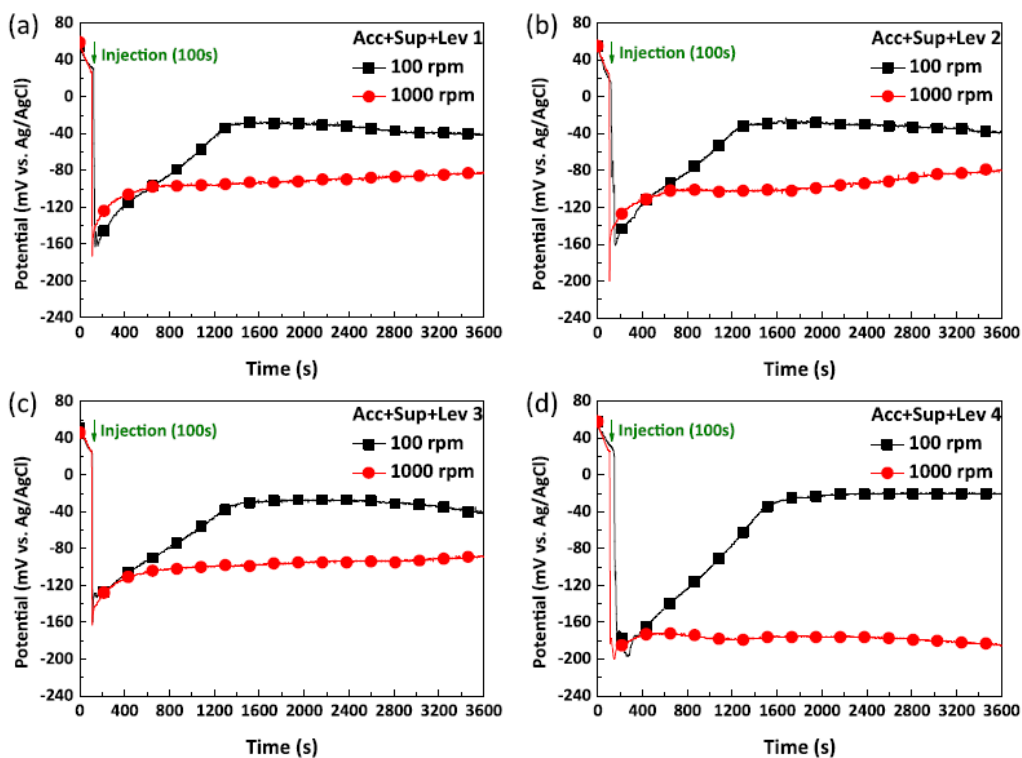


Fig. 1.7. The CDA model of the synthesized leveler with rotating disk electrode; (a) Lev 1, (b) Lev 2, (c) Lev 3, and (d) Lev 4. (Ref. 77)

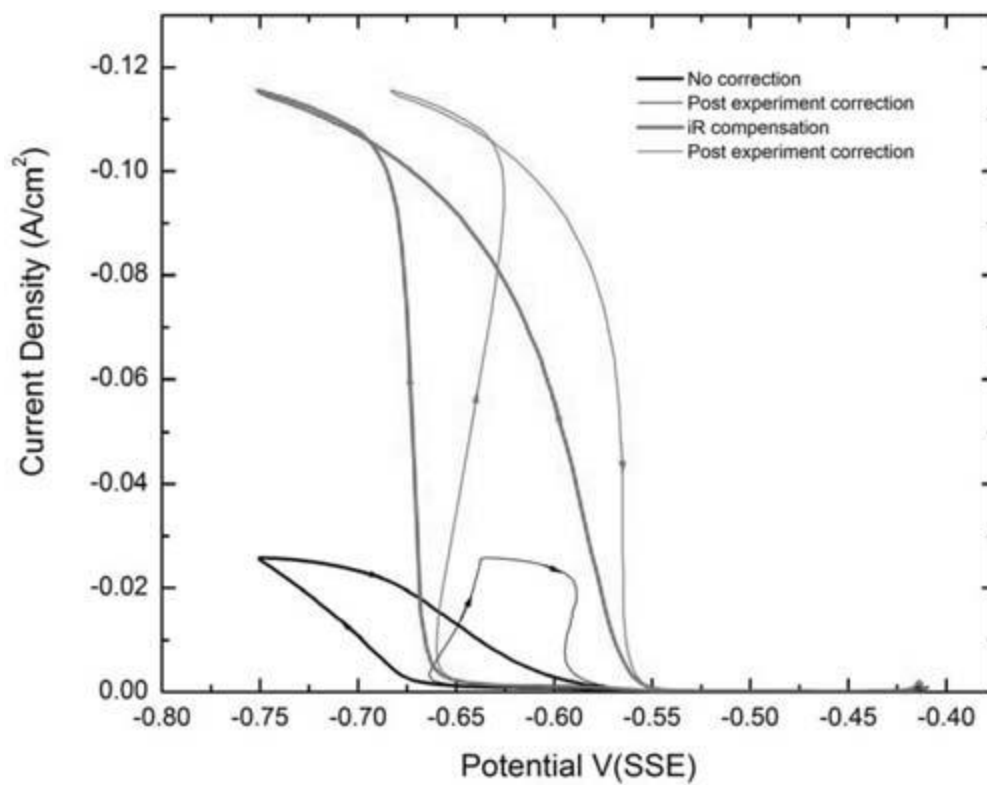


Fig. 1.8. The S-NDR voltammogram with Tetronic 701. (Ref. 78)

1.4. Decomposition of organic additive

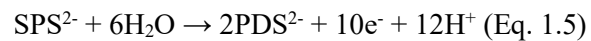
The organic additives play an important role in optimization of the Cu electrodeposition industry. In particular, maintaining the combination and concentration of organic additives determines the performance of the product. However, organic additives are decomposed chemically/electrochemically in the Cu electrodeposition process. Decomposition of organic additives changes the concentration and forms by-products, which deteriorates the Cu surface and performance to be optimized Cu in the Cu electrodeposition process. In **Fig. 1.9**, voids are formed in the Cu filling process (trench, micro-via, and TSV in semiconductor), and defects are created by decomposed organic additives in the subsequent chemical mechanical polishing (CMP) process.⁸⁰⁻⁹² Therefore, among many organic additives, decomposition studies have been conducted on SPS and PEG, which are representatively used in the industry.

1.4.1. SPS decomposition

SPS is known to be decomposed into MPS and 1,3-propane disulfonic acid (PDS) through electrochemical and chemical reactions in a Cu electrodeposition bath. SPS is a

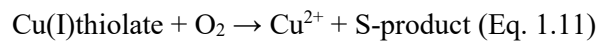
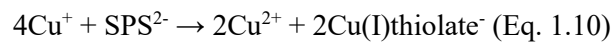
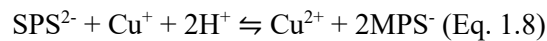
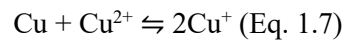
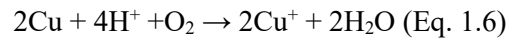
dimer of MPS, the bond of S-S is broken by electrons and oxidant. When H^+ attaches to the broken S-S bond, it forms a S-H bond which is reduced to MPS. The MPS is known to exhibit a higher acceleration effect than SPS, but it is not often used in industry because it is unstable in electrolyte. Finally, when S-S of SPS and S-H in MPS are continuously oxidized, PDS with little electrochemical/physical effect is produced. The SPS decomposition reactions are described in **Fig. 1.10**.^{66, 93-99}

First, looking at the electrochemical decomposition reaction of SPS in Eq. 1.5. It is known to be caused by participation of electron on anode in **Fig. 1.10(b)**. So, it is affected by the area and composition of the electrode surface and electrical energy (current/potential).



Second, it is known that the chemical decomposition of SPS is sequential oxidized by dissolved O_2 in the Cu electrodeposition process in **Fig. 1.10(a)**. Cu^+ ion is formed by corrosion reaction with acid solution and com-, disproportionation reactions by metallic Cu. (Eqs. 1.6 and 1.7) Thereafter, the SPS reacts with the formed Cu^+ ions, which makes the MPS by reduction, whereas the formed MPS undergoes an interconversion reaction

in which the formed MPS is oxidized to SPS again in the Cu^{2+} solution by Eq. 1.8. The formed MPS reacts with O_2 , which is oxidized back to SPS by Eq. 1.9. Through a Cu(I)thiolate complex formation reaction with Cu^+ ion by Eq. 1.10, it is oxidized with dissolved O_2 and finally decomposed into PDS by Eq. 1.11.^{87, 100}

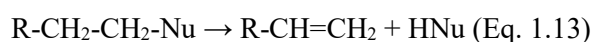


Cu^+ ion is known to be a very unstable material in aqueous solution, but it can exist relatively stable in solution by generating Cu(I)MPS⁻ together with MPS. Especially, in strong acidic solution with high H^+ concentration, the more SPS is converted to MPS by Eq. 1.8, the longer MPS can persist in Cu electrodeposition bath.¹⁰¹

1.4.2. PEG decomposition

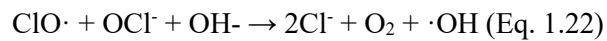
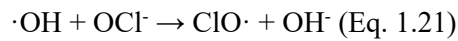
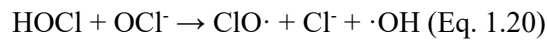
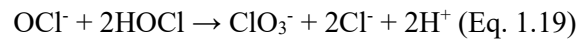
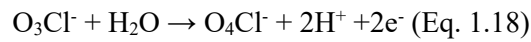
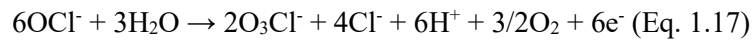
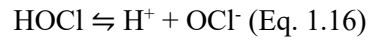
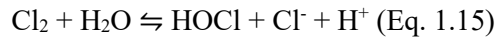
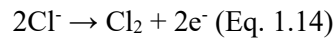
PEG consists of several bonds of ethylene glycol units. Under the electrolysis condition, PEG decomposes and gradually decreases of molecular weight. In addition, as the terminal group is oxidized, it has various oxidation forms (aldehyde, hydroxyl, ketone, carboxyl, vinyl, propyl group etc...). It is known that the decomposition of PEG is only degraded by chemical reactions in **Fig. 1.11**.^{102-105 106}

First, as shown in the **Fig. 1.11(a)**, nucleophilic substitution reaction is described in Eqs. 1.12 and 1.13. As shown in Eqs. 1.12 and 1.13, it is caused by the catalytic reaction of nucleophilic substitution substances such as Cu ions in Cu electrodeposition bath. This reaction occurs when PEG is attached to the electrode surface by bond breakdown. The C-C or C-O bond in PEG is broken by the S_N1 or S_N2 reaction, a continuous uni-molecular or bi-molecular elimination reaction occurs.¹⁰²



Second, the radical decomposition reaction in the **Fig.1.11(b)** is caused by hydroxyl

radicals formed in the Cu electrodeposition bath. Hydroxyl radicals are formed by a chain reaction (Eqs. 1.14~22) that occurs while generating HOCl by receiving electron along with chloride ions at the anode of Cu electrodeposition bath.¹⁰⁷



The formed hydroxyl radical breaks the C-O bond of PEG by hemolysis and decomposes it in the direction of molecular weight decrease.

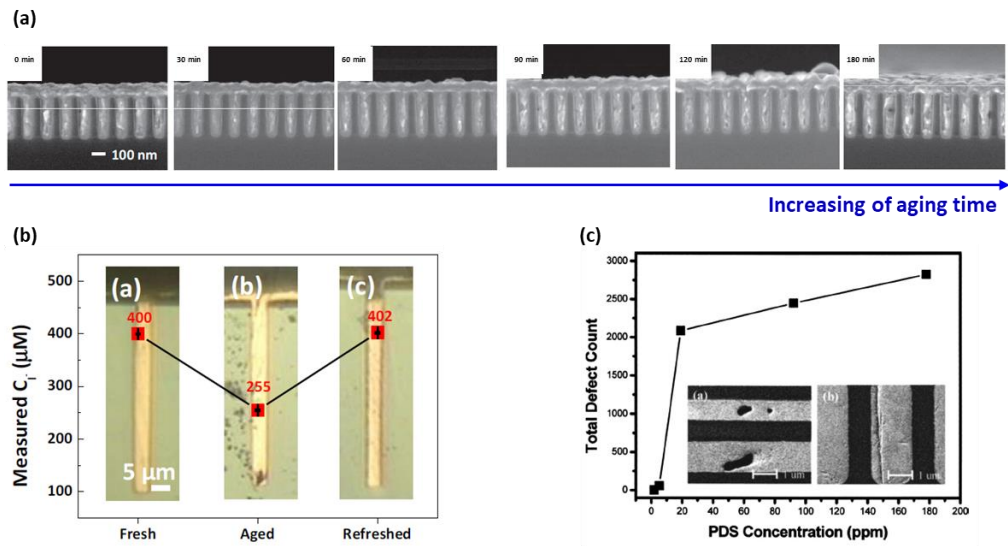


Fig. 1.9. The failure of Cu electrodeposition in various process. (a) trench filling performance, (b) TSV filling performance, and (c) Cu deposited surface after CMP. (Ref. 87, 92, and 81)

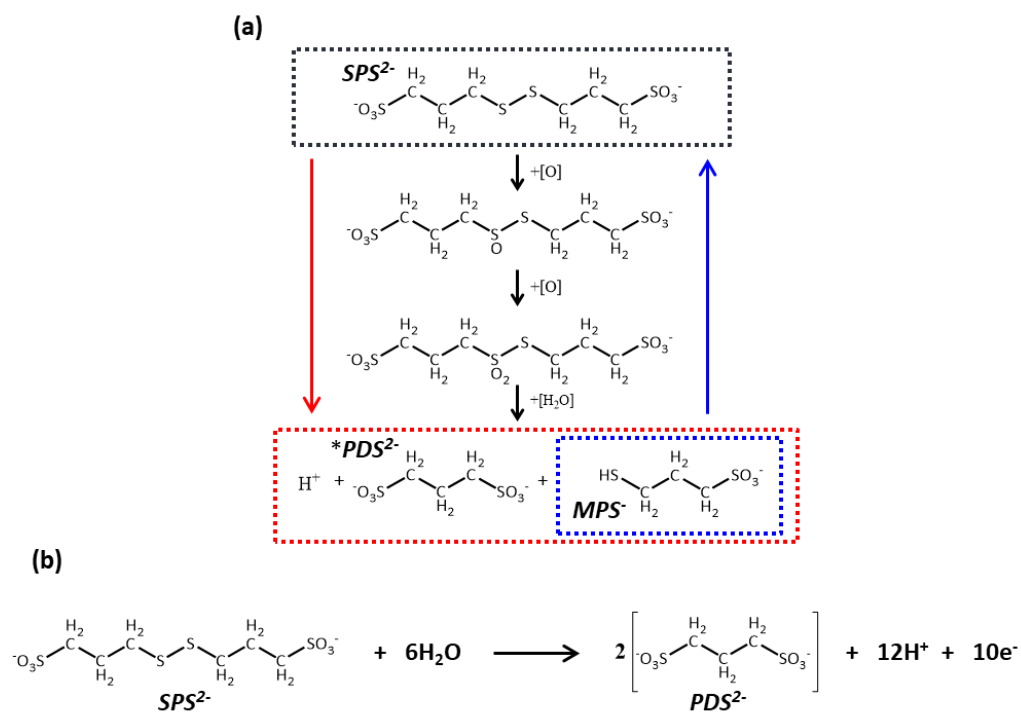


Fig. 1.10. Schematic diagram of SPS decomposition pathways (a) sequential oxidation,

(b) participation of electron on anode.

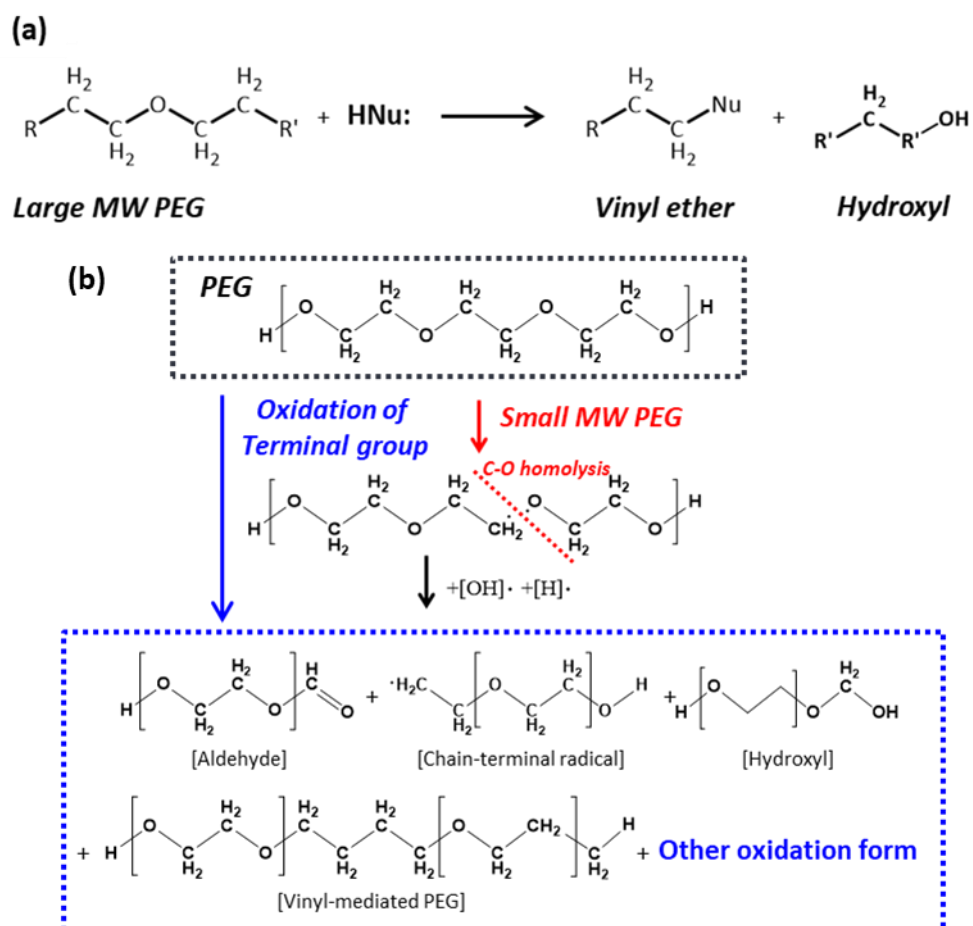


Fig. 1.11. Schematic diagram of PEG decomposition pathways (a) nucleophilic substitution reaction, (b) active radical decomposition.

1.5. Measurement of organic additive

Since the organic additive is degraded during the Cu electrodeposition process, it is important to accurately monitor and maintain the concentration of the organic additive. As studies on the decomposition of organic additives have been conducted, method for measuring the qualitative/quantitative of decomposition products have been developed. Analysis methods include electrochemical methods (Hull cell (HC), linear scan voltammetry (LSV), cyclic voltammetry stripping (CVS), cyclic pulse voltammetry stripping (CPVS)), spectroscopy methods (mass spectroscopy (MS), nuclear magnetic resonance (NMR), matrix-assisted laser desorption ionization-time of flight (MALDI-TOF), ultraviolet-visible spectroscopy (UV-Vis)), and chromatography methods (high-performance liquid chromatography (HPLC), solid phase extraction (SPE)).^{81, 108-113}

1.5.1. Cyclic voltammetry stripping (CVS) analysis

CVS is the most representative method to measure the concentration of organic additives in Cu electrodeposition bath. It is known as an analytical method with many merits, which is possible to measure the concentration of additives in a very small

quantity with simple pretreatment process. It is also powerful device in that real-time monitoring is possible. Since CVS is a method of calculation the change of the charge depending on the effect of the additives, the concentration of Cu that is reduced and oxidized on the electrode surface is determined by controlling various variables (vertex potential, rotating speed of electrode, scan rate, and calculation range)

The techniques of CVS experiment are largely divided into three types according to the additive. The suppressor is used as a basis for CVS focusing on the suppression effect by minimizing the other additives (accelerator, leveler) effect as it has the greatest effect on the same amount among additives. Therefore, the dilution titration CVS (DT-CVS) method is used to determine the effect of only the suppressor by diluting the electrodeposition solution. Since the accelerator should minimize the suppressor effect to exam the accurate concentration, it is measured by saturating the electrochemical effect of suppressor in the sample. At this time, the modified linear approximation technique CVS (MLAT-CVS) method is used to measure in a simple way by using a standard solution that knows the concentration of the accelerator. The leveler uses the method as the response curve CVS (RC-CVS) by formation of calibration curve. Additionally, our group has developed several modified CVS analysis methods in **Fig. 1.12~15.**^{108-110, 114}

Using the 2-step MLAT-CVS method in **Fig. 1.12**, it is possible to separate SPS and MPS to clearly (error < 10%) measure their concentration, respectively.¹⁰⁸ As shown in the **Fig. 1.13**, The measurement of average molecular weight of PEG method can accurately analyze the average MW of PEG within 9% error regardless of PEG MW distribution is symmetric or bimodal.¹¹⁰ Iodide ion concentration was successfully determined in various Cu acidic plating solution by potential control in **Fig. 1.14**. The inhibition of I drastically decreased when the vertex potential was set to a more negative value than -0.2 V due to the formation of CuI, which was further confirmed in effective coverage analysis.⁹² Selective suppressor concentration in over two-additives system was measured by iodide in the **Fig. 1.15**. Even CuI alone effectively inhibits the adsorption of SPS on the electrode surface. The synergistic interaction between CuI and PEG-PPG supported the re-formation of the passivation layer after the disruption by the inner diffusion of $\text{Cu}^{2+}/\text{Cu}^+$ ions in reverse sweep. Under the pre-optimized condition, modified CVS analysis was performed, and the Q/Q_0 plots showed the same response to CS in the CVS bath, irrespective of the CA in solutions.¹¹⁴

1.5.2. Spectroscopy (NMR, MALDI-TOF) analysis

CVS can clearly measure the concentration of target organic additives with electrochemically active one, but it cannot measure the disturbing effect of by-products formed by the decomposition process in the Cu electrodeposition bath and electrochemically inert additive. Therefore, spectroscopy analysis is used to compensate for CVS analysis. Qualitative/quantitative analysis is possible using by NMR analysis. $^1\text{H-NMR}$ and $^{13}\text{C-NMR}$ can be used to determine the structure of additives and decomposed by-products. In addition, it is possible to measure the quantitative analysis by calculating of the chemical shift peak area using an internal standard material. In the case of MALDI-TOF analysis, it is a method to check the distribution of the complex, such as polymer, it is possible to measure the molecular weight using a matrix material. It is particularly suitable for measuring PEG whose molecular weight decreases as it decomposes. In order to proceed with spectroscopy analysis, only additives in the solution should be extracted with high purity. Therefore, pre-treatment work is necessary.

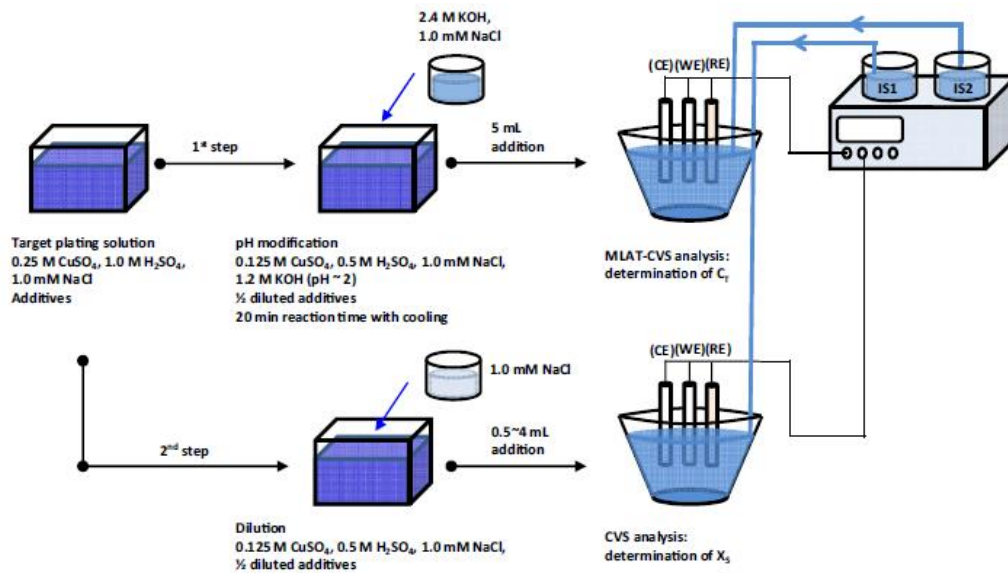


Fig. 1.12. Schematic diagram of 2-step MLAT-CVS method. (Ref. 108)

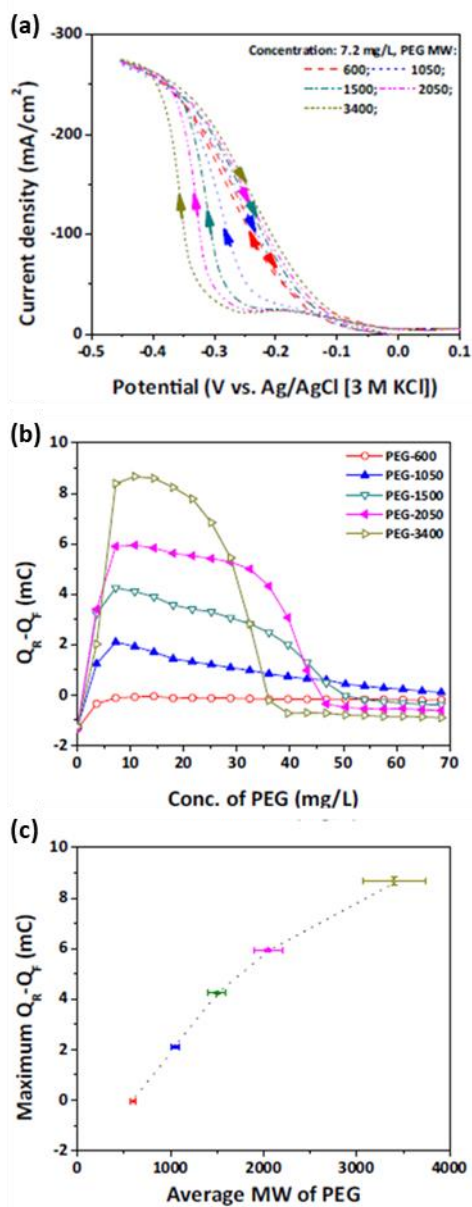


Fig. 1.13. Method of the average molecular weight of PEG. (a) influence of PEG molecular weight in CV, (b) Relation between the hysteresis area and PEG concentration for various MW_{PEG} , and (c) Calibration curve with maximum hysteresis area. (Ref. 110)

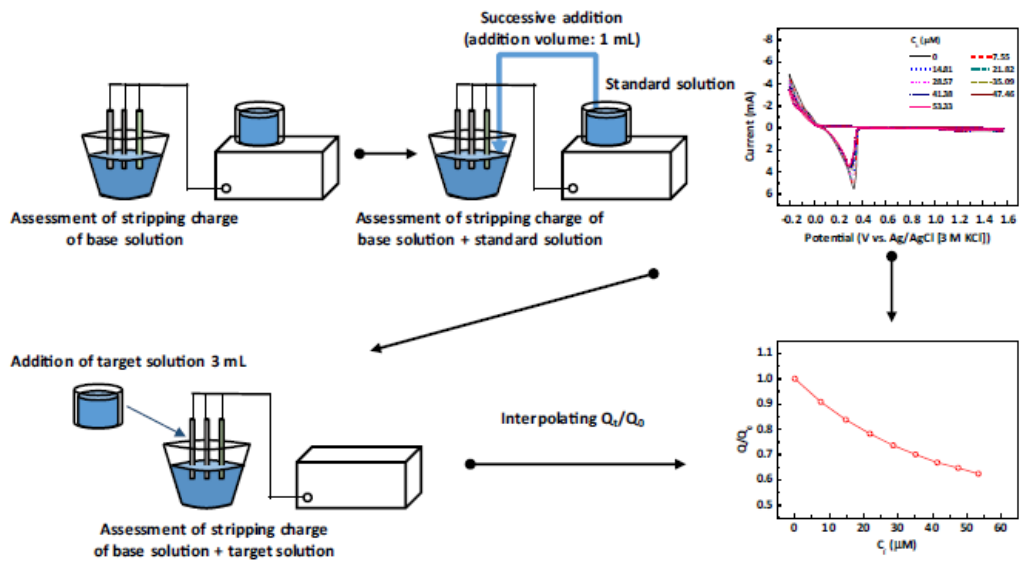


Fig. 1.14. Schematic diagram of iodide concentration method. (Ref. 92)

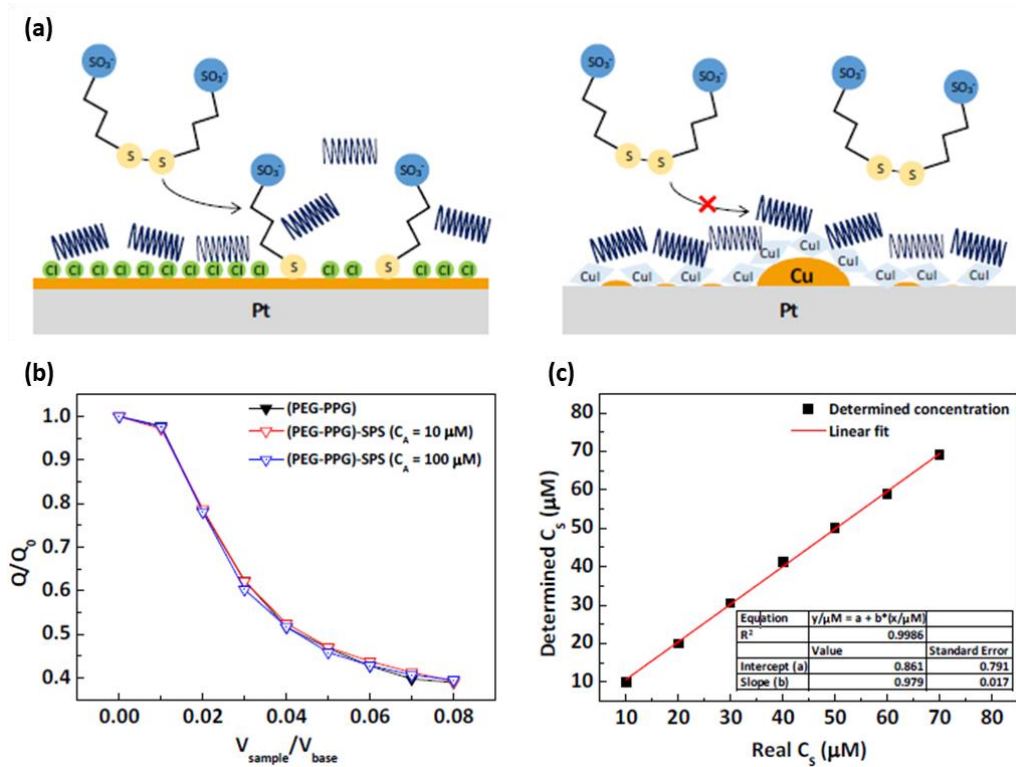


Fig. 1.15. Selective determination of PEG-PPG concentration by iodide ion. (a) formation of CuI inhibition layer, (b) elimination of anti-suppression action of SPS with I^- ion, and (c) determination of PEG-PPG concentration with small error and high linearity. (Ref. 114)

1.6. Purpose of this study

Research on the mechanism of additive behavior in Cu electrodeposition has been actively conducted. In recent years, the development of additive according to the electrodeposition process has been steadily progressing. In addition, research is developed in various ways to compensate for the problems of byproducts created by the decomposition of additives through technology that monitors the additive breakdown. However, studies on degradation of organic additive and preventing of decomposition have been relatively insufficient.

In this study, an in-depth approach was made to the decomposition mechanism of SPS and PEG, organic additives used as commercial additives in industry. The additive decomposition experiments were conducted at Cu plate (cathode) and Ir/IrO_x (anode) with membrane that was installed in the Cu electrolyte under three conditions; open-circuit; immersing each electrode in the solution, short-circuit; forming a closed-loop by connecting each electrode, and electrolysis; applying power in the circuit. Subsequently, the CVS analysis method developed in the laboratory was applied to measure the accurate concentration for SPS and correct average molecular weight for PEG, which calculates the decomposition rate according to the decomposition time. In addition, by-

products and were identified through qualitative analysis at each electrode using spectroscopy analysis; H-NMR, MALDI-TOF. So, reliability was secured through quantitative measurement and cross-checking with the results of the CVS analysis method. Through this, the decomposition reaction and key factor of organic additives were investigated.

Finally, while clearly grasping the key factors that decompose organic additive, a plan to decrease decomposition was searched. The reaction was identified by choosing a reducing agent that could be chemically/electrochemically applied to the Cu electrolyte by measurement of the additive decomposition concentration with and without the reducing agent. And it was checked whether it could be applied in practice through filling performance. Through this study, a method to increase the stability of the Cu electrodeposition bath used in the industry and to increase the economic efficiency was proposed.

CHAPTER II

Experimental

2.1. Degradation experiment

Decomposition experiments of organic additives in each electrode were conducted in three different environments: open-circuit, short-circuit, and electrolysis with various current density. The schematics of decomposition cells were shown in the **Fig. 2.1**. In the open-circuit condition, only the electrode was immersed in each electrolyte to deteriorate, and in the short-circuit condition, the immersed electrode was circuited to form a closed-loop. Electrolysis conditions were applied by various current. All decomposition experiments were conducted in a 2-electrode system, and a Cu plate (99.9% pure Cu, active area: 25 cm²) was used as the cathode, and an insoluble Ir/IrO_x (on Ti/TiO_x) plate was used as the anode. Each electrode was separated using an ion-conductive exchange membrane (Nafion N212) with 6 cm distance both Cu plate and Ir/IrO_x plate. The temperature was carried out at room temperature (18~22°C), and agitation was performed at 300 rpm using a stirrer bar. To examine the galvanic reaction in short-circuit conditions, galvanic current was measured using a multi-meter (DT4253,

HIOKI). In addition, when checking the effect of O₂, a pre-purging process was performed at 500 cc/min for 1 hour using N₂ purging, and a flow rate at 500 cc/min during the decomposition experiment by flow meter (Dwyer instrument, RMA-12-SSV).

2.1.1. Degradation of SPS

The decomposition experiment of SPS was largely carried out in two criteria (as sampled, and after 3 days). SPS reacts with the Cu⁺ ions formed in the solution to form Cu(I)MPS⁻ by interconversion reaction (Eqs. 1.8~1.10), and the reaction rate at which MPS is reduced to SPS depending on the acidity of the solution. Therefore, there was a difference in decomposition of SPS between the case of measuring the concentration by immediately sampling the decomposed electrolyte and measuring the concentration after 3 days.

The composition of the SPS decomposition base solution consisted of 0.25 M CuSO₄, 1 M H₂SO₄, and 1 mM NaCl. The organic additives were used as 50 μM SPS, 300 ppm PEG-3350. At this time, in the case of analyzing ¹H-NMR for quantitative analysis of SPS, the experiment was conducted by adding only SPS alone since the by-products of SPS and PEG-3350 are overlapped. The decomposition experiment process of SPS is as

follows.

- (1) After additives injected to the base solution, aging was performed for 10 hours under open-circuit, short-circuit, and electrolysis (10, 20, and 30 mA/cm²).
- (2) Aging samples were collected by 100 mL at 0, 2, 4, 6, 8, and 10 hours, respectively.
 - (2-1) In the cases of electrolysis, the consumption rates of Cu²⁺ ion and Cl⁻ ion were calculated and supplemented.
- (3) Immediate samples (as sampled) were measured using CVS by mixing the aging solution with titration solution (1.73 M NaOH and 1 mM NaCl) in a 1:1 ratio.
 - (3-1) After 3 days' samples were measured using CVS by mixing the aging solution with 1 mM NaCl solution in a 1:1 ratio.

2.1.2. Degradation of PEG

The composition of base solution for PEG decomposition consisted 0.25 M CuSO₄, 1 M H₂SO₄, 1 mM NaCl with 300 ppm PEG-3350. In the case of suppressor aging experiment, there was little difference in the decomposition between as sample and after 3 days, so PEG decomposition was performed using only after 3 days sample, and the sequence was as follows.

- (1) After additives inject to the base solution, aging was performed for 48 hours under open-circuit, short-circuit, and electrolysis (30, 40, and 50 mA/cm²).
- (2) Aging samples were collected by 100 mL at 0, 3, 6, 12, 24, and 48 hours, respectively.
- (2-1) In the cases of electrolysis, the consumption rates of Cu²⁺ ion and Cl⁻ ion were calculated and supplemented.
- (3) After collecting the samples, the concentration was measured using CVS.

2.1.3. Filling performance

The Filling base solution consisted of 0.93 M CuSO₄, 0.43 M H₂SO₄, 0.82 mM HCl with 24 μM SPS, which were optimized to fill the PCB micro-via substrate in the laboratory. And formaldehyde (HCHO) was added 10 mM as a reducing agent.

- (1) Decomposition was performed for 9 hours in open-circuit, and sampling was conducted every 3 hours.
- (2) The SPS decomposed samples for 0, 3, 6, and 9 hours were collected as 1.5 L, and the fresh 100 μM PEG-1500 and 100 μM NH₄Br were added to aging bath to perform a filling experiment.

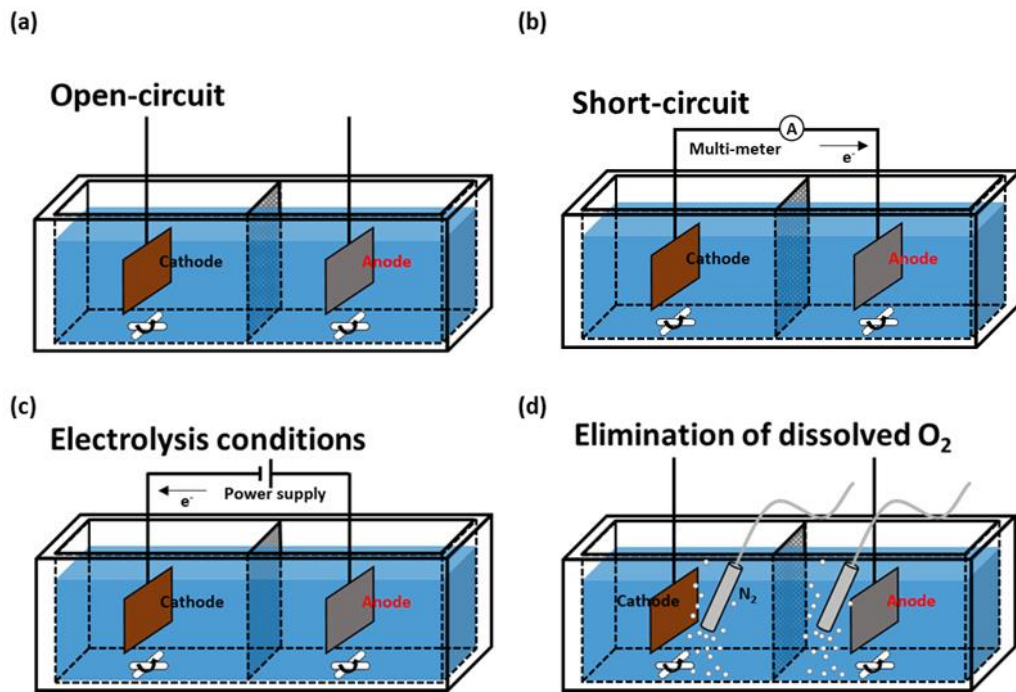


Fig. 2.1. The aging experiments were carried out under (a) open-circuit, (b) short-circuit, (c) electrolysis, and (d) elimination of dissolved O_2 in open-circuit.

2.2. Electrochemical analysis

In Cu electrodeposition, LSV analysis was used to confirm the electrochemical properties of the electrolyte and additives. The CVS analysis was applied to measure the concentration of SPS and average molecular weight of PEG.

2.2.1. LSV analysis

LSV was performed to confirm the electrochemical effect of the reducing agent, in a 3-electrode system in **Fig. 2.2(a)**, Cu (0.071, 0.1257 cm²) and Pt (0.196 cm²) were used as the working electrode (WE), Pt rod as the counter electrode (CE), and Hg/Hg₂SO₄ (saturated K₂SO₄) as the reference electrode (RE), respectively. The electrolyte consisted of 0.25 M CuSO₄, 1 M H₂SO₄, 1 mM HCl with 50 μM SPS and 300 ppm PEG-3350. As a reducing agent, hypophosphite (NaPO₂H₂), formaldehyde (HCHO), glyoxylic acid (OCHCO₂H), hydrazine (N₂H₄), and oxalic acid (COOH)₂ were examined in 100 μM (low concentration) and 10 mM (high concentration). The analysis was conducted at 25°C at a scan rate of 10 mV/s and various RDE rotation (0, 300, 1000 rpm). LSV was analyzed using potentiostats (Parstat 2273 and Par273A potentiostat (EG&G Princeton

Applied Research Corp.)).

2.2.2. CVS analysis

SPS concentration and PEG average molecular weight were measured by CVS analysis. As shown in the **Fig. 2.2(b)**, The CVS 3-electrode system consisted of Pt RDE (active area: 0.0314cm^2), Pt rod, and Ag/AgCl (3 M KCl) as working, counter, and reference electrode, respectively. During the CVS analysis, the Pt RDE as the working electrode was stirred at 2,000 rpm and at 30°C by a thermostat. First, the concentration of SPS (C_{SPS}) was measured by standard addition method in CVS, and average molecular weight of PEG (MW_{PEG}) was calculated by previous method.^{108, 110}

2.2.2.1. Measurement of SPS concentration (C_{SPS})

The concentration of SPS was measured using the standard addition method by CVS. The as sampled and after 3 days concentration of decomposition SPS was calculated. The potential was applied from 1.575 V, to vertex potential of -0.25 V, and swept back to 1.575 V again with the scan rate at 0.1 V/s. First, in order to measure the concentration

of SPS for the as sample condition, it was titrated to pH 2 to rapidly reduced Cu(I)MPS- to Cu²⁺ and SPS in the Cu electrodeposition bath to prevent more degradation of SPS with Cu⁺ ion. Virgin make-up solution of as sampled condition (VMS-A) is composed of 0.125 M CuSO₄, 0.5 M H₂SO₄, 0.86 M NaOH, 1 mM NaCl with mixing a 1:1 ratio of aged sample:titration solution (1.73 M NaOH, 1 mM NaCl) to make pH 2. In addition, after 3 days conditions virgin make-up solution (VMS-B) of SPS consisted of 0.125 M CuSO₄, 0.5 M H₂SO₄, 1 mM NaCl. In order to selectively measure only the concentration of SPS, it is made using 70 mM PEG-3350 saturated stock solution (satS). The experiment process of SPS concentration measurement by CVS is as follows, and the calculation results are shown in the **Fig. 2.3**.

$$m = \Delta(Q/Q_0)/\Delta(C_s \cdot V_s/V_i + V_s) \text{ (Eq.2.1)}$$

$$C_t = \Delta(Q_t/Q_0)/\Delta(V_t/V_i + V_t) \cdot (1/m) \text{ (Eq.2.2)}$$

- (1) Put VMS-A, B (49 mL) and SatS (1mL) into a CVS vessel.
- (2) Cyclic voltammetry stripping is measured repeatedly until the CVS solution and electrode are stabilized.
- (3) Measure each charge (Q) with 10 times injection of 0.5 mL standard solution (staS,

50 μ M SPS) in 50 mL of VMS (49 mL) and SatS (1 mL).

- (4) Obtain the charge ratio (Q_s/Q_0) vs. SPS concentration ($C_s \cdot V_s / (V_i + V_s)$) calibration curve by calculation the Q_0 value of VMS and Q_s (X: 0~10) obtained by (3) process
- (5) Calculate the slope (m) of the standard curve in Eq. 2.1.
- (6) The aging target sample was processed in the same manner as (1) ~ (5) to determine Q_t/Q_0 vs. addition number ($V_t / V_i + V_t$)
- (7) Calculated C_t by Eq. 2.2.

Here in, Q_0 is the stripping charge of VMS with satS, Q_s is the stripping charge of the addition staS, Q_t is the stripping charge of target solution, C_s is the SPS concentration in the StaS, C_t is the SPS concentration in target sample. In the sample solution, V_i is the volume of VMS-A, B with SatS, V_s is the volume of staS, and V_t is the volume of target sample solution.

2.2.2.2. Measurement of PEG average molecular weight (MW_{PEG})

The measurement of the PEG concentration is not easy to determine during decomposition process because PEG molecular weight was decrease but number of low molecular weight increase. Therefore, it is more accurate to use the measurement of

MW_{PEG} by previous method than to measure the PEG concentration. The measurement of MW_{PEG} method by CVS used the hysteresis area in CV formed by adsorption and desorption of PEG. PEG virgin make-up solution (VMS-P) consisted 0.25 M CuSO₄, 1 M H₂SO₄, 1 mM NaCl. The potential was applied from 1.575 V to sweep the vertex potential at -0.45 V. It was again swept back to 1.575 V with 0.1 V/s scan rate. During the analysis, the Pt RDE used as the working electrode with 2,000 rpm agitation. The temperature was maintained at 30°C using a thermostat.

To measure MW_{PEG}, Prior to carrying out the CVS analysis, the calibration curve between the maximum area of hysteresis (Q_b-Q_f) vs. MW_{PEG} (input data) was obtained. (Fig. 2.4) The hysteresis generally was evolved between 0.1 V and -0.45 V when a small amount of PEG (concentration of PEG (C_{PEG}): ~ 40 ppm) was added in the CVS vessel. Figs. 2.4(a), (b) showed that both MW_{PEG} and C_{PEG} affected the area of hysteresis. By plotting the area of hysteresis (Q_b-Q_f) vs. C_{PEG} , we obtained the maximum area of hysteresis as a function of MW_{PEG} in Figs. 2.4(c), (d). Using the individual data points in Fig. 2.4(d), a non-linear regression ($y=a+bc^x$, $a=435.038$, $b=515.473$, and $c=0.99956$) with an R^2 value of 0.9901 was carried out to obtain the master calibration curve. Using this method, the MW_{PEG} values in the bath under various aging conditions were calculated. The measurement of the MW_{PEG} is as follows, and the calculation result was

shown in the **Fig. 2.4**.

- (1) Put VMS-P (50 mL) into a CVS vessel.
- (2) Cyclic voltammetry stripping is measured repeatedly until the CVS solution and electrode are stabilized.
- (3) Measure each maximum charge ($Q_b^-Q_f$) with 10 times injection of 0.5 mL the stock solution (stoS, 1000 ppm PEG-X (S:200, 600, 1050, 1500, 2050, 3350, 6000, 10000 Da)) into 50 mL of VMS-P.
- (4) Obtain the maximum $Q_b^-Q_f$ (charge density) vs. MW_{PEG} (Da) calibration curve by calculation the hysteresis area value of VMS and addition of stoS obtained by process (3).
- (5) Calculate the master calibration curve by non-linear regression ($y=a+bc^x$, $a=435.038$, $b=515.473$, and $c=0.99956$) with an R^2 value of 0.9901 carried out in Fig. 2.2.
- (6) The aging target sample is processed in the same manner as in (1)~(5) to obtain the $Q_b^-Q_f$ vs. addition number graph.
- (7) Calculate the MW_{PEG} in aging target sample.

Here in, Q_b is the charge density of the backward scan, Q_f is the charge density of the forward scan.

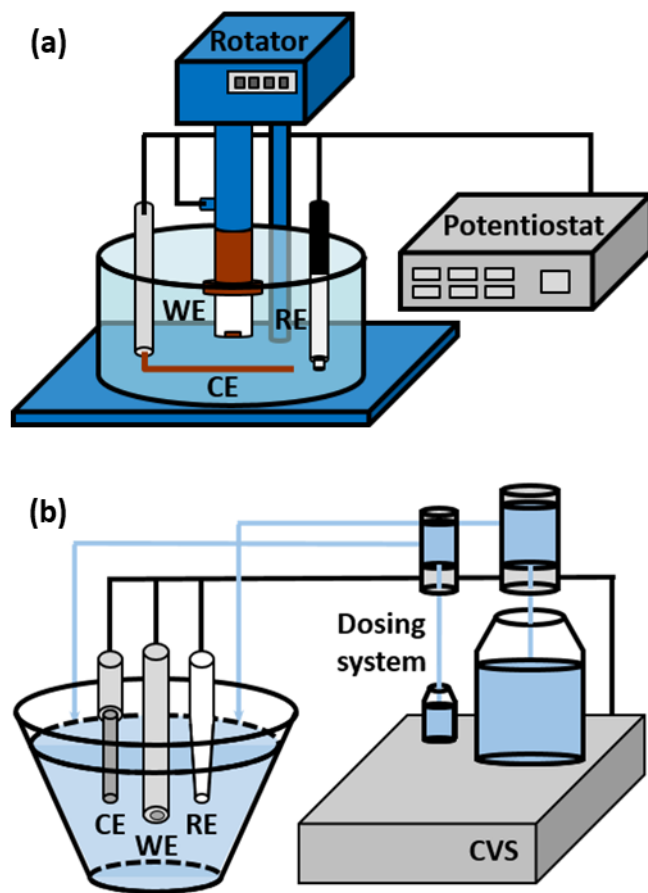


Fig. 2.2. Schematic diagram of electrochemical analysis (a) LSV, (b) CVS.

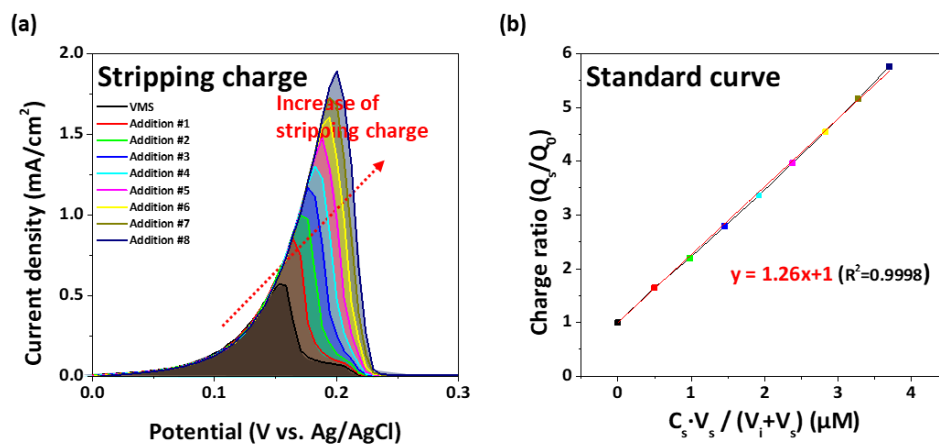


Fig. 2.3. Method of the C_{SPS} by CVS analysis. (a) cyclic voltammogram for the Cu stripping region with additions. (b) The calibration curve of the charge ratio (Q/Q_0) vs. additive concentration ($C_s \cdot V_s / (V_i + V_s)$).

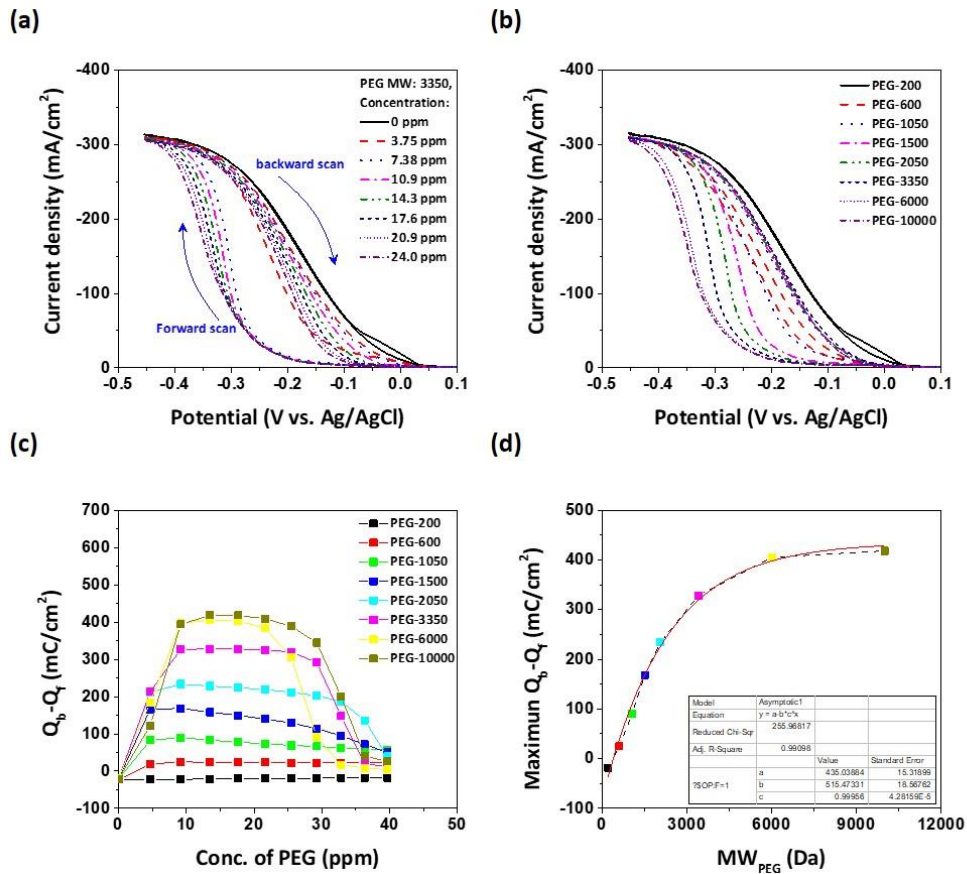


Fig. 2.4. Method of the MW_{PEG} by CVS analysis. Cyclic voltammogram for the Cu plating bath between -0.45 V and 0.1 V for different (a) C_{PEG} and (b) MW_{PEG} . The differences in the charge density between forward (Q_f) and backward (Q_b) scans for different C_{PEG} and MW_{PEG} are shown in (c). Calibration curve of the maximum value of ($Q_f - Q_b$) vs. a function of MW_{PEG} is shown in (d).

2.3. Spectroscopy analysis

A pretreatment process (solution extraction) is required to spectroscopically measure the additive contained in the Cu electrodeposition solution. The pretreatment process, as shown in the **Fig. 2.5**, is as follows.

- (1) Sampling: Draw off 100 mL the aging solution to be measured, and add an internal standard saccharin to 50 μM
- (2) Neutralization (#1): In order to minimize H^+ ion and OH^- ion of the aging solution and remove Cu^{2+} ions into CuOH sedimentation, 8 M KOH is added to the aging sample solution until pH reaches 7.
- (3) Precipitation (#2): In order to remove SO_4^{2-} ion contained in the neutralized solution, add to ethanol (EtOH) to lower the solubility and precipitate CuOH and K_2SO_4 , respectively.
- (4) Centrifugation (#3): Centrifuge for 10 minutes at 10,000 rpm to separate the precipitated CuOH and K_2SO_4 from the solution.
- (5) Filtration (#4): Unfiltered impurities in the solution are removed using a Polytetrafluoroethylene (PTFE) filter.
- (6) Evaporation (#5): EtOH (45°C) and H_2O (55°C) are evaporated using a vacuum

pump and chiller.

(7) Dissolution: Dissolve the remaining residue by adding D₂O for the NMR sample, and dihydroxybenzoic acid (DHB) for the MALDI-TOF sample.

Pretreated samples were analyzed using by ¹H-, ¹³C-NMR (600 MHz, Avance 600 FT-NMR, Bruker), MALDI-TOF (Voyager-DETM, Applied Biosystems Inc.) analysis of the additives contained in the sample and by-products of the additives. A qualitative and quantitative investigation was carried out using an internal standard material, which was performed by normalizing β-SPS (2.83 ppm) and α-PDS (3.00 ppm) peaks with saccharin (7.83, 7.89 ppm) in NMR data.

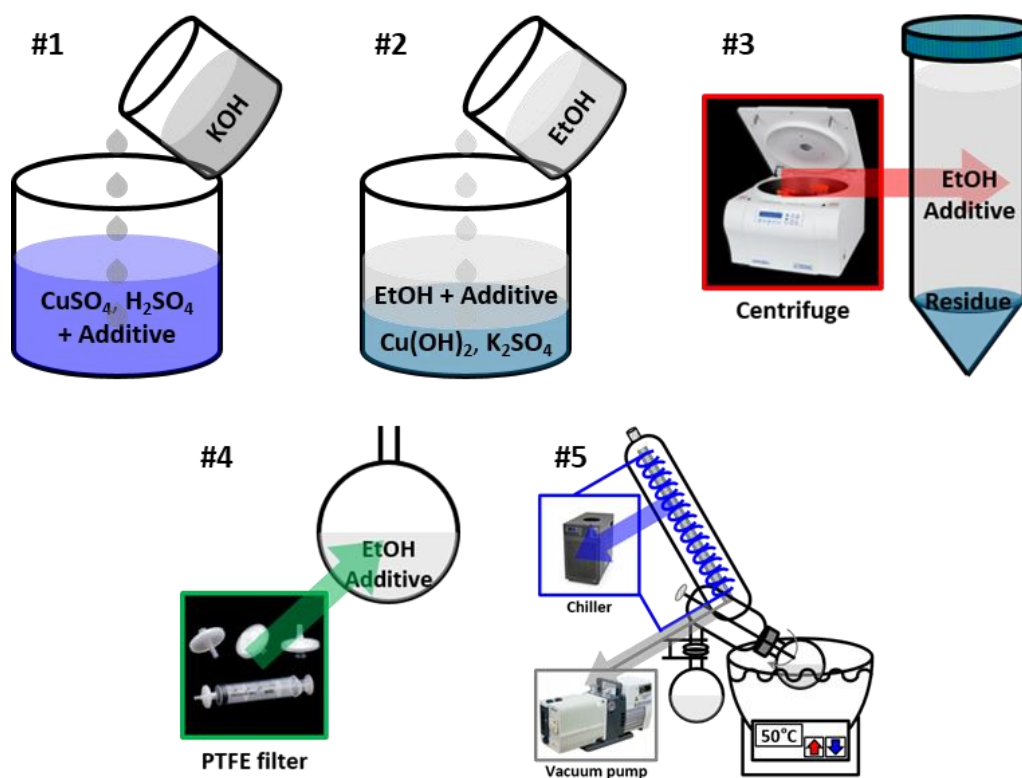


Fig. 2.5. Pretreatment of sample for spectroscopy analysis (MALDI-TOF, NMR).

2.4. Filling performance

To confirmed the effect of formaldehyde (HCHO) on the decomposition of SPS in Cu electrodeposition, the micro-via filling performance was conducted in a 3-additive system (100 μ M PEG-1500 (suppressor), 100 μ M NH_4Br (leveler)). Filling base solution consisted of 0.93 M CuSO_4 , 0.43 M H_2SO_4 , 0.82 mM HCl, which were optimized to fill the PCB substrate in the laboratory, and 1.5 L electrolyte was added to the cell as shown in **Fig. 2.6**. It was carried out in a 2-electrode system, patterned PCB substrate (Samsung Electro-Mechanics Co. Ltd.) having a size of $2.1 \times 2.2 \text{ cm}^2$ was used as the working electrode. Through laser drilling, the micro-via had a thickness of 130 μ m at the top, 100 μ m at the bottom, and a depth of 100 μ m. One unit of the substrate has approximately 1,750 micro-vias, and the average distance of via was 300 μ m. The surface of the substrate increased the adhesion by forming a Cu seed (3 μ m) through the desmear process. Ir/IrO_x on Ti/TiO_x was used as the counter electrode, and the upper part of the electrode was opened and covered with a proton-conducting Nafion membrane to remove oxygen generated during Cu electrodeposition. The electrolyte of PCB filling was injected from a nozzle installed in the bath, where the nozzle pressure was maintained at 49.03 kPa. The current density was 15 mA/cm² applied for 90 minutes.

The micro-via of the Cu electro-deposited substrate was embedded in acrylic resin, and then physically ground using silicon carbide abrasive disks (P240, P600, P1200, P4000), polycrystalline diamond suspension (average diameter: 1 μm), and colloidal silica (average diameter: 50 nm), sequentially. Finally, the cross section image of PCB micro-via was confirmed using an optical microscope (ICS-306B, SOMETECH).

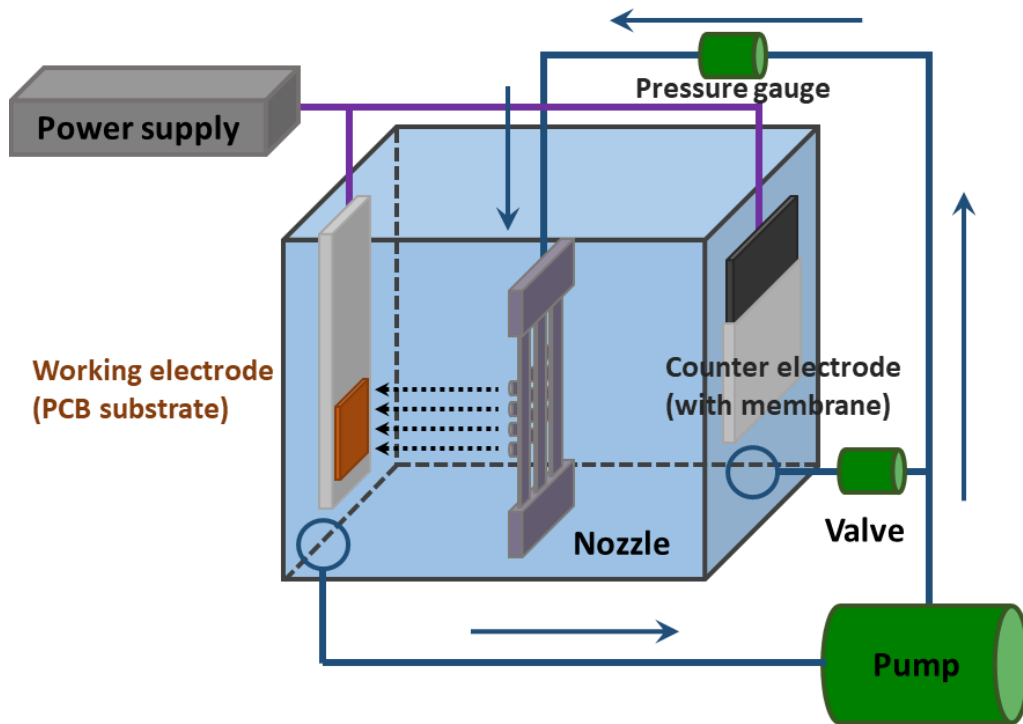


Fig. 2.6. Schematic diagram of flow cell for Cu micro-via filling.

CHAPTER III

Results and Discussion

3.1. Mechanism of SPS decomposition

The decomposition of SPS has been studied in our group. In particular, a method for confirming the effect of by-products through NMR analysis and monitoring the concentration of SPS was also suggested. While the decomposition reaction and by-products in the full cell were confirmed, the correct decomposition reaction in each electrode solution has not been obtained. Therefore, been done by dividing a catholyte and anolyte by a proton-conducting membrane into three conditions; open-circuit, short-circuit, and electrolysis. In addition, by removing dissolved oxygen in the solution, the effect of oxygen on the additive was investigated. The effect of active-radical was also examine using H_2O_2 to conduct an in-depth study of the decomposition reaction of SPS. Finally, the factors and mechanism of SPS decomposition were identified by NMR.

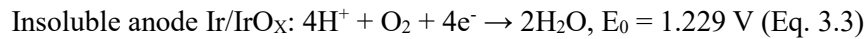
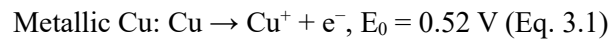
3.1.1. Measurement of C_{SPS} by CVS

First, the decomposition concentration of SPS was measured as sampled under open-circuit conditions using the CVS method. As shown in **Fig. 3.1**, the SPS concentration at the Cu cathode decreased, while that at the Ir/IrO_x insoluble anode was unchanged during 10 h aging process. It has been reported that the open-circuit decomposition of SPS at the Cu electrode surface is initiated by a Cu⁺ ion formed by Cu corrosion as well as by a disproportionation reaction in Eqs. 1.6~7.¹¹⁵⁻¹¹⁷ As mentioned earlier, Cu⁺ ions form Cu(I)thiolate through various reactions with SPS in solution Eqs. 1.10~11. The formed MPS and Cu(I)MPS⁻ undergo an additional oxidation reaction in an oxygen atmosphere. Therefore, the concentration of SPS gradually decreases with time in the reducing solution. According to Healy et al., it is suggested that SPS is oxidized to form an S-product, that is, PDS.¹⁰⁰ Since there is no metallic Cu in the oxidizing solution, Cu⁺ ions could not be formed, so that SPS could remain stable without decomposition. In addition, when an additional reaction was performed for 3 days after sampling, SPS degradation occurred as much as 16.79 μM after 10 hours of decomposition, is because Cu(I)MPS⁻ present in the solution for 3 days was further oxidized by Cu⁺ ion.

For the short-circuit in **Fig. 3.2**, the SPS decomposed at both the Cu plate (Cu) and the Ir/IrO_x (insoluble anode) with similar rates in as sampled and sampling after 3 days. In particular, when comparing the conditions of decomposition for 10 hours, the

condition after 3 days was further decomposed by 16.62 μM . This means that the decomposition of SPS occurred by Cu^+ ion even in the oxidizing electrode solution. To understand that Cu^+ ion was formed in the anolyte, galvanometric was measured using a multi-meter. As shown in **Fig. 3.3**, the current density was measured by sequentially addition metallic Cu, chloride, and additives in Cu plate and Ir/IrO_x plate solution with closed-loop. As a result of the measurement, in the absence of CuSO_4 , it was observed that electrons flow from metallic Cu to the insoluble electrode by 0.027 mA/cm^2 . This is because metallic Cu formed Cu ions according to the following reactions (Eqs. 3.1~3.3) by corrosion by strong acidic solution. When CuSO_4 first put in the catholyte, the current density changes in the negative direction, but it is recovered soon in **Fig. 3.3(a)**. Then, when CuSO_4 entered the anolyte, the current density increased to 0.113 mA/cm^2 . This is because a disproportionation reaction was formed near metallic Cu, was used a cathode, which made an electron moved to the Ir/IrO_x plate through the electric line. Conversely, an insoluble electrode, an anode, received electrons and reacts with Cu^{2+} ions to form Cu^+ ions in Eqs. 3.1~3.3. When NaCl was added to both electrode, the current density slightly increased to 0.127 mA/cm^2 , because the intermediate (Cu^+) stabilized as it formed into CuCl. The galvanometric experiment was carried out again to check the effect of changing of the addition order in **Fig. 3.3(b)**. First, in order to grasp the effect

of mass transfer, when increasing from 0 rpm to 300 rpm, 0.018 mA/cm^2 slightly increased to 0.025 mA/cm^2 . Then, addition CuSO_4 in the first to anolyte led to the increasing of current density significantly to 0.183 mA/cm^2 because of the disproportionation reaction. When Cu^{2+} ion was added to the catholyte, the current density decreased to 0.120 mA/cm^2 , possibly because disproportionation reaction additionally took place at the interface between Cu electrode and the catholyte as well as between the Ir/IrO_x plate to Cu plate. The addition of Cl^- ion and other additives slightly changed the current density, due to the Cu^+ formation by CuCl . Therefore, the current density formed in the short-circuit is the main factor owing to the disproportionation reaction that formed Cu^+ ion in a both electrolyte containing Cu^{2+} ion.



The concentration of SPS at catholyte and anolyte during electrolysis condition were shown in **Fig. 3.4**. Under the electrolysis, the SPS more rapidly degraded at the Ir/IrO_x plate bath than at the Cu plate bath because the electrochemical reaction (Eq. 1.5)

occurred. Especially, from **Table 3.1**, when the current density increased from 10 mA/cm² to 30 mA/cm², the decomposition of SPS occurred more rapidly at a rate of -17.232 μM/h to -24.394 μM/h in anolyte. On the other hand, it could be seen that the concentration of SPS decreased at a decomposition rate of about -2 μM/h under the three current density conditions in the catholyte, indicating that the decomposition was mainly caused by a chemical pathway rather than by an electrochemical pathway.

3.1.2. Analyzing the SPS decomposition by spectroscopy analysis

In order to clearly examine the degradation products, samples for as sampled and after 3 days' decomposition were measured using ¹H-NMR. In the presence of SPS, three characteristic peaks were observed at 2.12 ppm (-CH₂-), 2.83 ppm (-CH₂S-S), and 3.00 ppm (-CH₂SO₃⁻) in **Fig. 3.5(a)**. As a result of measuring the integrate area of peak, 3.00 ppm was calculated as 3.81, 2.83 ppm was 3.71, and 2.12 ppm was 4.45. After 5 hours' decomposition under the open-circuit condition, as sampled the peak intensity at 2.85 ppm decreased, while that at 3.00 ppm increased, indicating the oxidation of thiol or disulfide functional group to sulfonate. Note that the characteristic peaks of MPS (-CH₂S⁻) and Cu(I)MPS (-CH₂S-Cu⁺) were not analyzed by ¹H-NMR, because it was all

reduced to SPS during the pH titration process, of pretreatment for NMR analysis. When the sample was measured 3 days after decomposition, the peak area of 2.83 ppm decreased further to 0.23 and 3.00 ppm increased to 5.95. This was because almost all of the S-S functional groups are decomposed and most of them were oxidized to SO_3^- terminal group, resulting in PDS.

Fig. 3.5(b) showed the concentrations of SPS and PDS at each stage obtained from CVS and NMR measurements. Right after the aging experiment, the SPS concentration of as sampled condition was measured 34.67 μM from initial 50.18 μM , which implies that about 69% of the accelerator species (SPS, MPS, and Cu(I)MPS^-) remained in the bath. However, only 3.02 μM SPS remained after aging for 3 days after the experiment despite the absence of metallic Cu. On the other hand, the concentration of PDS was increased with aging. The results of comparing the concentration of SPS through CVS and $^1\text{H-NMR}$ are shown in **Fig. 3.5(c)**. As a result of comparison, the SPS concentration was similarly measured by CVS and NMR analysis.

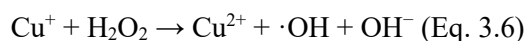
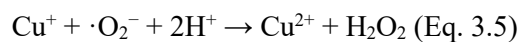
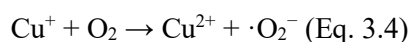
3.1.3. Verification of SPS decomposition factor

Based on the Figs. 3.1~3.5, the consumption rate of SPS under three condition; open-

circuit, short-circuit, and electrolysis (10, 20, and 30 mA/cm²) at both electrode was evaluated in **Fig. 3.6(a)**. In the catholyte, the SPS consumption rates were in the range from 1.20 to 1.39 μM/h under non-electrolytic conditions. Consumption rate increased to 2.23 μM/h when applying the current density of 20 mA/cm², possibly because of the incorporation of accelerator species into the growing Cu film and formation of Cu⁺ ion on deposited Cu surface during the Cu reduction.^{85, 118-120} In the anolyte, the consumption rate was nearly 0 μM/h under the open-circuit condition, but it increased to 0.98 μM/h when a short-circuit was formed, by the reaction of Cu⁺ ion. Under the electrolysis condition, the consumption rate further increased, up to 21.28 μM/h, due to the anodic oxidation reaction. At the re-measurement of concentration for 3 days later, the apparent consumption rate increased when the SPS decomposition was caused by the Cu⁺ ion (condition #1~#5). When the decomposition was caused by anodic oxidation, no further consumption was observed.

In order to investigate the oxygen effect on the SPS decomposition, dissolved oxygen in the electrolyte was removed by N₂ purging. As shown in the **Fig. 3.7**, initial sample #1 was measured as 49.19 μM, and the decomposition for 3 days with eliminating the dissolved O₂ by N₂ purging #2 was measured as 48.62 μM with little decomposition. On the other hand, it was confirmed that the decomposition for 3 days in the air was

completely processed to 0.25 μM . Therefore, the decomposition of SPS might result from the reactive Cu^+ ion, which led to the formation of the reactive O_2 species via the reaction of Eqs. 3.4~3.8.¹²¹⁻¹²⁶



The Cu^+ ion, which is continuously generated by corrosion and disproportionation reactions (Eqs. 1.6~1.7), reacted with dissolved O_2 in accordance with reactions (Eqs. 3.4~3.8) to form reactive oxygen ($\cdot\text{O}_2^-$), hydrogen peroxide (H_2O_2), or free radical of hydroxides ($\cdot\text{OH}$), respectively. The free radical led the decomposition of Cu(I)MPS^- to PDS. Cu^+ ions acted as a catalyst to form free-radicals, which helped to form the Cu(I)MPS^- . Regarding this issue, Brennan et al. presented that the most of MPS was converted to SPS and PDS in the presence of Cu^{2+} and O_2 within 24 hours, while it was metastable in Cu^{2+} -free condition. They suggested that this might be associated with the

interaction of Cu^+ with O_2 , which played a critical role in partitioning between MPS $^-$ dimerization to SPS^{2-} or to SPS^{2-} -sulfone to disulfone that may result in PDS generation.¹²⁷ Healy's et al. and Frank's et al. Presented that the voltammetry of aged Cu solution depended on O_2 contents in bath, indicating that dissolved O_2 is concerned with SPS decomposition reaction.^{95, 100} D'Urzo et al. and Koh et al. also showed that the concentration of SPS did not decrease when O_2 was not present, using ion chromatography and mass spectroscopy analysis.^{94, 96} Based on our results as well as previous works, it could be concluded that both Cu^+ and dissolved O_2 played critical roles on SPS decomposition, in a way such as forming $\cdot\text{O}_2^-$, H_2O_2 , $\cdot\text{OH}$.

In addition, in order to check the effect of hydroxyl radical formed in the electrolyte, it was confirmed whether decomposition of SPS occurred when H_2O_2 or Cu^{2+} source was directly added to form $\cdot\text{OH}$ in the solution by NMR analysis. As shown in the **Fig. 3.8**, there was no decomposition of SPS without H_2O_2 and with Cu^{2+} , which meant that the decomposition factor did not exist in the Cu electrodeposition bath. On the other hand, with H_2O_2 condition, SPS was decomposed as 0 μM with Cu^{2+} ion and as 24.96 μM without Cu^{2+} ion. When H_2O_2 and Cu^{2+} ions were present in the solution, more decomposition of SPS occurred due to the additional formation of $\cdot\text{OH}$ by Eqs. 3.5~3.6.

So, to summarize, as shown in **Fig. 3.9**, Cu^+ ion was sequentially formed by metallic

Cu with disproportionation reaction in the solution. After that, $\cdot\text{OH}$ was formed as it was oxidized by dissolved O_2 , and free-radicals cut the S-S and S-H bond of organic additives, and finally formed PDS.

Table 3.1. Rate of SPS Breakdown under Electrolytic Conditions

	Current density (mA/cm²)	Slope (μM/h)	Intercept (μM)	R-square
Cu plate	10	-2.0717	50.144	0.9942
	20	-2.2536	49.855	0.9704
	30	-1.9223	48.939	0.985
Ir/IrO_x plate	10	-17.232	48.703	0.9777
	20	-21.283	49.708	1
	30	-24.394	47.317	0.9764

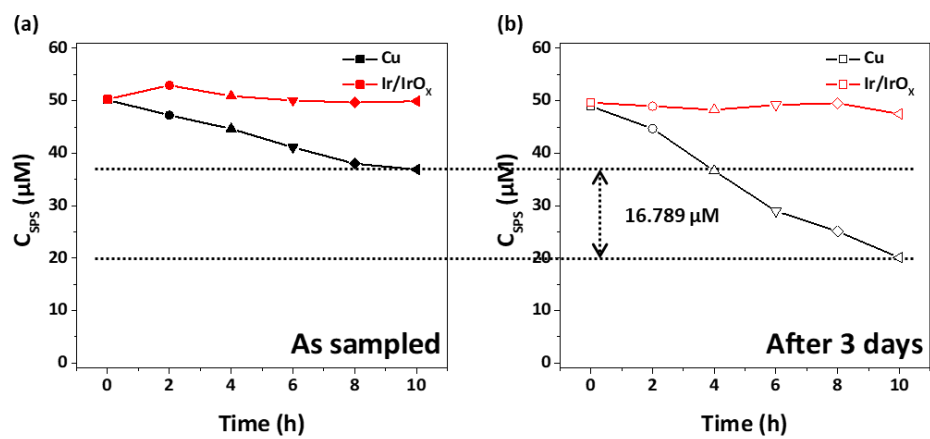


Fig. 3.1. Concentration of SPS measured by CVS during the aging experiment under the open-circuit. The measurements were carried out twice, (a) as sampled the aging experiment and (b) after 3 days later.

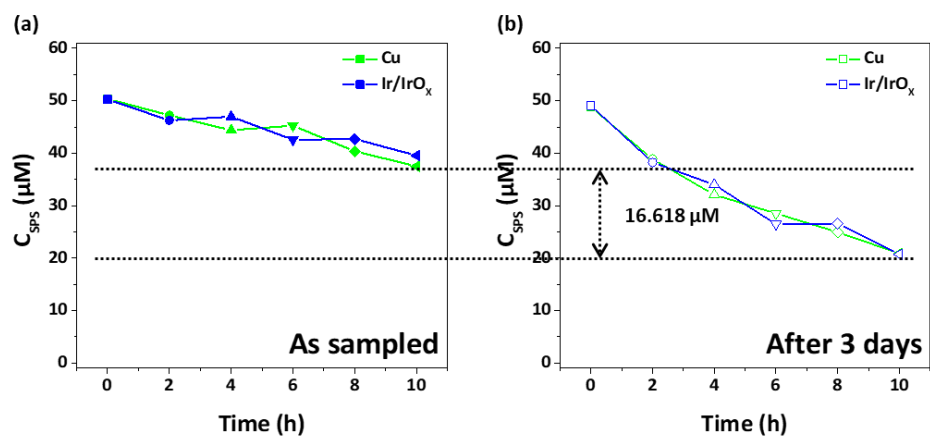


Fig. 3.2. Concentration of SPS measured by CVS during the aging experiment under the short-circuit. The measurements were carried out twice, (a) as sampled the aging experiment and (b) after 3 days later.

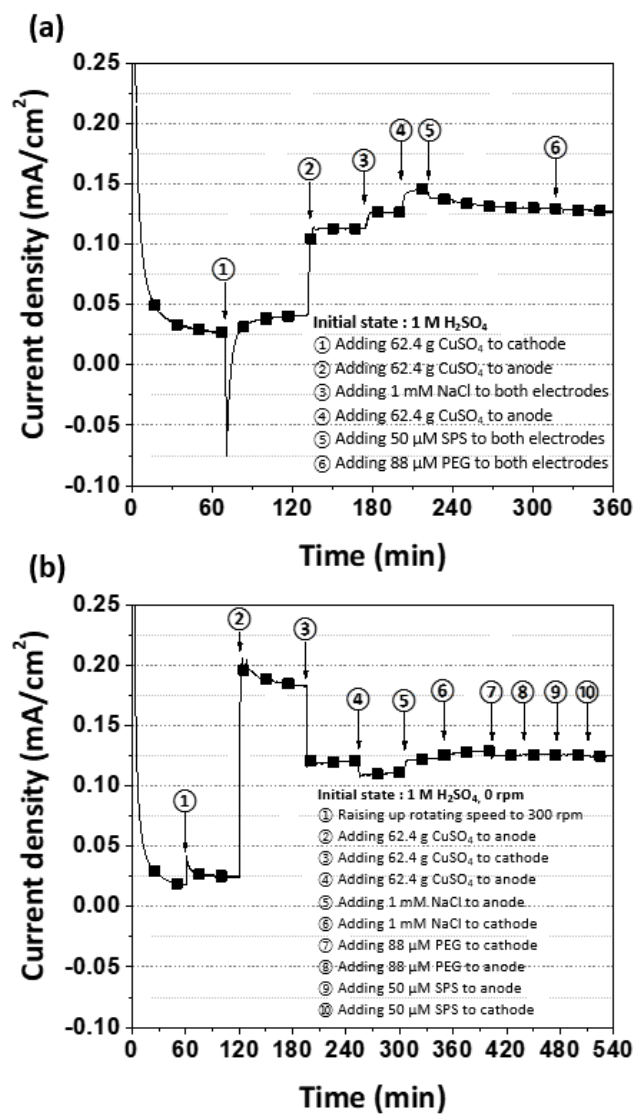


Fig. 3.3. Measurement of current flow under the short-circuit by multi-meter with two different addition sequences. Input the materials in the (a) Cu plate to Ir/IrO_x plate, (b) Ir/IrO_x plate to Cu plate.

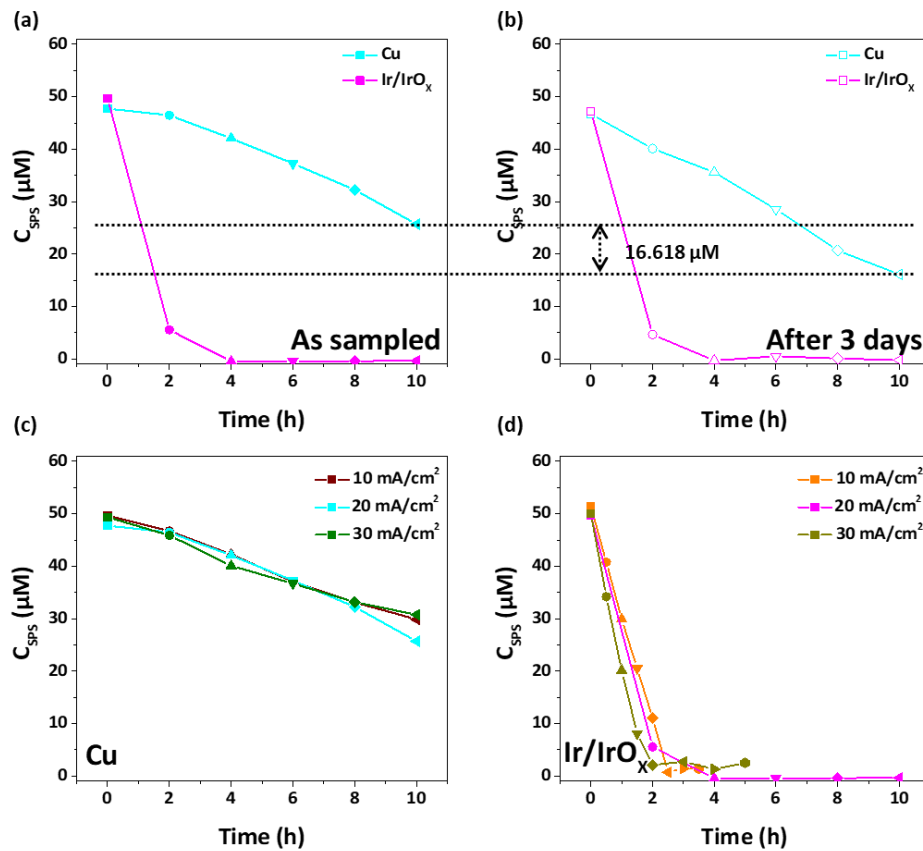


Fig. 3.4. Concentration of SPS measured by CVS during the aging experiment under the electrolysis condition (20 mA/cm^2). The measurements were carried out twice, (a) as sampled the aging experiment and (b) after 3 days later. The effects of the current density on the breakdown rate are shown in (c) and (d), respectively.

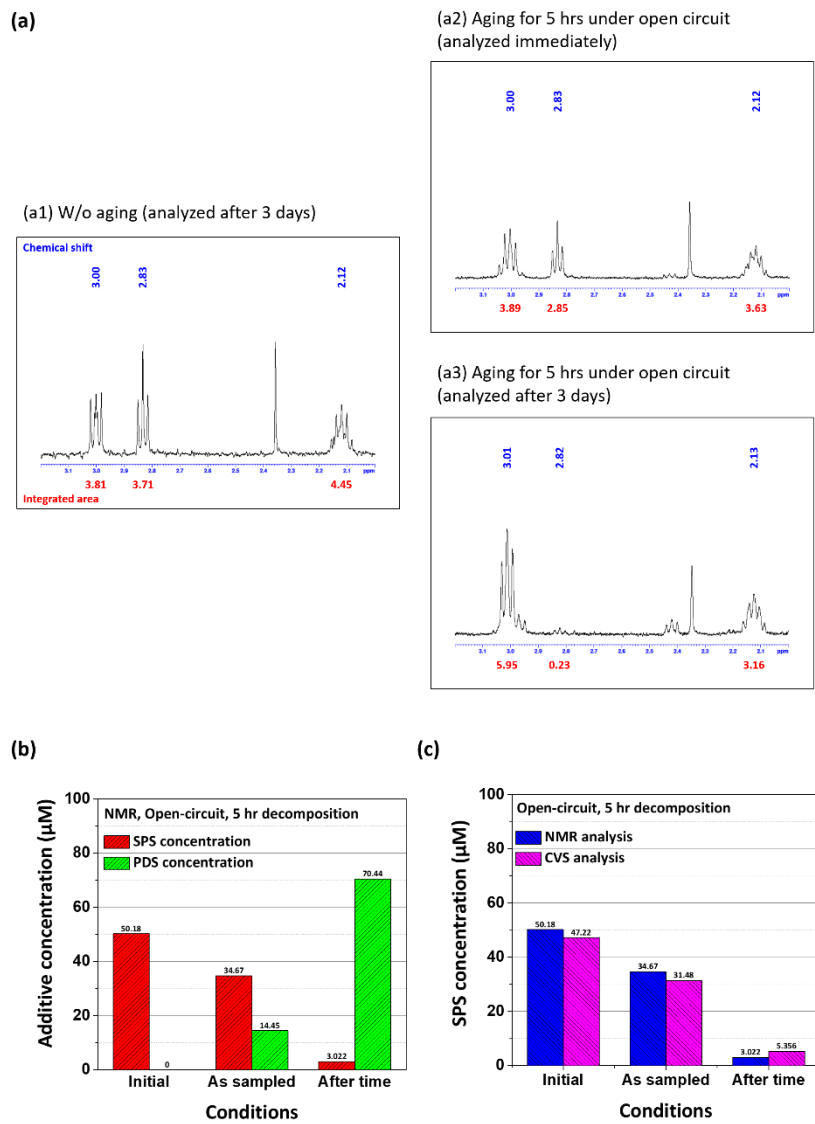


Fig. 3.5. (a) ^1H -NMR spectrum of accelerator species obtained from electrolytes (a1) without aging, (a2) with aging for 5 h under the open-circuit, and (a3) 3 days later. Concentration of accelerator species analyzed are presented at (b) SPS and PDS concentration by ^1H -NMR and (c) SPS concentration by ^1H -NMR and CVS, respectively.

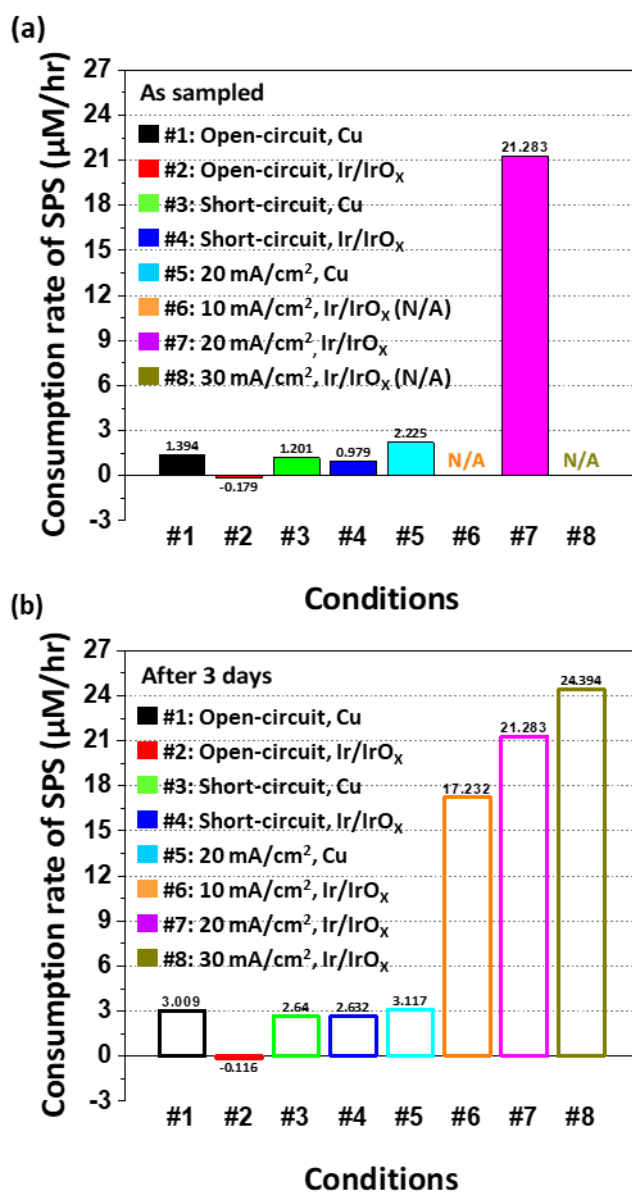


Fig. 3.6. Consumption rates of SPS at electrodes under various conditions measured (a) immediately and (b) 3 days later.

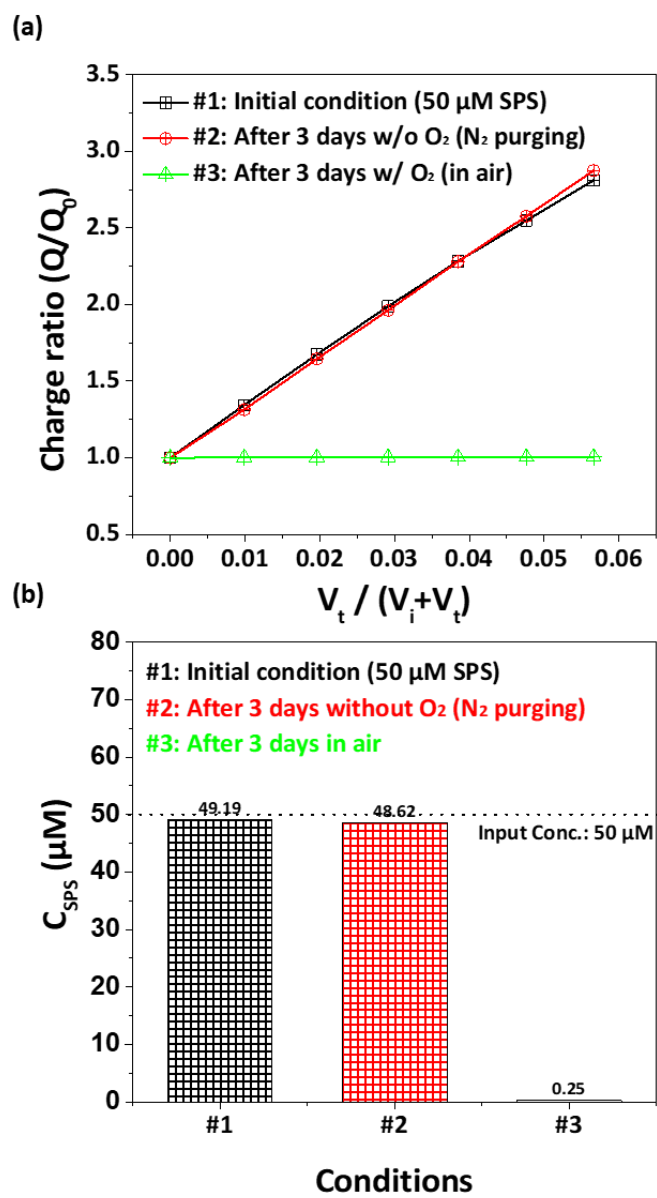


Fig. 3.7. The concentrations of SPS by CVS after aging for 3 days under open-circuit w/ and w/o N_2 purging (a) raw data and (b) C_{SPS} .

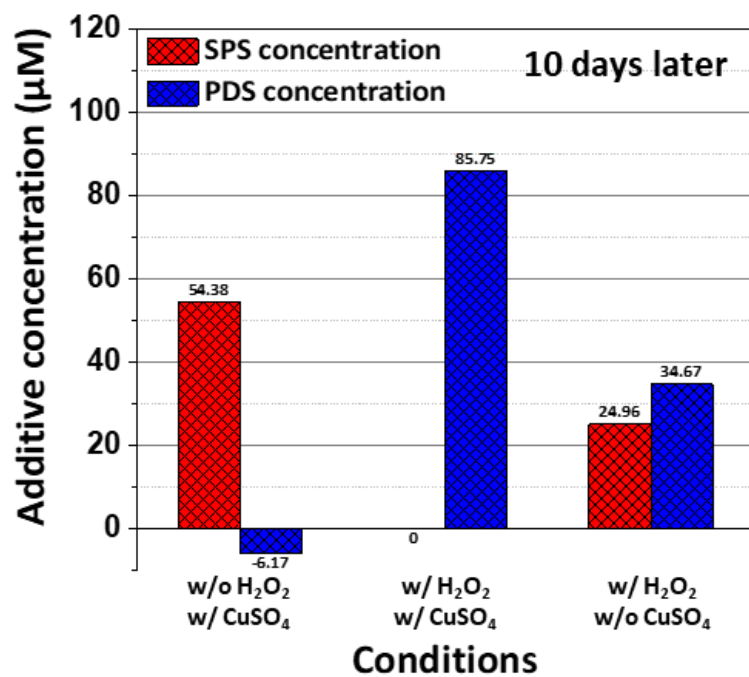


Fig. 3.8. The concentrations of additives by NMR w/ and w/o Cu²⁺ and H₂O₂ after aging for 10 days.

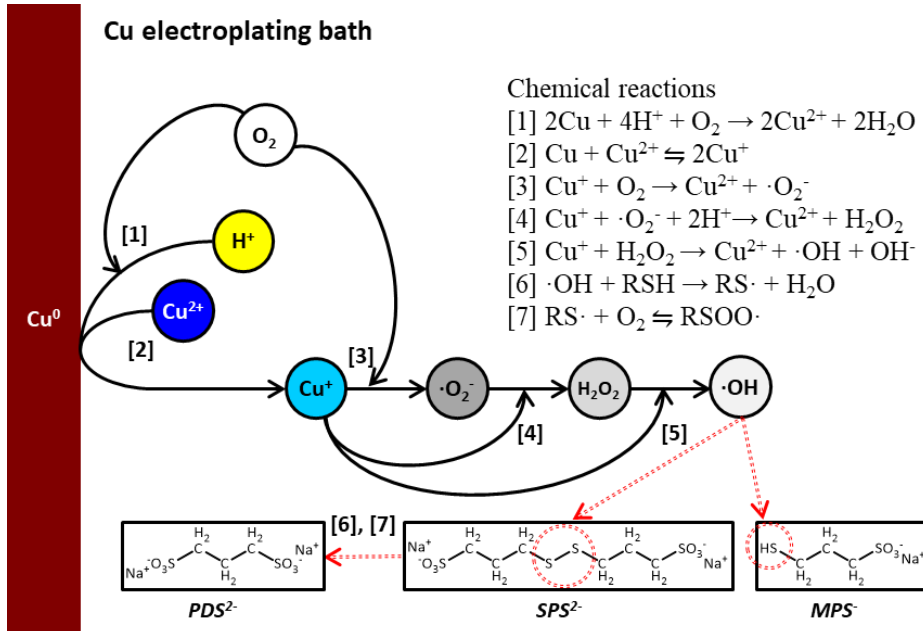


Fig. 3.9. Schematic diagram of the SPS chemical decomposition reactions.

3.2. Mechanism of PEG decomposition

The decomposition of PEG has been studied in our group. In particular, MALDI-TOF, NMR, and gel permeation chromatography (GPC) analysis have been done to investigate the decrease of by-products and molecular weight of PEG. In addition, a method for monitoring the average molecular weight of PEG using CVS was introduced by Choe et al.¹¹⁰ However, the only decomposition reaction and products in the full cell was studied, but the correct decomposition reaction in each electrode solution has not been done. Therefore, the electrolyte was separated into catholyte and anolyte using a proton-conductive membrane into three conditions; open-circuit, short-circuit, and electrolyte. In addition, by removing dissolved oxygen in the solution, the effect of oxygen on the additive was investigated. Finally, the factors and mechanism of PEG decomposition were identified by MALDI-TOF and NMR analysis.

3.2.1. Measurement of MW_{PEG} by CVS

MW_{PEG} was analyzed in order to elucidate the mechanism of PEG decomposition under open-circuit, short-circuit, and electrolysis (30, 40, and 50 mA/cm²) conditions.

First, the breakdown of PEG was examined in the open-circuit conditions. As shown in the **Fig. 3.10**, in the catholyte, the maximum Q_b - Q_f value decreased from 327.4 to 136.9 mC/cm^2 after 48 h aging time, corresponding to the MW_{PEG} values of 3494.15 Da and 1226.45 Da, respectively, whereas in the anolyte, little change in MW_{PEG} was observed for 48 h, from 3528.9 Da to 3286.4 Da, which implied that the PEG was stable in the acidic Cu electrolyte in the absence of the metallic Cu. When the Cu metal was contacted with an acidic bath, the reactions denoted in Eqs. 1.6~1.7 occurred, resulting in the formation of Cu^+ . In addition, if there were no surface sites to which PEG could be adsorbed, PEG would not be decomposed in a Cu electrolytic solution.

Under the short-circuit condition, MW_{PEG} decreased in both electrolytes at nearly same rates (**Fig. 3.11**). Especially, after 48 hour of aging experiment, the MW_{PEG} was measured 975.6 and 988.9 Da in the catholyte and anolyte, respectively. In the short-circuit condition, as in the decomposition of SPS, Cu^+ ion was formed at both electrodes, which occurred through Eqs. 3.1~3.2. The galvanic current density between the Cu plate and Ir/IrO_x plate was 0.127 mA/cm^2 , in good agreement with our previous study. Assuming that all of the electrons were consumed in the reactions denoted using Eqs. 3.1~3.2, the rate of Cu^+ formation at the Ir/IrO_x was estimated to be 13.16 $\mu\text{mol}/\text{s}\cdot\text{m}^2$.

The results for the decrease in MW_{PEG} under the electrolysis condition (30, 40, and 50

mA/cm²) were shown in **Fig. 3.12**. MW_{PEG} decreased more rapidly at the catholyte than at the anolyte at all current densities. It was also found that the current density had almost no influence on the rate of the PEG decomposition in both electrolyte, implying that the decomposition of PEG did not follow a direct electrochemical reaction that involved electron transfer. Rather, PEG degradation appeared to be closely related to active radicals such as $\cdot\text{OH}$.

3.2.2. Analyzing the PEG decomposition by spectroscopy analysis

MALDI-TOF and ¹H-NMR analysis were conducted for representative samples (under 30 mA/cm² electrolysis condition) for a detailed examination of the breakdown byproducts of PEG and cross-checking to compare the CVS results. Using MALDI-TOF analysis, MW_{PEG} was calculated using the following Eq. 3.9, where N_i : number of molecules, M_i : molecular weight.

$$M_n = \frac{\sum N_i M_i}{\sum N_i} \text{ (Eq. 3.9)}$$

As depicted in **Fig. 3.13**, PEG molecular weight distribution changed due to aging

process. Prior to aging, a symmetric PEG molecular weight distribution with a peak at approximately 3350 m/z was observed for both electrolytes. As the aging progressed, the population of the low molecular weight of PEG in the 400~2500 m/z range gradually increased. After 48 h, the MW_{PEG} became bimodal, with a broad peak at approximately 1000 m/z and a peak of initial PEG at 3350 m/z. the MW_{PEG} values obtained by CVS and MALDI-TOF were similar, confirming the accuracy of the CVS analysis in **Fig. 3.14**. However, because of the matrix material of MALDI-TOF, it was difficult to measure a small molecular weight of PEG under 300 m/z or less. In addition, with the CVS analysis, it was not affordable to measure the MW_{PEG} because the small molecular weight of PEG under 200 Da or less had a relatively small inhibitory effect. Therefore, it could be similarly measured MALDI-TOF and CVS.

The structure of the PEG decomposition products in the fresh and aged baths was examined via $^1\text{H-NMR}$ analysis. Saccharin with the chemical shifts of 7.82 and 7.89 ppm was used as the internal standard to correct the chemical shift of the analyte, which varied with pH. As presented in **Fig. 3.15(a)**, black line was the pristine result, peaks at 3.70 ppm and 4.80 ppm were observed for the pure PEG-3350 that dissolved in D_2O . These peaks were assigned to $-\text{CH}_2-\text{O}$ and $-\text{OH}$, respectively. The PEG in the fresh Cu electrodeposition bath that was preliminarily extracted by pretreatment steps showed the

peaks of pure PEG (3.70, 4.80 ppm), and some minor peaks at 1.04, 1.17, 1.28, 1.90, and 2.17 ppm (propyl group, ethyl ether, ketone, unassigned, respectively). Unassigned minor peak may be related to the impurities in the electrodeposition bath and the breakdown products of PEG removed during the sample extraction.¹²⁸⁻¹³² In **Fig. 3.15(b)~(d)**, ¹H-NMR spectra of PEG in three aged baths conditions; open-circuit, short-circuit, and electrolysis was presented. After decomposition of PEG in open-circuit condition, the PEG byproducts at the Ir/IrO_x did not show any additional chemical shift peaks, indicating the absence of chemical decomposition. For other cases, new peaks were formed at the chemical shifts close to 6.43, 8.47, 9.26, and 9.67 ppm and were assigned to aldehyde (9.26 and 9.67 ppm), formic ester (8.47 ppm), and vinyl groups (6.43 ppm).^{88, 107, 133, 134}

3.2.3. Verification of PEG decomposition factor

Based on **Figs. 3.10–3.12**, the values of MW_{PEG} obtained after aging was carried out for 48 h in various conditions; open-circuit, short-circuit, and electrolysis were compared in **Fig. 3.16**. The initial MW_{PEG} was nearly measured 3350 Da. Under open-circuit condition, MW_{PEG} decreased to 1226.4 Da (#1) in catholyte, and changed only slightly 3286.4 Da (#2) in anolyte. The MW_{PEG} values in short-circuit condition were observed to be 975.6 Da (#3) and 988.9 Da (#4) at Cu plate and Ir/IrO_x plate baths, respectively. This is because, like the Cu electrodeposition of SPS, Cu⁺ ion was formed in the electrolyte by corrosion (Eq. 1.6) and disproportionation (Eq. 1.7) reactions, and Cu⁺ ion and dissolved oxygen react to form active radical ($\cdot\text{OH}$). Subsequently, the formed active radical in the Cu electrodeposition bath with metallic Cu broke the C-O bond of PEG. Under the electrolysis conditions, for the current densities of 30, 40, and 50 mA/cm², the MW_{PEG} values in catholyte were close to 2500 Da (2470.7 at 30 mA/cm² (#5), 2437.3 at 40 mA/cm² (#7), and 2515.84 in 50 mA/cm² (#9)). MW_{PEG} values in anolyte were 1728.7 (#6), 1462.5 (#8), and 1480.0 (#10) Da, respectively, indicating that the amount of decomposed PEG was nearly independent of the applied current densities at both electrodes. A comparison between the MW_{PEG} values obtained in the catholyte showed

that PEG decomposition occurred more rapidly under open-circuit condition than under the electrolysis condition in which the Cu^+ ion was reduced to metallic Cu on the cathode, contributing to the lesser extent of the formation of the Cu^+ ion in the electrolysis conditions than in the open-circuit conditions.

Fig. 3.17 showed the ratio of -OH/-CH₂-O for various aging conditions by ¹H-NMR analysis. The -OH/-CH₂-O ratio of the pristine PEG was obtained as 0.968. With pretreatment, the ratio of -OH/-CH₂-O increased to 1.219, possibly due to residue of H₂O molecular after evaporation step. For the cases where Cu^+ ion was involved (#3, #5, #6, #7, #9, #11) the intensity ratio of -OH/-CH₂-O increased to 1.67~2.29, indicative of the breakdown of -CH₂-O bond. In contrary, for anodic conditions (#8, #10, #12), the intensity ratio of -OH/-CH₂-O decreased to 0.621~0.752. That meant that the further oxidation of molecular terminal to aldehyde, formic ester, and vinyl groups became more dominant, which was possibly due to the higher concentration of ·OH during electrolysis.

Previous studies have indicated that hydroxyl radicals initiate the decomposition of PEG, that is, these active radicals break the C-O bond in PEG.¹³⁵⁻¹³⁸ Considering the results presented in **Fig. 3.10** and the previous data in SPS decomposition, it was concluded that PEG spontaneously decomposed when the metallic Cu was contacted by the bath, most likely due to the presence of the Cu^+ ion by disproportionation reaction.

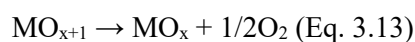
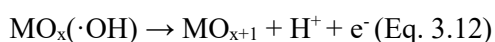
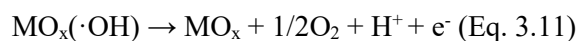
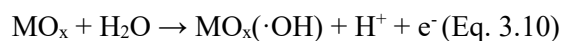
Fig. 3.18 presents MW_{PEG} measured by CVS after open-circuit aging for 48 h with and without N_2 purging to check the oxygen effect in the PEG decomposition. In the presence of O_2 (in air), the MW_{PEG} decreased to 988.2 Da after open-circuit aging for 48 h. However, under de-aeration, MW_{PEG} decreased to 1764.7 Da in Fig. 3.19(b), which indicated that the PEG degradation possible, took place even in the absence of O_2 .

PEG was stable in electrodeposition bath where there was no decomposition source like metallic Cu or current flowing etc. Also in our study, PEG did not decompose for 48 h in anolyte under the open-circuit aging in **Fig. 3.10(c)**. That is, the reactive Cu^+ ion should be involved in decomposition pathway in anyway. The contact of metallic Cu and Cu^{2+} produced the reactive Cu^+ ion on the solution. Considering equilibrium constant ($K=6.757 \times 10^{-7}$ M), the Cu^+ ion concentration in 0.25 M CuSO_4 should be 0.41 mM.¹³⁹ However, as suggested by many papers the oxidation of Cu^+ by dissolved oxygen in the Eq. 3.4 is very instantaneous, so that the actual concentration of Cu^+ is quite low.^{140, 141} In the case of de-aerating the electrolyte where the concentration of Cu^+ ion is supposed to be high, the PEG molecules is still formed to be slightly decomposed. It could be suggested the PEG would be decomposed, following the different path like direct Cu^+ ion reaction.

Comparing to breakdown products by the $^1\text{H-NMR}$ analysis with and without N_2

purging, byproducts (aldehyde, formic ester, and vinyl groups) were formed after aging PEG with dissolved O₂ in Fig. 3.19(a). However, under de-aeration, both HO- and its further oxidized forms like aldehyde and vinyl groups were not clearly detected. In addition, the intensity ratio of -OH/-CH₂-O clearly increased from 1.22 to 1.83 in Fig. 3.19(b), which implied that the breakdown of -CH₂-O to -H₂-OH + HO-, or -CH₃ + HO-. It could be thought that the breakdown pathway under de-aerated condition is totally different to that under conventional condition.

Meanwhile, at the Ir/IrOX plate, the ·OH was also generated during water splitting via the reactions denoted using Eqs. 3.10~3.13.^{142, 143}



Won et al. also insisted that ·OH radical could be created at the anode by Cl⁻ that acted to carry out the hypochlorite formation reaction. To examine the effect of the Cl⁻ ion, aging under electrolysis conditions (30 mA/cm²) was also carried out in the absence of

the Cl⁻ ion with the results shown in **Fig. 3.20**. It is observed from **Fig. 3.20(a)** that MW_{PEG} was unchanged in catholyte for 48 h; this was due to the low stability of Cu⁺ ion in the aqueous conditions in the absence of the halide, resulting in a low ·OH concentration. Comparison of **Fig. 3.12** and **Fig. 3.20(c)** showed that the rate of PEG decomposition at the anode is slightly decreased in the absence of Cl⁻, demonstrating that PEG degradation was possible even in the absence of the Cl⁻ ion.

In summary, as shown in the **Fig. 3.21**, obtained products were related to the active radical decomposition reaction or direct Cu⁺ ion catalytic reaction, suggesting that the decompositions of PEG under open-circuit, short-circuit, and electrolysis conditions were caused by chemical reactions.

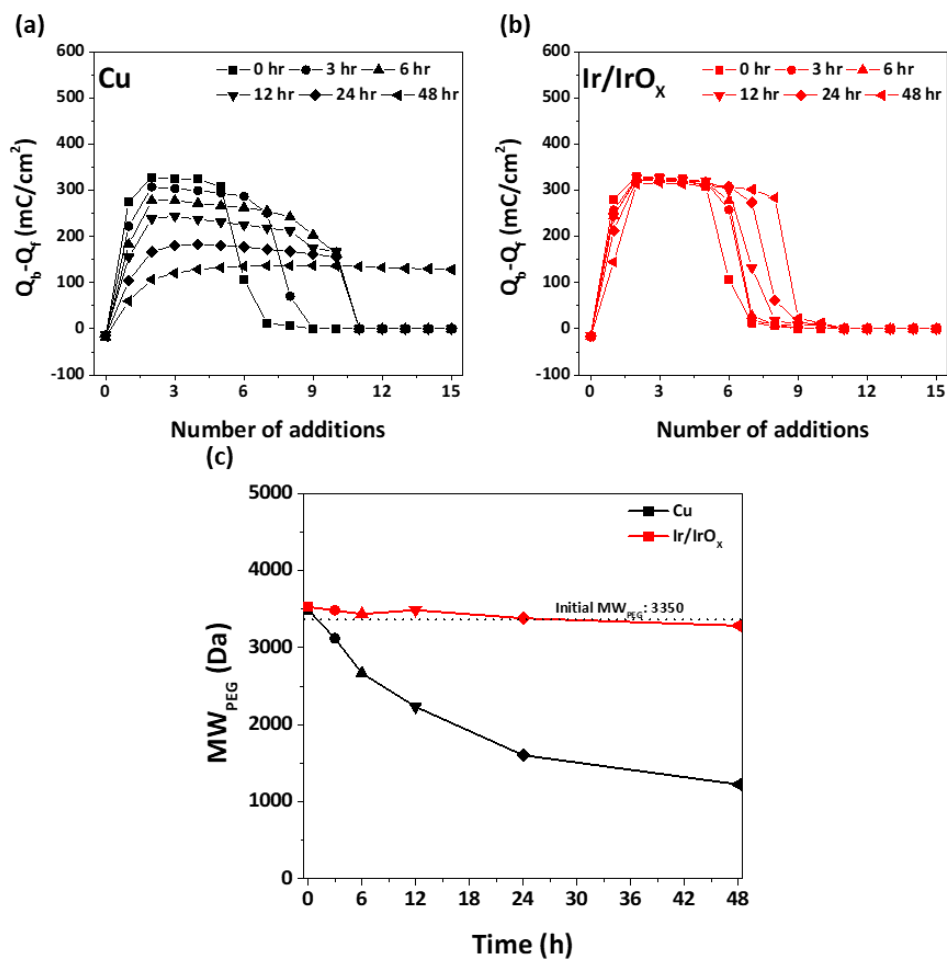


Fig. 3.10. Value of $Q_b - Q_f$ as a function of the amount of the aged solution (1 mL/addition) at (a) the Cu plate and (b) Ir/IrO_x plate added into VMS (50 mL). The aged solution was obtained under open-circuit conditions in a membrane cell. The MW_{PEG} values in the aged solution measured by CVS is presented in (c).

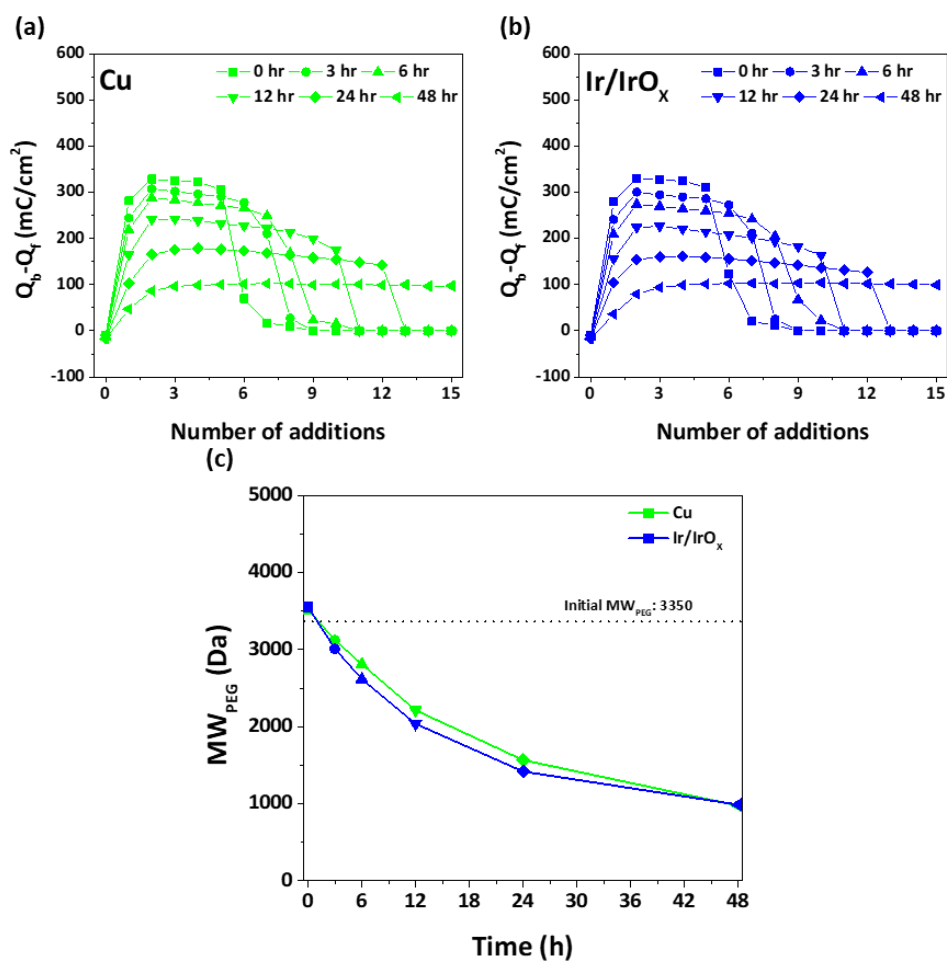


Fig. 3.11. Value of $Q_b - Q_f$ as a function of the amount of the aged solution (1 mL/addition) at (a) the Cu plate and (b) Ir/IrO_x plate added into VMS (50 mL). The aged solution was obtained under short-circuit conditions in a membrane cell. The MW_{PEG} values in the aged solution measured by CVS is presented in (c).

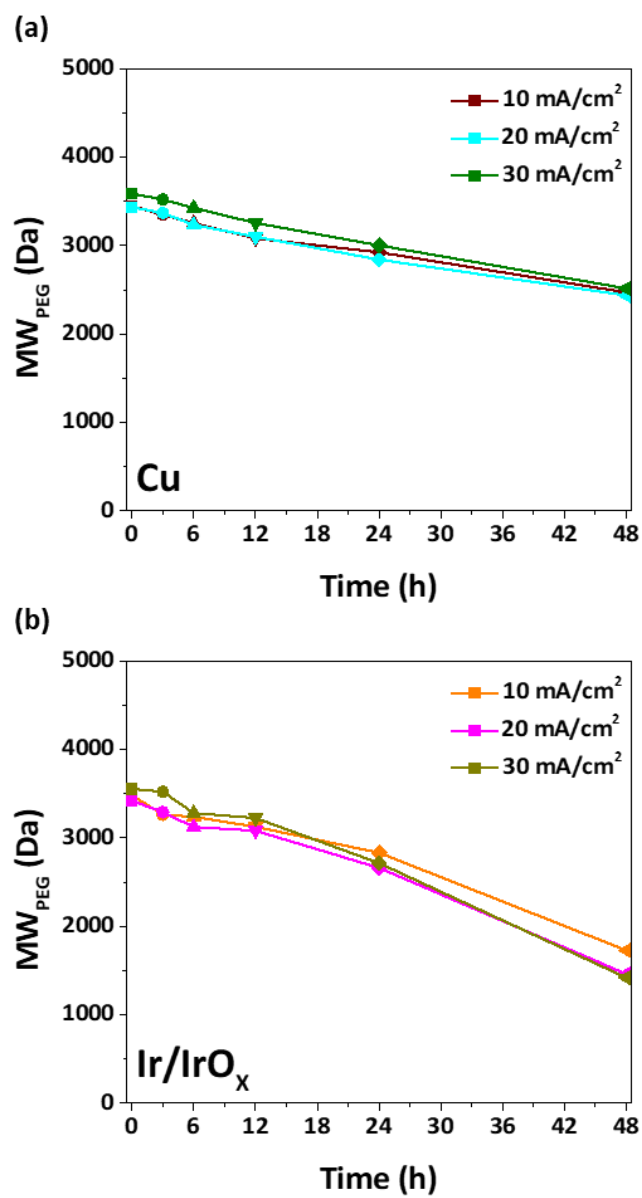


Fig. 3.12. Changes in MW_{PEG} during electrolysis at 30 mA/cm², 40 mA/cm², and 50 mA/cm² in (a) Cu plate and (b) Ir/IrO_x plate.

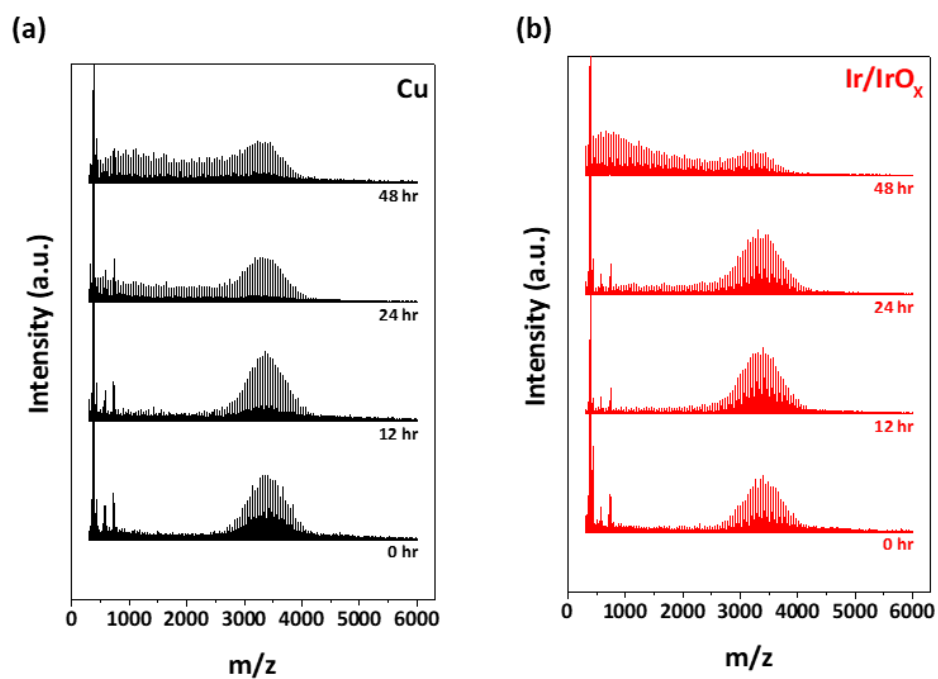


Fig. 3.13. MW_{PEG} measured by MALDI-TOF during the degradation experiment under electrolysis conditions (30 mA/cm²) at (a) the Cu plate, and (b) Ir/IrO_x plate.

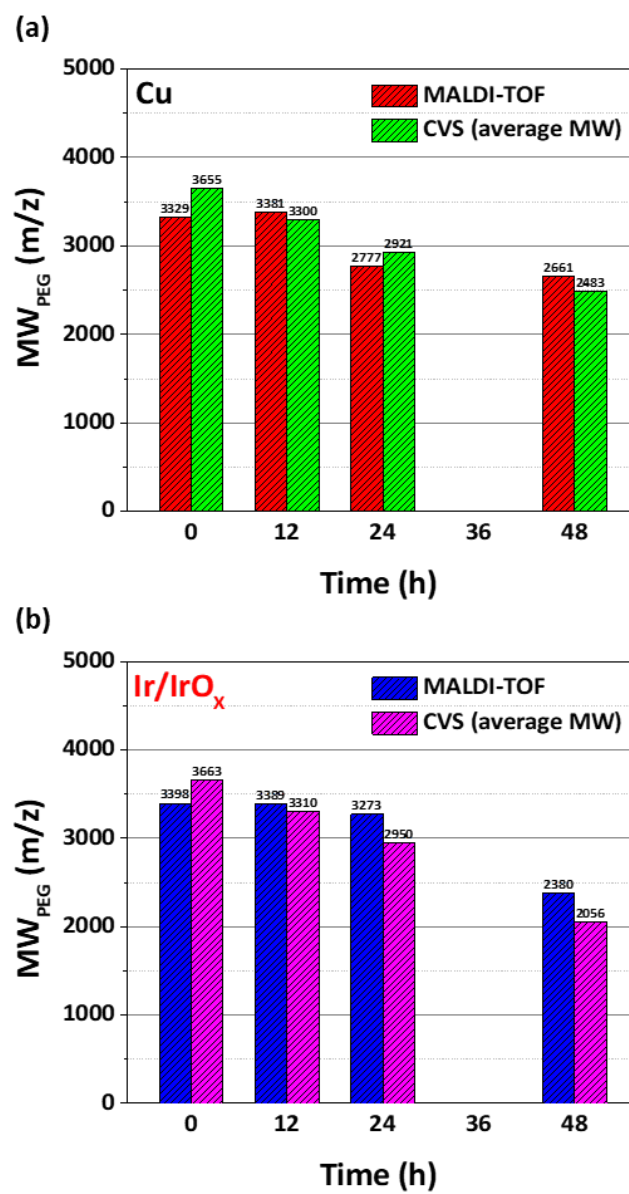


Fig. 3.14. Comparison between the MW_{PEG} values obtained with MALDI-TOF and with CVS analysis at (a) the Cu plate and (b) Ir/IrO_x plate.

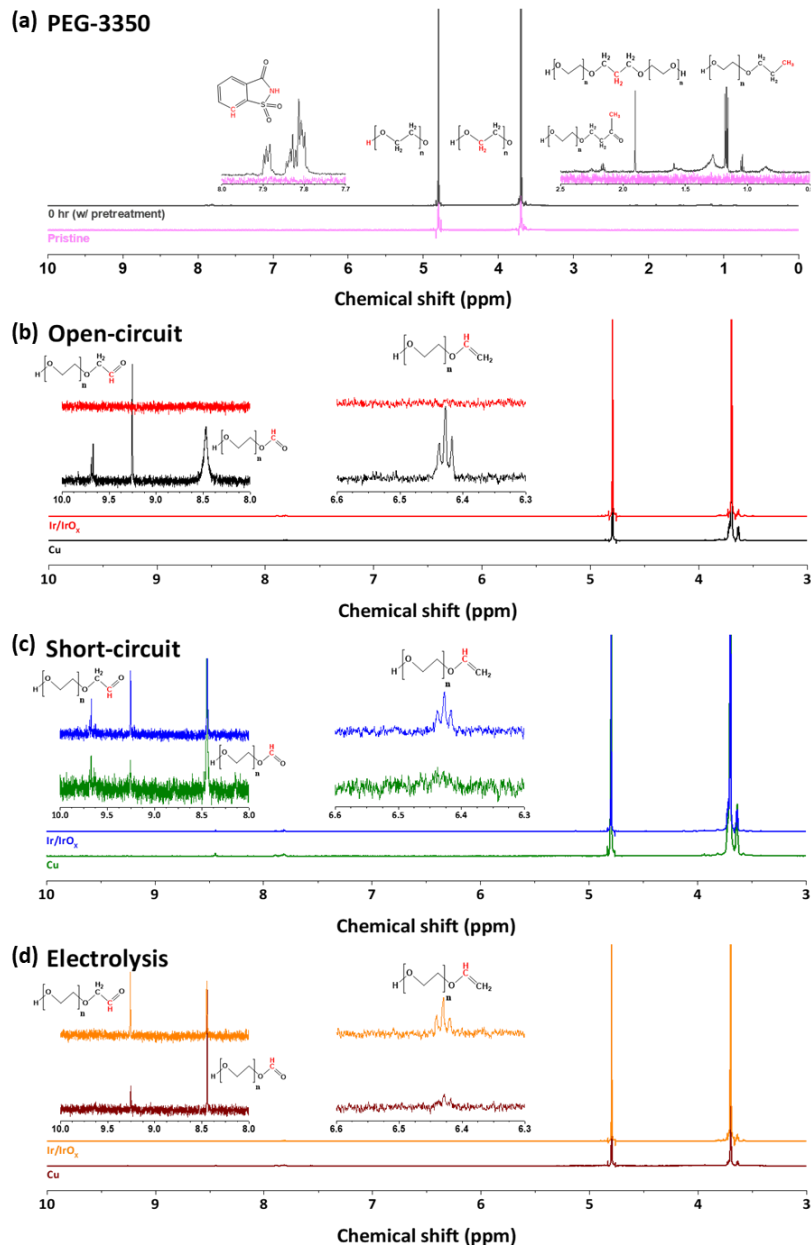


Fig. 3.15. ^1H -NMR spectra of PEG after aging for 48 h, (a) pristine PEG and PEG in the fresh bath; (b) PEG aged under open-circuit conditions; (c) PEG aged under short-circuit conditions; (d) PEG aged under electrolysis conditions with 30 mA/cm^2 .

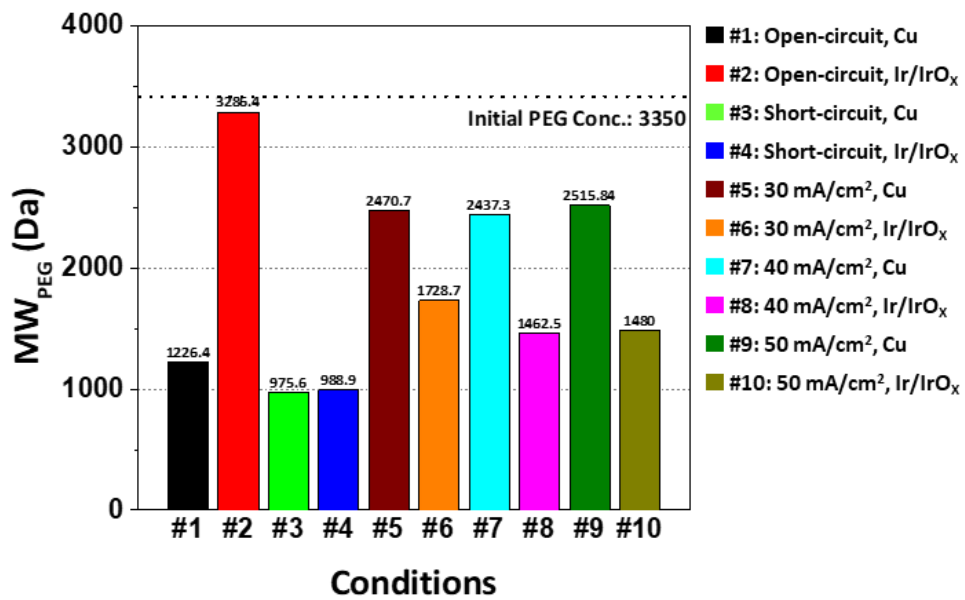


Fig. 3.16. MW_{PEG} after 48 h aging under various conditions (open-circuit, short-circuit, and electrolysis).

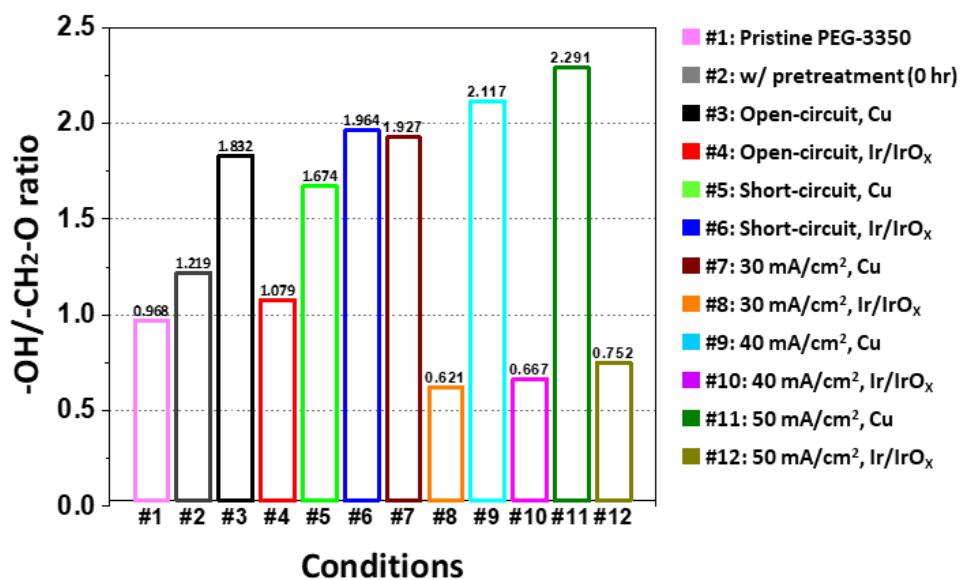


Fig. 3.17. Intensity ratio of -OH/-CH₂-O for PEGs aged for 48 h under various conditions.

Intensity ratio was obtained by integrating peaks at 3.7 ppm (-CH₂-O) and 4.8 ppm (-OH).

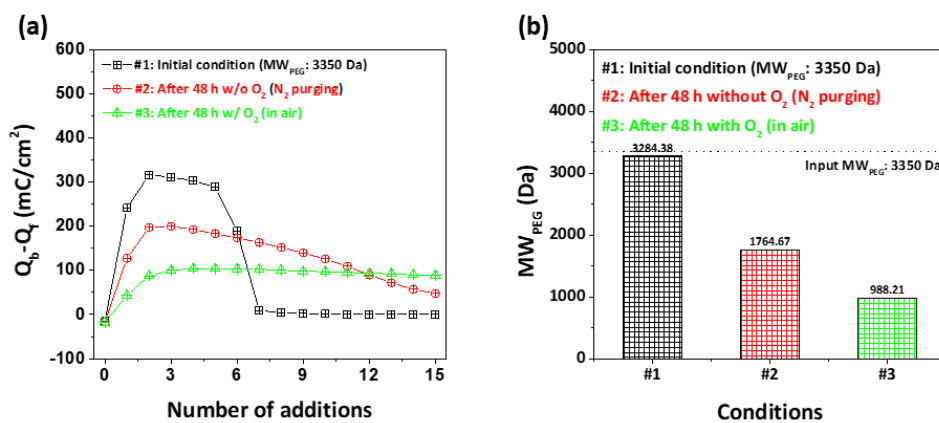


Fig. 3.18. Value of $Q_b - Q_f$ as a function of the amount of the aged solution (1 mL/addition) at the Cu plate added into VMS (50 mL). The aged solution was obtained under open-circuit aging with and without N₂ purging. The MW_{PEG} values in the aged solution measured by CVS is presented in (b).

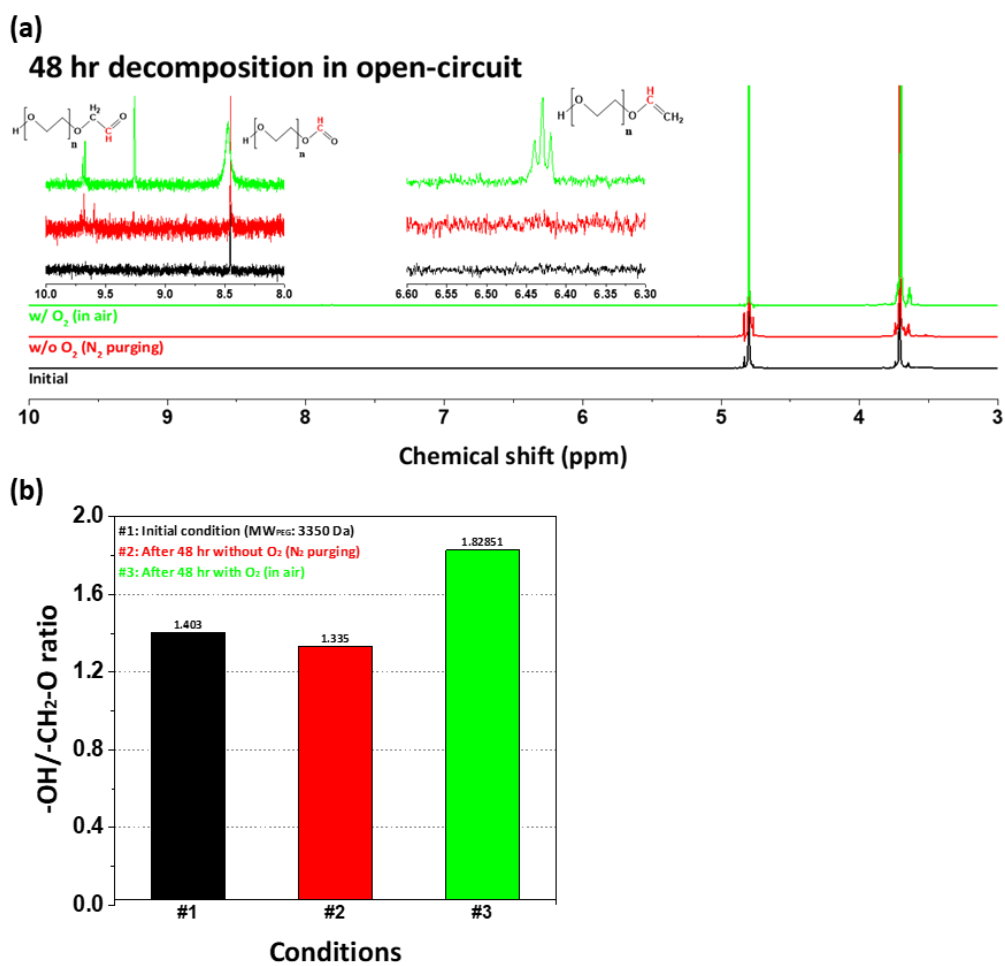


Fig. 3.19. (a) ^1H -NMR spectra of PEG; fresh PEG, aged PEG under open circuit condition with N_2 purging, and that aged without N_2 purging. (b) Intensity ratio of $-\text{OH}/-\text{CH}_2-\text{O}$ for various conditions.

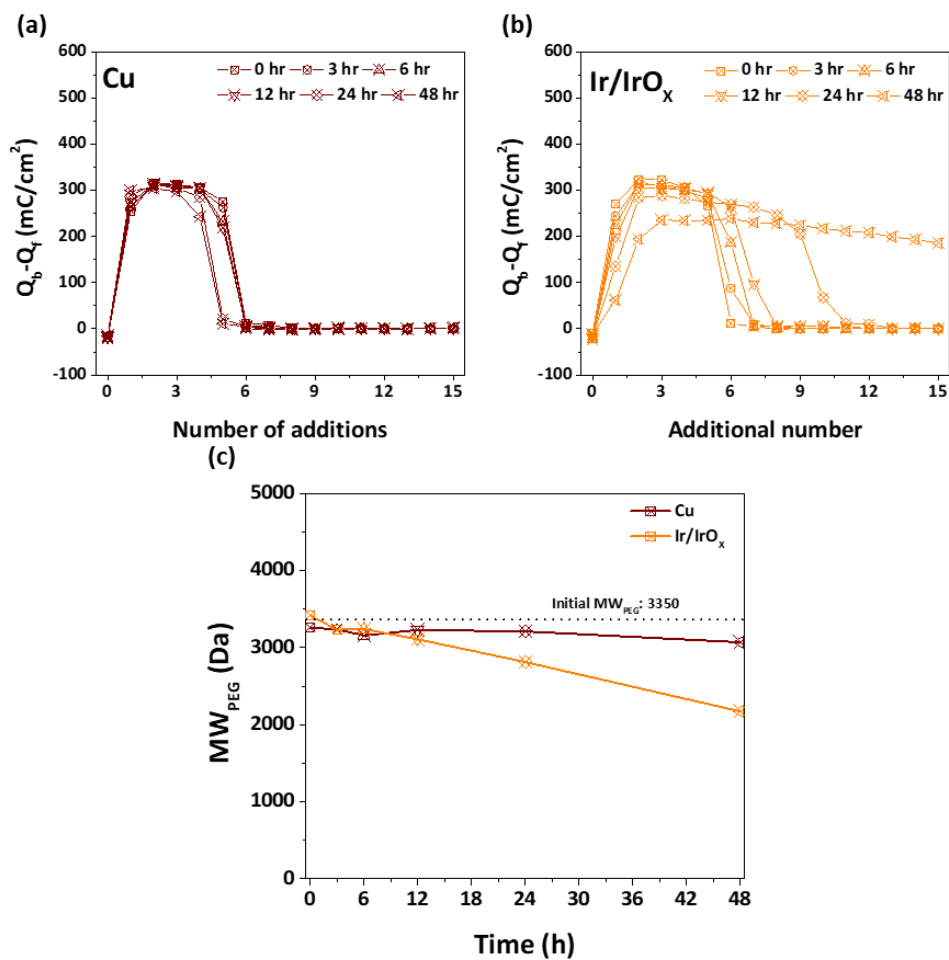


Fig. 3.20. $Q_b - Q_f$ as a function of the amount of Cl⁻-free aged solution (1 mL/addition) at (a) the Cu plate and (b) Ir/IrO_x plate added into VMS (50 mL). The aged solution was obtained under electrolysis conditions with 30 mA/cm². The MW_{PEG} values in the aged solution measured via CVS is presented in (c).

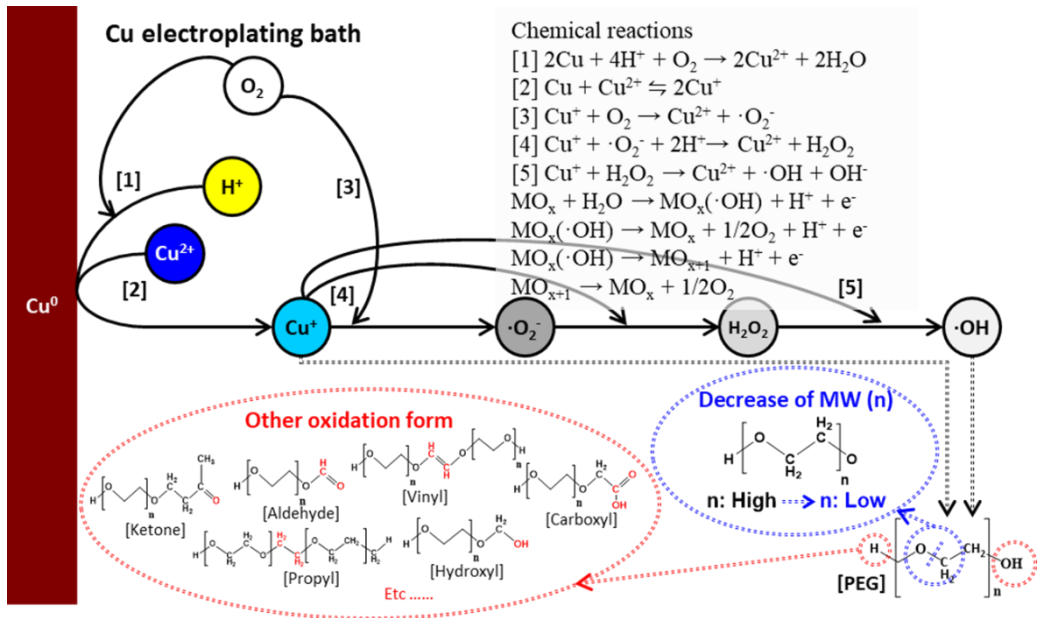


Fig. 3.21. Schematic diagram of the PEG chemical decomposition reactions.

3.3. Decrease of additive decomposition

In the current industry, as a method to reduce the decomposition of additives, ionic conducting membrane is used to prevent direct electrochemical reactions at the anode. However, since this method only aims at additive that are electrochemically decomposed, breakdown of the additive due to a decomposition factor formed by chemical reactions in the solution cannot be prevented. In order to solve this problem, the chemical reaction was investigated through the decomposition mechanism of SPS and PEG, in which was confirmed the factor of degradation. Methods that could be eliminated by analyzing the decomposition factor were suggested, and it was confirmed that decomposition was controlled by applying it in practice.

3.3.1. The factor of additive decomposition

As a result of confirming the decomposition factor of the additive, it was confirmed that SPS was decomposed only by active radical formed in the electrolyte, and that PEG was degraded not only by active radical but also by direct Cu^+ ion. Therefore, in order to decrease decomposition, the formation of active radical and Cu^+ ion must be

suppressed. As a method to remove active radical that are unavoidably formed in the electrolyte, two approaches were largely examine.

First, a reducing agent was introduced to make the active radical react with other substances before the active radical broke the weak bond of SPS. The reducing agent was selected as a material that did not affect the Cu electrodeposition bath, and then the actual decomposition concentration of SPS was measured with reducing agent. Finally, the filling performance was confirmed with the decomposed solution to secure the reliability of the electrolyte. Through the previous study and following Eq. 1.4, Eqs. 3.5~3.7, it was found that the decomposition factors are largely three kinds of Cu^+ ion, dissolved O_2 , and active radical.^{139, 144-146} In order to prevent decomposition, it is necessary to suppress the formation of decomposition factor. However, in the industrial process, it is practically impossible to remove dissolved oxygen present in a solution because of economic burden. Therefore, we focused on a method that could remove Cu^+ ion and active radical in the solution.

The second method is to reduce decomposition by change of the electrolyte properties lowering the concentration of Cu^+ ion present in the solution and decreasing of the concentration of active radical. This method is covered in detail in appendix.

3.3.2. Selection of reducing agent in Cu electrodeposition bath

First, five kinds of reducing agents used in the industry were selected: hypophosphite (NaPO_2H_2), formaldehyde (HCHO), glyoxylic acid (OCHCO_2H), hydrazine (N_2H_4), and oxalic acid (COOH)₂. Electrochemical analysis was conducted to evaluate the effect of reducing agents on Cu electrodeposition. Linear sweep voltammetry (LSV) was performed using fresh Cu electrolyte by adding 100 μM of each of the reducing agent in order to examine the possible side effect by them in **Fig. 3.22**. In the low potential region at -0.4 to -0.6 V, there seemed to be a slight difference in current density, but the voltammograms were almost identical for all reducing agents. The electrochemical response was also similar between -0.2 and -1.0 V (vs. $\text{Hg}/\text{Hg}_2\text{SO}_4$) when the forced convection was stronger 300 rpm and 1000 rpm. Furthermore, even after the addition of 100 μM reducing agents, there was no apparent effect on the voltammetric response. To understand the effect of the reducing agents on the decomposition of SPS, an aging experiment of SPS was proceeded under the open-circuit condition. The C_{SPS} during the 10 h aging process and the corresponding consumption rates were shown in **Fig. 3.23(a)** and **(b)**, respectively. The results indicated that when the aging was done for 10 h without the addition of a reducing agent, the SPS decomposed at a consumption rate 12.70 $\mu\text{M}/\text{h}$.

Note that the consumption rates were determined between 0 and 4 h, where the concentration of SPS linearly decreased. The consumption rates of SPS, when reducing agent were added, were measured 12.23 $\mu\text{M/h}$ (NaPO_2H_2), 11.91 $\mu\text{M/h}$ (HCHO), 12.06 $\mu\text{M/h}$ (OCHCO_2H), 12.65 $\mu\text{M/h}$ (N_2H_4), and 12.21 $\mu\text{M/h}$ ($(\text{COOH})_2$), respectively. The rate of SPS degradation slightly decreased when the reducing agent were added, and especially formaldehyde was determined to be the most effective for inhibiting SPS decomposition. However, due to the low concentration of the reducing agents, there was not a large change in the SPS consumption rates. Therefore, it was selected again by increasing the concentration of the reducing agent.

There was no visible change when 100 μM of a reducing agent was injected into the Cu electrolyte. The Cu electrodeposition bath was maintained for 10 h after the addition of the reducing agent without the formation of precipitates. In the **Fig. 3.24**, the increase of reducing agent concentration to 10 mM in Cu electroplating bath occurred the precipitation of hydrazine (blue-green precipitate) or oxalic acid (sky-blue precipitate) immediately due to the formation of hydrazinium sulfate (white) and cupric oxalate (bluish-white), respectively. The solubility of hydrazinium sulfate with 30 g/L in water, decreased as the amount of sulfuric acid increased due to the increase in the concentration of sulfate. LSV analysis was performed again with an increase in the

concentrations of the reducing agents from 100 μM to 10 mM (100 times more concentrated) at Cu RDE in **Fig. 3.25(a)~(c)** and Pt RDE in **Fig. 3.25(d)~(f)**. There were no observable changes in the voltammograms of the Cu RDE after the addition of the reducing agent, except in the case of hydrazine. When hydrazine was added in the Cu electroplating bath, a higher current density was obtained between -0.4 and -0.85 V owing to the acceleration Cu reduction, which indicated that hydrazine affected the Cu reduction process. In addition, CVS analysis was used to measure the concentration of SPS. So, electrochemical analysis on the Pt RDE was also needed. In the case of formaldehyde, glyoxylic acid, and oxalic acid, there were no apparent differences in the voltammograms obtained between -0.4 and -1.0 V compared to the voltammogram obtained when a reducing agent was not present. However, when hypophosphite, which is known to reduce metallic phosphite, was added, a peak was detected in the range of -0.4 to -0.5 V (vs. $\text{Hg}/\text{Hg}_2\text{SO}_4$) in **Fig. 3.25(d)~(f)**.¹⁴⁷ Note that the measurement of SPS concentration with NaPO_2H_2 was excluded because accurate measurement was not possible.

In the open-circuit condition, the aging of SPS was conducted by increasing the concentrations of the reducing agents to 10 mM, and the results were presented in **Fig. 3.26**. The SPS degraded at a rate of 12.70 $\mu\text{M}/\text{h}$ when no reducing agents were added.

The consumption rate of SPS decreased with the addition of reducing agents. The concentration of SPS measured using CVS analysis was unreliable at initial condition when hydrazine and oxalic acid were added, due to the formation of precipitates and an accelerating effect resulting in a measurement error, as presented in **Fig. 3.25**. The consumption rates of SPS in the presence of hydrazine and oxalic acid were 4.50 and 6.25 $\mu\text{M}/\text{h}$, respectively. However, when formaldehyde and glyoxylic acid were added, the SPS decomposed at much lower rates of 0.75 and 1.46 $\mu\text{M}/\text{h}$, respectively. In addition, CVS was used to determine the SPS concentration in order to check the consumption rates of SPS as a result of the concentration of formaldehyde and glyoxylic acid. Each reducing agent was added to the Cu bath and samples were taken every 2 h in **Fig. 3. 27**. The consumption rate of SPS under these condition was 0.32 and 0.65 $\mu\text{M}/\text{h}$ for formaldehyde and glyoxylic acid, respectively, indicating that the decomposition of SPS decreased when the concentration of reducing agent increased.

Among the five reducing agents, formaldehyde and glyoxylic acid effectively inhibited the decomposition of SPS without apparent side effect (precipitation or electrochemical response). In particular, when using formaldehyde, it was confirmed that the rate of decomposition of SPS decreased in about 2 times compared to glyoxylic acid. Therefore, formaldehyde was utilized to investigate micro-via filling performance in Cu

electrodeposition bath.

3.3.3. Effect of reducing agent (formaldehyde)

The process of micro-via filling was performed using HCHO, which has the best effect. In this case, in order to focus only the effect of SPS, the solution containing only SPS was aged, and the optimized 100 μM PEG-1500 and 100 μM NH_4Br were freshly added to perform the filling process. Open-circuit aging was conducted by adding SPS to the Cu electrodeposition bath with and without formaldehyde.

In the case of formaldehyde-free condition, after aging for 3, 6, and 9 h, the electrolyte was sampled, and the SPS concentration were measured by CVS. As shown in **Fig. 3.28(a)**, at the initial condition where 24 μM of SPS was present, the surface of the PCB substrate was shiny (top view), and the micro-via was fully filled. After aging the electrolyte for 3, 6, and 9 h under the open-circuit condition, the filling performance gradually decreased and the substrate surface became rough. Furthermore, SPS concentration during the 9 h period, measured using CVS analysis, were determined in **Fig. 3.28(b)**. After 3, 6, and 9 h of aging, the concentration of SPS decreased from 25.96 μM to 17.10, 9.67, and 6.09 μM , respectively. The SPS breakdown during the aging process resulted in the insufficient filling of the micro-via in the PCB substrate.

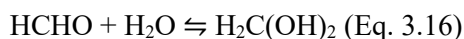
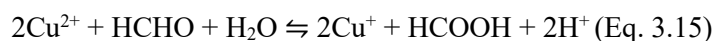
In the case of formaldehyde addition, the initial filling performance was excellent, and

the substrate surface was shiny in **Fig. 3.29(a)**. After being aged under the open-circuit condition for 9 h, the filling performance and the shiny surface of the PCB substrate were maintained. During this period, the SPS concentration determined by CVS analysis was relatively consistent 26.93 μM in initial, 25.16 μM in 3 h, 24.75 μM in 6 h, and 24.00 μM in 9 h in **Fig. 3.29(b)**. These results indicated that SPS was less oxidized when formaldehyde was added compared to when it was not added.

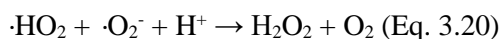
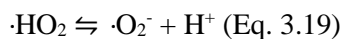
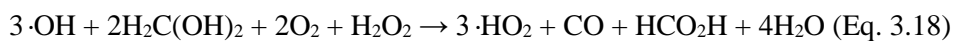
The decomposition of SPS could thus be decreased by the addition of reducing agents. In particular, formaldehyde had the best performance among the reducing agents. It has been suggested that the degradation of SPS is initiated by the hydroxyl radical, which is formed via the reaction between Cu^+ and dissolved O_2 . Here, Cu^+ ion was produced via a disproportionation reaction by Eq. 1.7. Subsequently, as the Fenton-like reaction occurred between dissolved O_2 and Cu^+ ion, the active radical ($\cdot\text{OH}$) was formed, which led to the oxidation of SPS.¹⁴⁷⁻¹⁵⁶

Typically, when formaldehyde was used in electro-less deposition, it is oxidized to formate and methanol by the Cannizzaro reaction (Eqs. 3.14~3.15) in alkaline solution.^{157, 158} The reducing agent acted as an electron donor in the electro-less deposition, enabling Cu^{2+} to be reduced to metallic Cu in the presence of a complexing agent such as ethylenediaminetetraacetic acid (EDTA), in alkaline solution. However, in a neutral

solution, formaldehyde existed as methylene glycol in Eqs. 3.16~17.



When hydroxyl radical is formed due to the reaction between Cu^+ ion and dissolved O_2 in the Cu electrodeposition bath, they react with the methylene glycol in Eq. 3.18. Subsequently, formic acid (HCOOH), hydrogen peroxide (H_2O_2), and active radical are intermediate products that lead to the formation of hydroxyl ($\cdot\text{OH}$), hydroperoxy ($\cdot\text{HO}_2$), and superoxide ($\cdot\text{O}_2^-$) by successive reactions in Eqs. 3.19~3.21. Finally, the oxidation of formaldehyde leads to the formation of carbon monoxide (CO), carbon dioxide (CO_2), and water (H_2O).





In summary, since formaldehyde was oxidized by the active radical in place of the SPS, the rate of SPS decomposition decreased in **Fig. 3.30**. In addition, when formaldehyde was added as a reducing agent, there were few side effects on Cu electrodeposition. The micro-via in the PCB substrate was fully filled regardless of the presence of formaldehyde, which indicated that the formaldehyde did not affect the filling performance of the Cu electrodeposition.

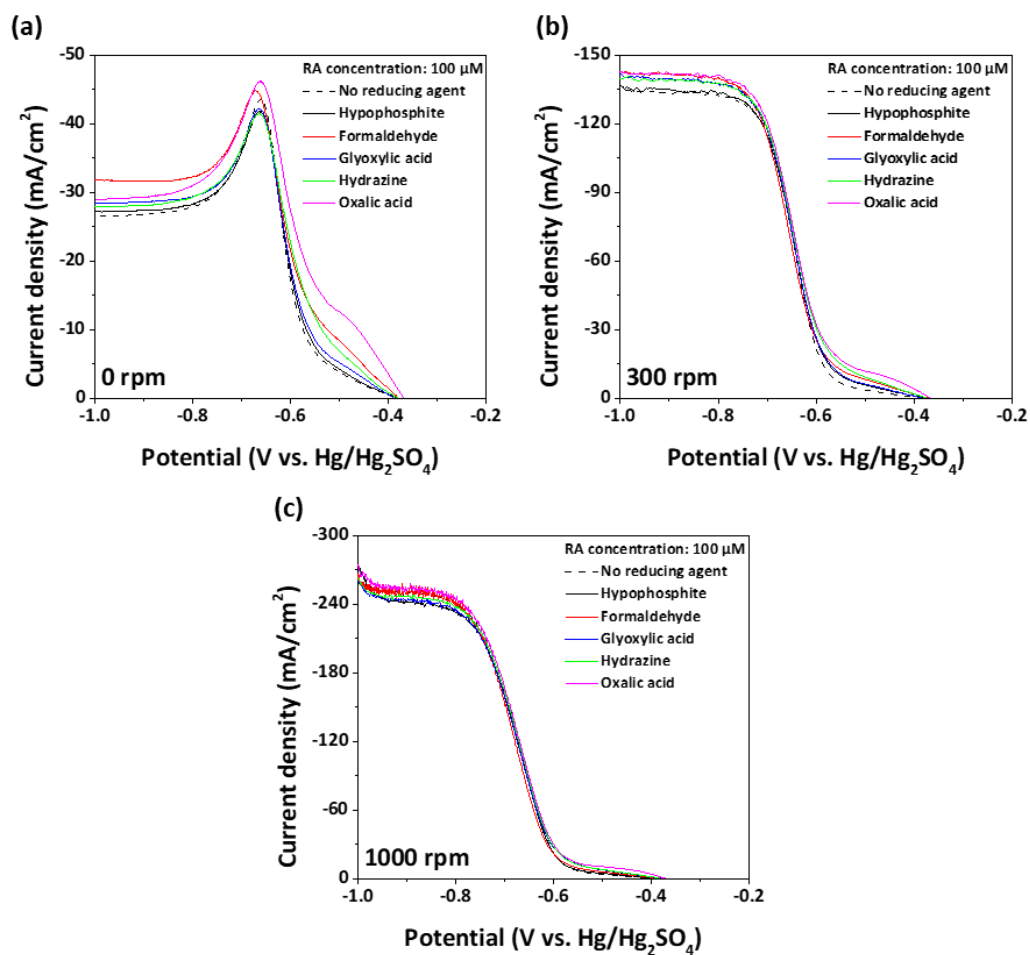


Fig. 3.22. The voltammograms of the Cu bath with a Cu RDE (VMS# 1, 50 μM SPS, and 88 μM PEG-3350), with and without the addition of 100 μM of each reducing agent, with a rotating speed of (a) 0 rpm, (b) 300 rpm, and (c) 1000 rpm.

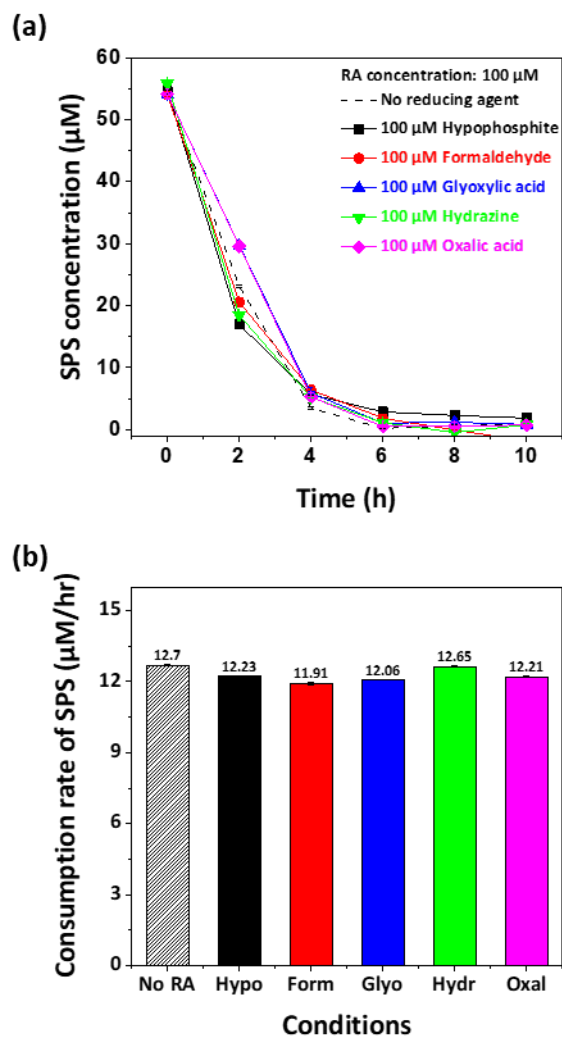


Fig. 3.23. (a) The concentrations of SPS in the Cu bath during open-circuit aging with and without the addition of 100 μM of each reducing agent, and (b) corresponding consumption rates.

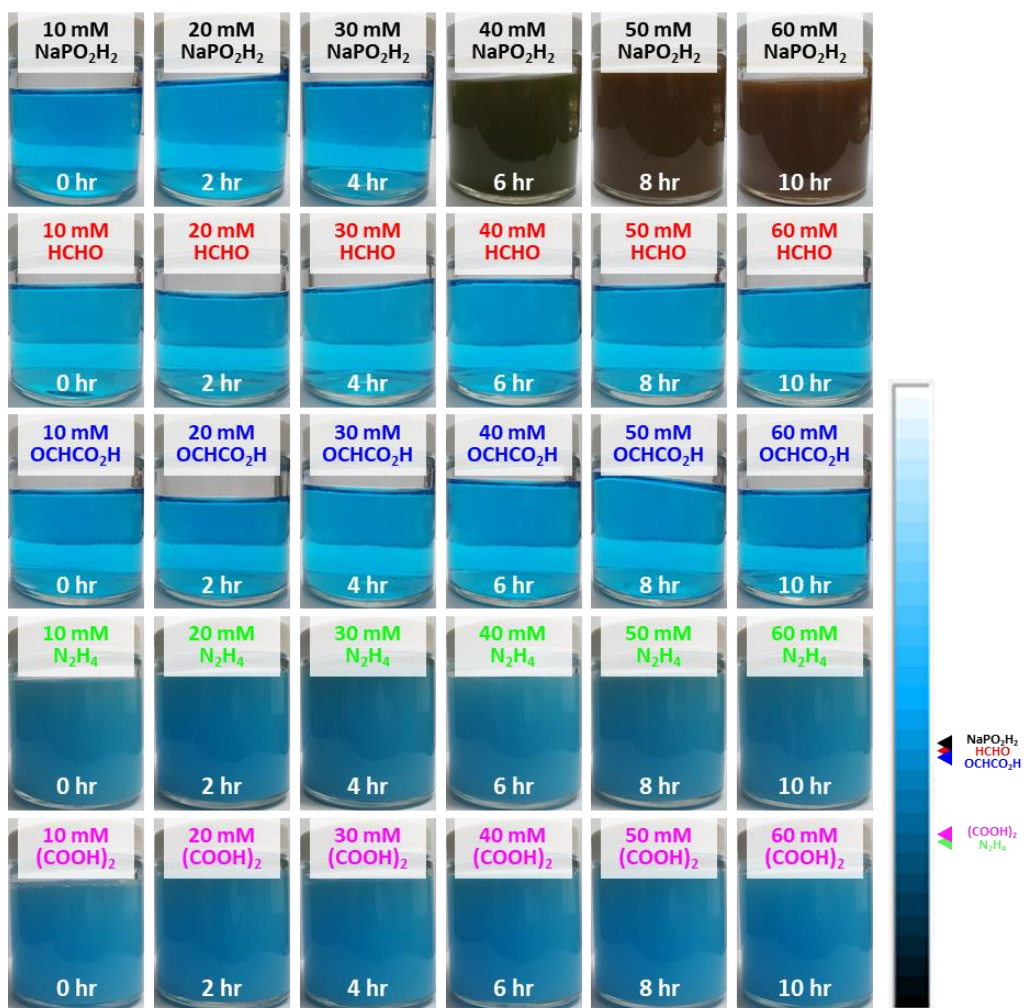


Fig. 3.24. Photographic images of the Cu bath with 10 mM of each reducing agent over a 10 h period.

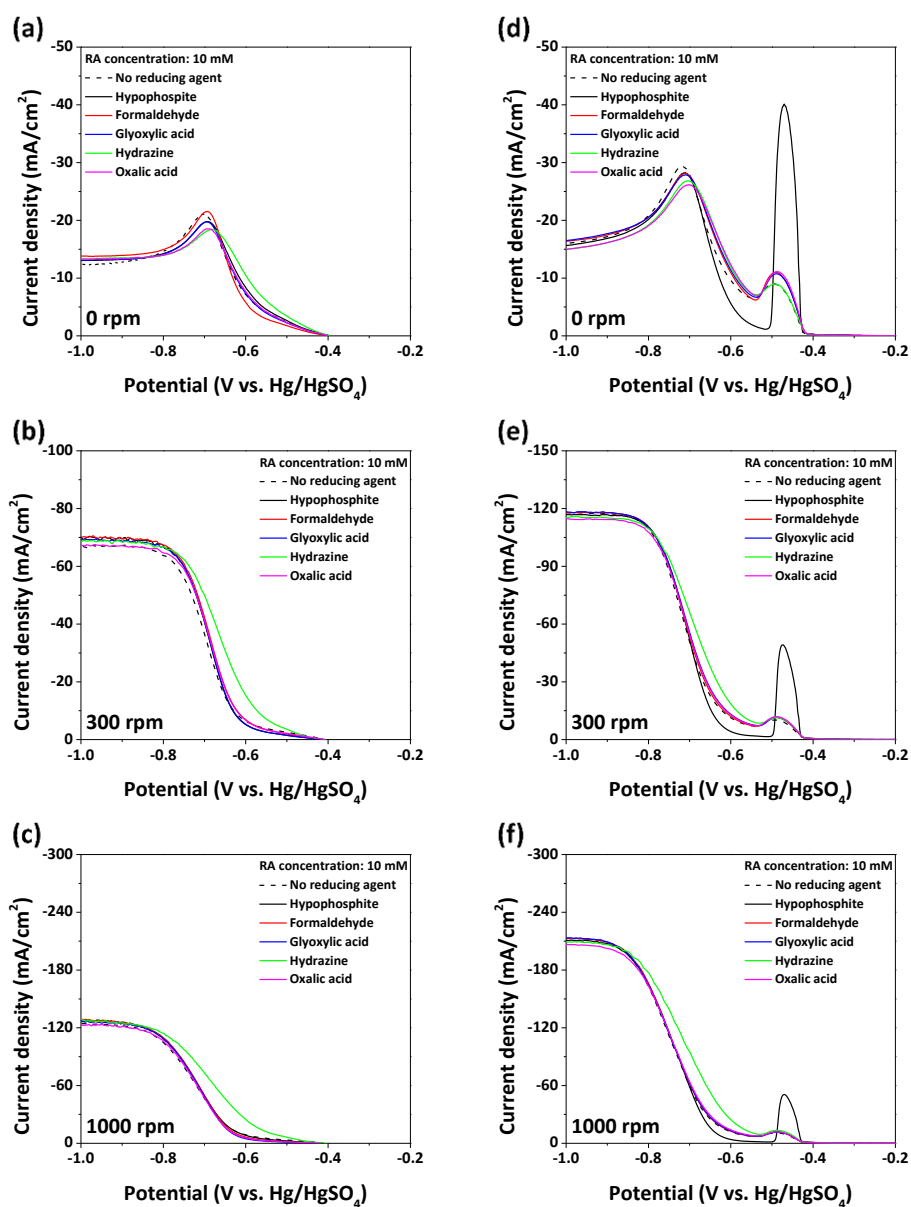


Fig. 3.25. The voltammograms of the Cu bath (VMS#1, 50 μ M SPS, and 88 μ M PEG-3350) with 10 mM of each reducing agent on the Cu RDE ((a) 0 rpm, (b) 300 rpm, (c) 1000 rpm), and on the Pt RDE ((d) 0 rpm, (e) 300 rpm, (f) 1000 rpm).

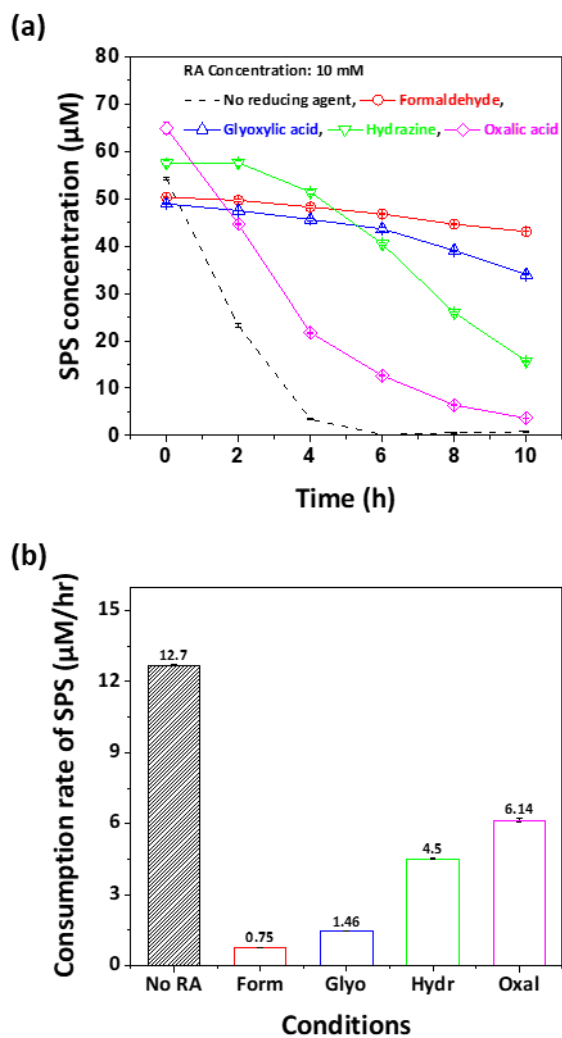


Fig. 3.26. (a) The concentrations of SPS in the Cu bath (VMS#1, 50 μM SPS) during open-circuit aging with and without 10 mM of each reducing agent, and (b) corresponding consumption rates.

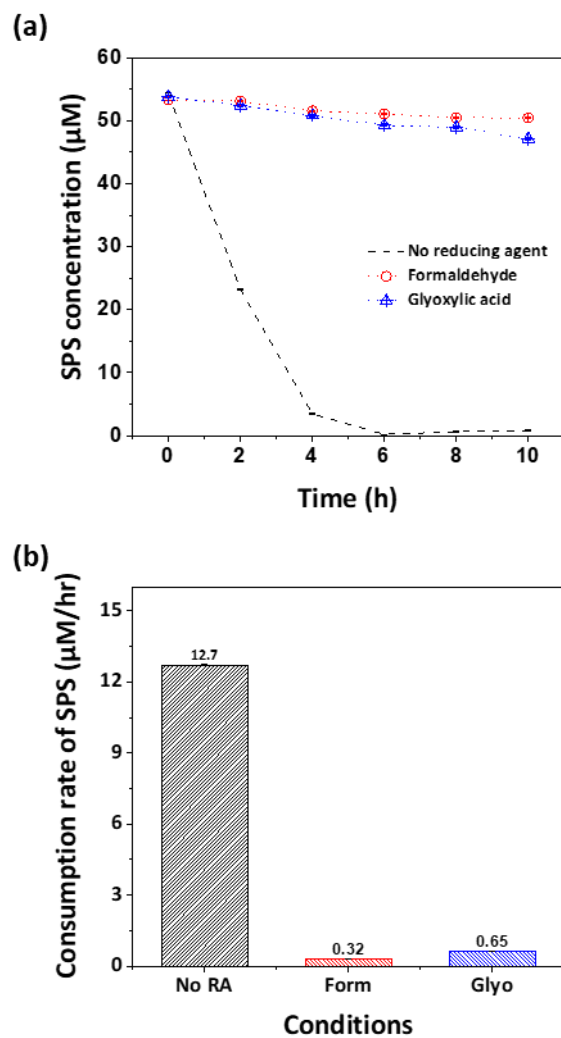
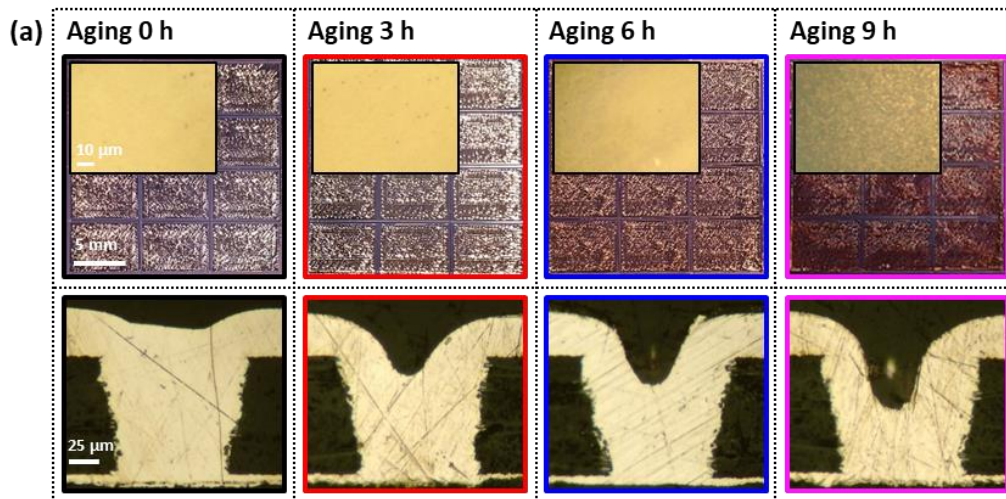


Fig. 3.27. (a) SPS concentration during open-circuit aging, and (b) corresponding consumption rates. The Cu bath initially consisted of VMS#1, 50 μM SPS, and 10 mM of each reducing agent was added to the electrolyte, which was sampled every 2 h.



(b)

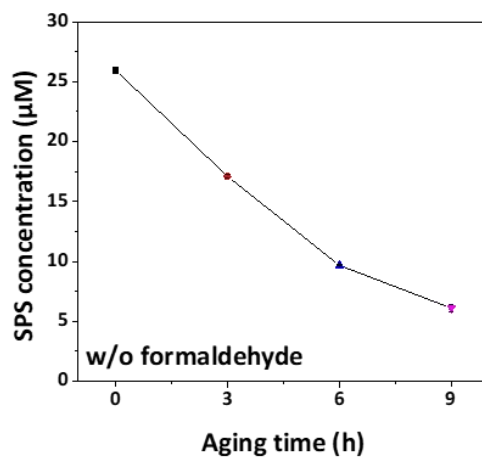
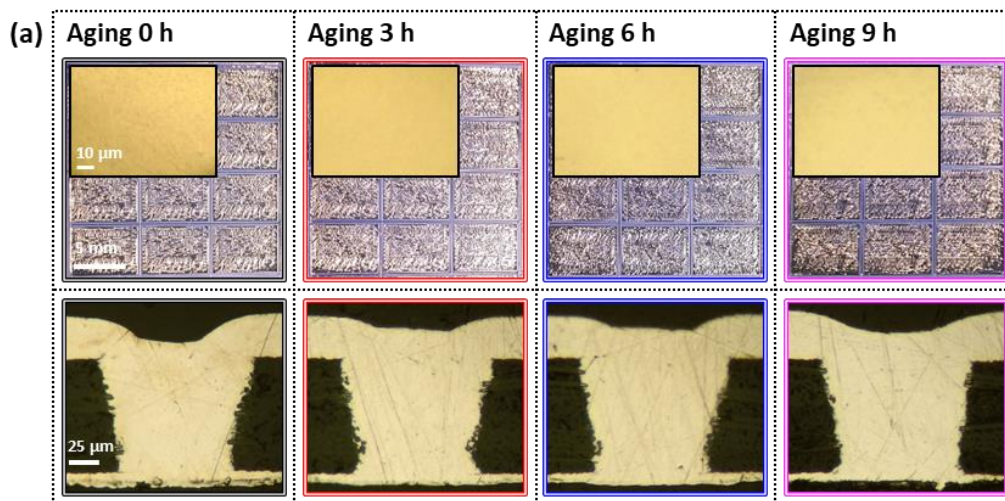


Fig. 3.28. (a) Optical microscopy (OM) images of the PCB surface and micro-via after electrodeposition for 90 min using fresh and aged baths without the addition of formaldehyde (initial concentration= VMS#2 and 24 μM SPS; supplement after aging= 100 μM PEG-1500 and 100 μM NH_4Br) (b) SPS concentration measured by CVS analysis.



(b)

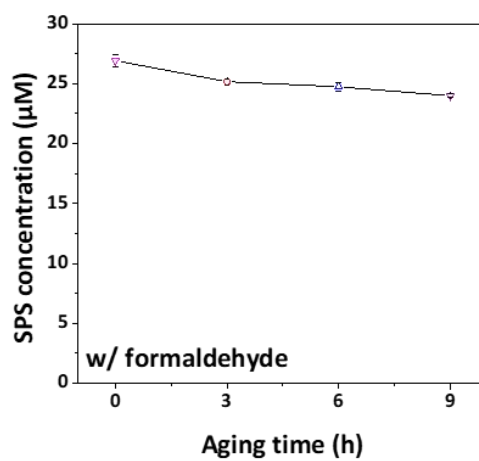


Fig. 3.29. (a) Optical microscopy (OM) images of the PCB surface and micro-via after electrodeposition for 90 min using fresh and aged baths with the addition of formaldehyde (initial concentration = VMS#2 and 24 μM SPS, 10 mM formaldehyde; supplement after aging = 100 μM PEG-1500 and 100 μM NH_4Br) (b) SPS concentration measured by CVS analysis.

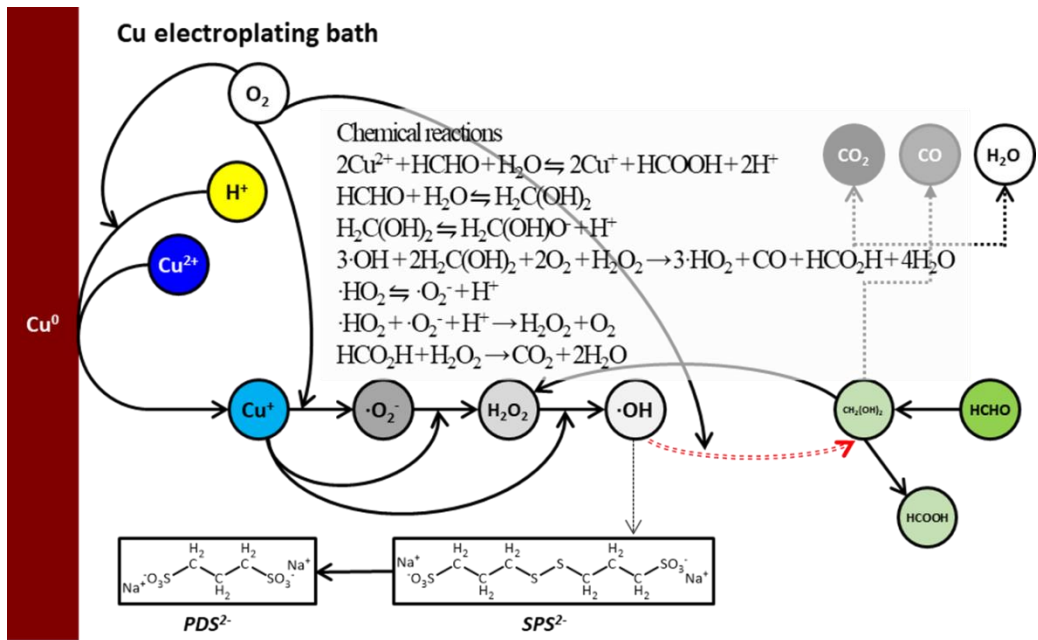


Fig. 3.30. Schematic diagram of the reduction of formaldehyde by active radicals.

CHAPTER IV

Conclusion

In this study, the additive decomposition mechanisms were investigated with ion-conducting membrane under the various conditions (open-circuit, short-circuit, and electrolysis). At first, the rates of SPS decomposition at the Cu plate and Ir/IrO_x plate were measured by the standard addition-CVS method, and the factor affecting the decomposition was examined. In the open-circuit condition, Cu⁺ ions were formed through Cu corrosion from the Cu metal and the disproportionation reaction between the Cu electrode and Cu²⁺ ions; the formed Cu⁺ ions reacted with SPS to form Cu(I)MPS⁻. Because of the reactivity of Cu⁺, Cu(I)MPS⁻ was further oxidized to PDS via the reaction with dissolved oxygen. Note that uncomplexed MPS was reduced to SPS rather than to PDS, while SPS remained stable in the bath. Though SPS was stable at the insoluble anode (Ir/IrO_x), it began to decompose when the circuit was closed because of the formation of Cu⁺ ions by the galvanic disproportionation reaction between Cu²⁺ in the anolyte and the catholyte. Under electrolysis, SPS at the Cu plate was consumed via the reaction with Cu⁺ ions as well as by physical incorporation, while that at the Ir/IrO_x plate decomposed via anodic oxidation.

Second, the reliability of the MW_{PEG} values obtained by CVS was verified by the comparison to the MW_{PEG} values obtained by MALDI-TOF analysis. Under the open-circuit conditions, the Cu^+ ion produced via a disproportionation reaction promoted the formation of $\cdot\text{OH}$ radicals and initiated the PEG breakdown. The $\cdot\text{OH}$ radical broke the C-O bond which is the weakest bond of PEG, leading to a decrease in MW_{PEG} . Under the short-circuit conditions, PEG degradation occurred at both electrodes due to the flow of the galvanic current, resulting in the formation of Cu^+ ion at the Ir/IrO_x. Under the electrolysis conditions, PEG degradation proceeded both at the Cu and the Ir/IrO_x plate, albeit at different rates, and PEG decomposition at the Cu plate was due to the Cu^+ ions formed during Cu^{2+} reduction, while PEG decomposition at the Ir/IrO_x plate was caused by the $\cdot\text{OH}$ radicals formed during water splitting. Under electrolytic conditions, the rate of PEG breakdown at the Cu plate was reduced compared with those of the other two cases (open-circuit and short-circuit conditions), indicating a low Cu^+ concentration. In addition, the PEG degradation occurred even when dissolved O₂ removed, which meant that direct Cu^+ ion catalytic reaction was generated in Cu electrodeposition bath. PEG by-products (aldehyde, formic ester, and vinyl group) were not identified in the anolyte of the open-circuit conditions, but were observed in other conditions, indicating that PEG decomposition proceeded via an active radical-induced chemical

reaction at both electrodes.

Through the additive decomposition mechanism, the factor of SPS and PEG degradation were identified to Cu^+ ion, O_2 , and active radical. As a method to suppress the chemical decomposition of SPS, we investigated the effect of reducing agents, which are used in electro-less deposition, on the chemical decomposition of SPS in a Cu electroplating bath. SPS can be chemically decomposed by active radicals such as $\cdot\text{O}_2^-$ and $\cdot\text{OH}$, which are formed by the reaction between Cu^+ ions and O_2 . Therefore, to reduce the chemical breakdown of SPS (i.e., to suppress the formation of active radicals), we added reducing agents to the Cu plating bath and tested the voltammetric response, bath performance, and stability of SPS under the open-circuit condition. Firstly, we selected a reducing agent that has few side effects on Cu electrodeposition. Among the five candidates (hypophosphite, formaldehyde, glyoxylic acid, hydrazine, and oxalic acid), formaldehyde and glyoxylic acid were electrochemically inactive in the cathodic potential region and did not form precipitates up to a concentration of 10 mM, and they were thus determined to be the most promising candidates. The addition of formaldehyde resulted in the least SPS decomposition during aging and thus proved to be the most efficient by about 40 times compared to without formaldehyde. We evaluated the stability of SPS in the presence of formaldehyde under the open-circuit condition.

Consequently, when formaldehyde was absent, the concentration of SPS sharply decreased (25.96 μM (initial) \rightarrow 6.09 μM (9 h)) after open-circuit aging owing to the chemical decomposition of SPS, resulting in imperfect filling. However, when formaldehyde was present in the Cu bath, SPS decomposition rarely happened (26.93 μM (initial) \rightarrow 24.00 μM (9 h)), and the filling performance was maintained for up to 9 h. It is expected that formaldehyde is oxidized by the free radicals in place of the SPS, whereby the rate of SPS oxidation decreases. These results indicated that the addition of formaldehyde improved the chemical stability of additives with little side effect on bath performance.

References

1. IEEE, The international roadmap for devices and systems: 2020 - Executive summary, (2020).
2. IEEE, The international roadmap for devices and systems: 2020 - more moore, (2020).
3. P. C. Andricacos, C. Uzoh, J. O. Dukovic, J. Horkans and H. Deligianni, *Ibm Journal of Research and Development*, **42**, 567 (1998).
4. J. J. Kelly, C. Y. Tian and A. C. West, *J Electrochem Soc*, **146**, 2540 (1999).
5. J. H. Yun, G. B. Han, Y. M. Lee, Y. G. Lee, K. M. Kim, J. K. Park and K. Y. Cho, *Electrochem Solid St*, **14**, A116 (2011).
6. W. C. Gau, T. C. Chang, Y. S. Lin, J. C. Hu, L. J. Chen, C. Y. Chang and C. L. Cheng, *J Vac Sci Technol A*, **18**, 656 (2000).
7. T. P. Moffat, J. E. Bonevich, W. H. Huber, A. Stanishevsky, D. R. Kelly, G. R. Stafford and D. Josell, *J Electrochem Soc*, **147**, 4524 (2000).
8. K. Kondo, T. Matsumoto and K. Watanabe, *J Electrochem Soc*, **151**, C250 (2004).
9. M. J. Kim, H. C. Kim and J. J. Kim, *J Electrochem Soc*, **163**, D434 (2016).
10. S. Y. Lee, H. Jung, N.-K. Kim, H.-S. Oh, B. K. Min and Y. J. Hwang, *Journal of the American Chemical Society*, **140**, 8681 (2018).
11. A. Augustin, P. Huilgol, K. R. Udupa and U. Bhat K, *J Mech Behav Biomed*, **63**, 352 (2016).
12. A. Dutta, M. Rahaman, N. C. Luedi, M. Mohos and P. Broekmann, *ACS Catalysis*, **6**, 3804 (2016).

13. X. Chen, D. A. Henckel, U. O. Nwabara, Y. Li, A. I. Frenkel, T. T. Fister, P. J. A. Kenis and A. A. Gewirth, *ACS Catalysis*, **10**, 672 (2020).
14. T. T. H. Hoang, S. Ma, J. I. Gold, P. J. A. Kenis and A. A. Gewirth, *ACS Catalysis*, **7**, 3313 (2017).
15. Y. Huang, M. Hao, X. Nian, H. Qiao, X. Zhang, X. Zhang, G. Song, J. Guo, X. Pang and H. Zhang, *Ceramics International*, **42**, 11876 (2016).
16. E. R. Mamleyev, F. Falk, P. G. Weidler, S. Heissler, S. Wadhwa, O. Nassar, C. N. Shyam Kumar, C. Kübel, C. Wöll, M. Islam, D. Mager and J. G. Korvink, *ACS Applied Materials & Interfaces*, **12**, 53193 (2020).
17. R. D. Mikkola and C. Linlin, in *Proceedings of the IEEE 2000 International Interconnect Technology Conference (Cat. No.00EX407)*, p. 117 (2000).
18. T. P. Moffat, D. Wheeler, M. D. Edelstein and D. Josell, *IBM Journal of Research and Development*, **49**, 19 (2005).
19. W.-P. Dow, H.-H. Chen, M.-Y. Yen, W.-H. Chen, K.-H. Hsu, P.-Y. Chuang, H. Ishizuka, N. Sakagawa and R. Kimizuka, *J Electrochem Soc*, **155**, D750 (2008).
20. W. P. Dow, M. Y. Yen, S. Z. Liao, Y. D. Chiu and H. C. Huang, *Electrochim Acta*, **53**, 8228 (2008).
21. K. Kondo, R. N. Akolkar, D. P. Barkey and M. Yokoi, *Copper Electrodeposition for Nanofabrication of Electronics Devices*, New York, NY: Springer New York, New York, NY (2014).

22. M. V. P. Pessoa and J. M. J. Becker, *Res Eng Des*, **31**, 175 (2020).
23. D. Mourtzis, *Int J Prod Res*, **58**, 1927 (2020).
24. K. Hollstein and K. Weide-Zaage, in *2020 Pan Pacific Microelectronics Symposium (Pan Pacific)*, p. 1 (2020).
25. W.-P. Dow, H.-H. Chen, M.-Y. Yen and C.-W. Liu, *ECS Transactions*, **2**, 259 (2019).
26. H. P. Kiran Pulidindi, "Oxygen-free Copper Market Size, By Grade (Copper Oxygen-free Electronic (Cu-OFE), Copper Oxygen-free (Cu-OF)), By Product (Wire, Strips, Rods, Busbars), By Industry (Electronics & Electrical, Automotive), Industry Analysis Report, Regional Outlook, Application Potential, Price Trends, Competitive Market Share & Forecast, 2020–2026", *Global Market Insights, GMI1411*, p. 192, (2020).
27. "Global Electroplating Market Size By Type, By End-Use, By Geographic Scope And Forecast", *Verified Market Research*, 16394, p. 105, (2019).
28. J. G. Ryan, R. M. Geffken, N. R. Poulin and J. R. Paraszczak, *IBM Journal of Research and Development*, **39**, 371 (1995).
29. S. Miura and H. Honma, *Surface and Coatings Technology*, **169-170**, 91 (2003).
30. G. Schneider, D. Hambach, B. Niemann, B. Kaulich, J. Susini, N. Hoffmann and W. Hasse, *Applied Physics Letters*, **78**, 1936 (2001).
31. R. Changsup, K. Kee-Won, A. L. S. Loke, L. Haebum, T. Nogami, V. M. Dubin, R. A. Kavari, G. W. Ray and S. S. Wong, *IEEE Transactions on Electron Devices*, **46**, 1113 (1999).
32. M. J. Kim, T. Lim, K. J. Park, S.-K. Kim and J. J. Kim, *J Electrochem Soc*, **160**, D3081 (2013).

33. D. Wheeler, T. P. Moffat and D. Josell, *J Electrochem Soc*, **160**, D3260 (2013).
34. J. Reid, *Jpn J Appl Phys I*, **40**, 2650 (2001).
35. D. Grujicic and B. Pesic, *Electrochim Acta*, **47**, 2901 (2002).
36. L. Bonou, M. Eyraud, R. Denoyel and Y. Massiani, *Electrochim Acta*, **47**, 4139 (2002).
37. M. H. Lee, Y. Lee, J. H. Oh, Y. G. Kim, S. K. Cho and J. J. Kim, *J Electrochem Soc*, **164**, D1051 (2017).
38. S.-E. Bae and A. A. Gewirth, *Langmuir*, **22**, 10315 (2006).
39. N. T. M. Hai, T. T. M. Huynh, A. Fluegel, M. Arnold, D. Mayer, W. Reckien, T. Bredow and P. Broekmann, *Electrochim Acta*, **70**, 286 (2012).
40. P. Broekmann, A. Fluegel, C. Emnet, M. Arnold, C. Roeger-Goepfert, A. Wagner, N. T. M. Hai and D. Mayer, *Electrochim Acta*, **56**, 4724 (2011).
41. C. Y. Chang, Y. H. Chen, H. Li, C. Y. Chiu, Y. H. Yu, P. C. Chiang, Y. Ku and J. N. Chen, *J Environ Eng-Asce*, **127**, 908 (2001).
42. J. W. Gallaway and A. C. West, *J Electrochem Soc*, **155**, D632 (2008).
43. J. W. Gallaway, M. J. Willey and A. C. West, *J Electrochem Soc*, **156**, D146 (2009).
44. M. E. H. Garrido and M. D. Pritzker, *J Electrochem Soc*, **155**, D332 (2008).
45. K. R. Hebert, S. Adhikari and J. E. Houser, *J Electrochem Soc*, **152**, C324 (2005).
46. M. R. H. Hill and G. T. Rogers, *J Electroanal Chem*, **86**, 179 (1978).
47. Y. Jin, K. Kondo, Y. Suzuki, T. Matsumoto and D. P. Barkey, *Electrochem Solid St*, **8**, C6 (2005).

48. A. Kreider, D. P. Barkey and E. H. Wong, *J Electrochem Soc*, **161**, D663 (2014).
49. T. M. T. Huynh, F. Weiss, N. T. M. Hai, W. Reckien, T. Bredow, A. Fluegel, M. Arnold, D. Mayer, H. Keller and P. Broekmann, *Electrochim Acta*, **89**, 537 (2013).
50. W. P. Dow, M. Y. Yen, W. B. Lin and S. W. Ho, *J Electrochem Soc*, **152**, C769 (2005).
51. M. Hayase, M. Taketani, K. Aizawa, T. Hatsuzawa and K. Hayabusa, *Electrochem Solid St*, **5**, C98 (2002).
52. J. J. Kelly and A. C. West, *J Electrochem Soc*, **145**, 3477 (1998).
53. J. J. Kelly and A. C. West, *J Electrochem Soc*, **145**, 3472 (1998).
54. S. L. Ko, J. Y. Lin, Y. Y. Wang and C. C. Wan, *Thin Solid Films*, **516**, 5046 (2008).
55. Y. B. Li, W. Wang and Y. L. Li, *Appl Surf Sci*, **255**, 3977 (2009).
56. J. Mendez, R. Akolkar and U. Landau, *J Electrochem Soc*, **156**, D474 (2009).
57. D. Stoychev and C. Tsvetanov, *J Appl Electrochem*, **26**, 741 (1996).
58. H. Yang, R. Krause, C. Scheunert, R. Liske, B. Uhlig, A. Preusse, A. Dianat, M. Bobeth and G. Cuniberti, *J Electrochem Soc*, **165**, D13 (2018).
59. H. L. Yang, A. Dianat, M. Bobeth and G. Cuniberti, *J Electrochem Soc*, **164**, D196 (2017).
60. J. J. Kelly, *J Electrochem Soc*, **145**, 3472 (1998).
61. N. Xiao, D. Y. Li, G. F. Cui, N. Li, Q. Li and G. Wu, *Electrochim Acta*, **116**, 284 (2014).
62. L. Yang, A. Radisic, J. Deconinck and P. M. Vereecken, *J Electrochem Soc*, **161**, D269 (2014).
63. J. J. Kim, S.-K. Kim and J.-U. Bae, *Thin Solid Films*, **415**, 101 (2002).
64. M. Sung, H. C. Kim, T. Lim and J. J. Kim, *J Electrochem Soc*, **164**, D805 (2017).

65. M. A. Pasquale, L. M. Gassa and A. J. Arvia, *Electrochim Acta*, **53**, 5891 (2008).
66. P. M. Vereecken, R. A. Binstead, H. Deligianni and P. C. Andricacos, *IBM Journal of Research and Development*, **49**, 3 (2005).
67. H. M. Chen, S. J. Parulekar and A. Zdunek, *J Electrochem Soc*, **155**, D349 (2008).
68. J. P. Healy, D. Pletcher and M. Goodenough, *J Electroanal Chem*, **338**, 179 (1992).
69. T. P. Moffat, D. Wheeler and D. Josell, *J Electrochem Soc*, **151**, C262 (2004).
70. M. J. Willey and A. C. West, *J Electrochem Soc*, **154**, D156 (2007).
71. S. K. Kim, D. Josell and T. P. Moffat, *J Electrochem Soc*, **153**, C616 (2006).
72. T. P. Moffat, D. Wheeler, S. K. Kim and D. Josell, *J Electrochem Soc*, **153**, C127 (2006).
73. M. L. Walker, L. J. Richter and T. P. Moffat, *J Electrochem Soc*, **153**, C557 (2006).
74. D. Josell, T. P. Moffat and D. Wheeler, *J Electrochem Soc*, **154**, D208 (2007).
75. D. Josell, D. Wheeler and T. P. Moffat, *J Electrochem Soc*, **159**, D570 (2012).
76. W. P. Dow, H. S. Huang, M. Y. Yen and H. C. Huang, *J Electrochem Soc*, **152**, C425 (2005).
77. M. H. Lee, Y. Lee, M. Sung, S. K. Cho, Y. G. Kim and J. J. Kim, *J Electrochem Soc*, **167**, 102505 (2020).
78. T. P. Moffat and D. Josell, *J Electrochem Soc*, **159**, D208 (2012).
79. T. M. Braun, D. Josell and T. P. Moffat, *Electrochim Acta*, **375**, 137925 (2021).
80. Y.-D. Chiu and W.-P. Dow, *J Electrochem Soc*, **160**, D3021 (2013).
81. C.-C. Hung, W.-H. Lee, S.-Y. Hu, S.-C. Chang, K.-W. Chen and Y.-L. Wang, *J Electrochem Soc*, **155**, H329 (2008).

82. S.-K. Kim and J. J. Kim, *Electrochemical and Solid-State Letters*, **7**, C98 (2004).
83. R. Kimizuka, H. Toda, T. Eda, K. Kishimoto, R. Oh, H. Honma and O. Takai, *J Electrochem Soc*, **162**, D584 (2015).
84. R. Kimizuka, H. Toda, T. Eda, K. Kishimoto, Y. Takaya, R. Oh and O. Takai, *ECS Transactions*, **64**, 23 (2015).
85. L. T. Koh, G. Z. You, C. Y. Li and P. D. Foo, *Microelectronics Journal*, **33**, 229 (2002).
86. W. Wang, Y.-B. Li and Y.-L. Li, *Appl Surf Sci*, **255**, 4389 (2009).
87. S. Choe, M. J. Kim, H. C. Kim, S. K. Cho, S. H. Ahn, S.-K. Kim and J. J. Kim, *J Electrochem Soc*, **160**, D3179 (2013).
88. S. Choe, M. J. Kim, H. C. Kim, T. Lim, K. J. Park, K. H. Kim, S. H. Ahn, A. Lee, S.-K. Kim and J. J. Kim, *J Electroanal Chem*, **714-715**, 85 (2014).
89. K. W. Kim, E. H. Lee, J. S. Kim, K. H. Shin and B. I. Jung, *Electrochim Acta*, **47**, 2525 (2002).
90. F. Wafula, L. Yin, P. Borgesen, D. Andala and N. Dimitrov, *J Electron Mater*, **41**, 1898 (2012).
91. B. H. Wu, C. C. Wan and Y. Y. Wang, *J Appl Electrochem*, **33**, 823 (2003).
92. Y. Yoon, Y. S. Ham, T. Y. Kim, S. Choe and J. J. Kim, *J Electrochem Soc*, **165**, H213 (2018).
93. T. H. Bailey, Q. Wang and M. West, *ECS Transactions*, **2**, 131 (2007).
94. L. D'Urzo, H. Wang, A. Pa and C. Zhi, *J Electrochem Soc*, **152**, C243 (2005).
95. A. Frank and A. J. Bard, *J Electrochem Soc*, **150**, C244 (2003).
96. L. T. Koh, G. Z. You, S. Y. Lim, C. Y. Li and P. D. Foo, *Microelectronics Journal*, **32**, 973 (2001).

97. W.-H. Lee, C.-C. Hung, S.-C. Chang and Y.-L. Wang, *J Electrochem Soc*, **157**, H131 (2010).
98. T. P. Moffat, B. Baker, D. Wheeler and D. Josell *Electrochemical and Solid-State Letters*, **6**, C59 (2003).
99. T. Y. Kim, M. Sung, Y. Yoon, K. H. Lee, S. Choe and J. J. Kim, *J Electrochem Soc*, **166**, G61 (2019).
100. J. P. Healy, D. Pletcher and M. Goodenough, *J Electroanal Chem*, **338**, 167 (1992).
101. H. Shen, H. C. Kim, M. Sung, T. Lim and J. J. Kim, *J Electroanal Chem*, **816**, 132 (2018).
102. L. D'Urzo, H. H. Wang, C. Tang, A. Pa and C. Zhi, *J Electrochem Soc*, **152**, C697 (2005).
103. J. P. Healy, D. Pletcher and M. Goodenough, *J Electroanal Chem*, **338**, 155 (1992).
104. H. Kawasaki, Y. Takeda and R. Arakawa, *Anal Chem*, **79**, 4182 (2007).
105. S. H. Liu, T. C. Li, C. Chen, J. M. Shieh, B. T. Dai, K. Hensen and S. S. Cheng, *Jpn J Appl Phys 1*, **45**, 3976 (2006).
106. T. Y. Kim, S. Choe and J. J. Kim, *Electrochim Acta*, **357**, 136803 (2020).
107. Y. S. Won, D. Cho, Y. Kim, J. Lee and S. S. Park, *J Appl Polym Sci*, **117**, 2083 (2010).
108. S. Choe, M. J. Kim, K. H. Kim, H. C. Kim, Y. Jeon, T. Y. Kim, S.-K. Kim and J. J. Kim, *J Electrochem Soc*, **163**, D33 (2016).
109. S. Choe, M. J. Kim, K. H. Kim, H. C. Kim, J. C. Song, S.-K. Kim and J. J. Kim, *J Electrochem Soc*, **162**, H294 (2015).
110. S. Choe, M. J. Kim, T. Lim, Y. S. Ham, S. K. Kim and J. J. Kim, *J Electrochem Soc*, **163**, D747 (2016).

111. E. Garcia-Cardona, E. H. Wong and D. P. Barkey, *J Electrochem Soc*, **158**, D143 (2011).
112. R. Palmans, S. Claes, L. E. Vanatta and D. E. Coleman, *J Chromatogr A*, **1085**, 147 (2005).
113. S. Yang and K. H. Carlson, *J Chromatogr A*, **1038**, 141 (2004).
114. Y. Yoon, H. Kim, T. Y. Kim, K. H. Lee, S. Choe and J. J. Kim, *Electrochim Acta*, **339** (2020).
115. S. K. Cho, T. Lim, H. K. Lee and J. J. Kim, *J Electrochem Soc*, **157**, D187 (2010).
116. S. M. Mayanna and T. H. V. Setty, *Corros Sci*, **15**, 627 (1975).
117. A. Shaban, E. Kalman and J. Telegdi, *Electrochim Acta*, **43**, 159 (1998).
118. A. Chrzanowska, R. Mroczka and M. Florek, *Electrochim Acta*, **106**, 49 (2013).
119. N. T. M. Hai, J. Odermatt, V. Grimaudo, K. W. Krämer, A. Fluegel, M. Arnold, D. Mayer and P. Broekmann, *The Journal of Physical Chemistry C*, **116**, 6913 (2012).
120. R. Mroczka, R. Łopucki and G. Żukociński, *Appl Surf Sci*, **463**, 412 (2019).
121. K.-D. Asmus, in *Methods in Enzymology*, p. 168, Academic Press (1990).
122. S. D. Aust, L. A. Morehouse and C. E. Thomas, *Journal of Free Radicals in Biology & Medicine*, **1**, 3 (1985).
123. B. Halliwell, *Toxicol Ind Health*, **9**, 1 (1993).
124. B. Halliwell and J. M. Gutteridge, *The Biochemical journal*, **219**, 1 (1984).
125. A. N. Pham, G. Xing, C. J. Miller and T. D. Waite, *Journal of Catalysis*, **301**, 54 (2013).
126. H. C. Sutton and C. C. Winterbourn, *Free Radical Bio Med*, **6**, 53 (1989).
127. R. G. Brennan, M. M. Phillips, L.-Y. O. Yang and T. P. Moffat, *J Electrochem Soc*, **158**, D178 (2011).

128. G. Gallet, S. Carroccio, P. Rizzarelli and S. Karlsson, *Polymer*, **43**, 1081 (2002).
129. G. Gallet, B. Erlandsson, A. C. Albertsson and S. Karlsson, *Polym Degrad Stabil*, **77**, 55 (2002).
130. D. S. G. Hu and H. J. Liu, *J Appl Polym Sci*, **51**, 473 (1994).
131. K. J. Voorhees, S. F. Baugh and D. N. Stevenson, *Thermochim Acta*, **274**, 187 (1996).
132. C. C. Chen, *J Electrochem Soc*, **141**, 2942 (1994).
133. K. Fukatsu and S. Kokot, *Polym Degrad Stabil*, **72**, 353 (2001).
134. R. Mroczka and A. Slodkowska, *Electrochim Acta*, **339** (2020).
135. S. Han, C. Kim and D. Kwon, *Polym Degrad Stabil*, **47**, 203 (1995).
136. S. Han, C. Kim and D. Kwon, *Polymer*, **38**, 317 (1997).
137. K. J. Voorhees, S. F. Baugh and D. N. Stevenson, *J Anal Appl Pyrol*, **30**, 47 (1994).
138. K. J. Voorhees, D. N. Stevenson, Y. H. Sun and G. E. Maciel, *J Mater Sci*, **32**, 2115 (1997).
139. E. Gileadi and V. Tsionsky, *J Electrochem Soc*, **147**, 567 (2000).
140. L. Ciavatta, D. Ferri and R. Palombari, *J Inorg Nucl Chem*, **42**, 593 (1980).
141. M. Mokmeli, B. Wassink and D. Dreisinger, *Hydrometallurgy*, **121**, 100 (2012).
142. A. J. Copley and D. R. Gabe, *TI Met Finish*, **81**, 37 (2003).
143. O. Simond, V. Schaller and C. Comminellis, *Electrochim Acta*, **42**, 2009 (1997).
144. M. R. Gunther, P. M. Hanna, R. P. Mason and M. S. Cohen, *Archives of Biochemistry and Biophysics*, **316**, 515 (1995).
145. G. Oster and G. K. Oster, *Contraception*, **10**, 273 (1974).

146. T. E. Patten and K. Matyjaszewski, *Accounts of Chemical Research*, **32**, 895 (1999).
147. D. Torres, L. Madriz, R. Vargas and B. R. Scharifker, *Electrochim Acta*, **354**, 136705 (2020).
148. J. J. Byerley and W. K. Teo, *Can J Chemistry*, **47**, 3355 (1969).
149. C. Gabrielli, L. Beitone, C. Mace, E. Ostermann and H. Perrot, *Electrochim Acta*, **52**, 6012 (2007).
150. N. Nobari, M. Behboudnia and R. Maleki, *Appl Surf Sci*, **385**, 9 (2016).
151. Y. Shacham-Diamand, V. Dubin and M. Angyal, *Thin Solid Films*, **262**, 93 (1995).
152. Y. Y. Shacham-Diamand, *Electrochemical and Solid-State Letters*, **3**, 279 (1999).
153. R. Touir, H. Larhzil, M. EbnTouhami, M. Cherkaoui and E. Chassaing, *J Appl Electrochem*, **36**, 69 (2006).
154. I. A. Vardanyan, G. A. Sachyan and A. B. Nalbandyan, *Combustion and Flame*, **17**, 315 (1971).
155. F. Liao, X. Han, C. Xu and H. Chen, *Journal of Materials Science: Materials in Electronics*, **28**, 13869 (2017).
156. L. Yu, L. Guo, R. Preisser and R. Akolkar, *J Electrochem Soc*, **160**, D3004 (2013).
157. W. J. Mcelroy and S. J. Waygood, *J Chem Soc Faraday T*, **87**, 1513 (1991).
158. J. E. A. M. Vandenmeerakker, *J Appl Electrochem*, **11**, 387 (1981).

국문초록

구리 전해 도금은 높은 생산성과 경제성으로, 4차 산업혁명 시대에서 다양한 산업인 반도체, 2차 전지, 그리고 촉매에 적용되는 뿌리 기술 중 하나이다. 전착된 구리의 성질을 조절하기 위해서, 유기 첨가제는 구리 전해 도금에서 중요한 역할로 사용된다. 하지만, 유기 첨가제는 구리 전해 도금 공정 속에서 불안정하여 여러가지 분해 경로를 통해 점차 분해됩니다. 안정적이고 고효율의 구리 전해 도금 시스템을 설계하려면, 작동조건에서 첨가제의 분해를 이해하는 것이 굉장히 필요하다. 본 연구에서는 각 전극에서 비스-설퍼프로필 다이설파이드 (SPS) 및 폴리에틸렌 글라이콜 (PEG)의 분해 메커니즘을 규명하고, 첨가제의 분해 인자를 확인하였다. 이를 통해서, 첨가제의 분해를 제어할 목적으로 분해 인자를 억제하는 방법을 제시하였다.

구리 전해 도금 공정 속에서 가속제로 사용되는 SPS의 음극 및 양극에서의 분해 메커니즘을 순환 전류 탈착 (CVS)과 수소-핵 자기 공명 (NMR) 분석 방법을 이용하여 세 가지 조건; 개방 회로, 무전원 폐쇄 회로 및 전기 분해 조건 아래에서 시험하였다. 개방 회로 환원액에서 SPS는 용해된 산소와 함께 일가 구리 이온 (Cu^+)에 의해 형성된 활성

라디칼($\cdot\text{OH}$)에 의한 화학 반응을 통해 음극에서 일가 구리-머캡토 프로페인 설페이드(Cu(I)MPS^-)로 산화된 후, 최종적으로 프로페인 다이설페이드(PDS)로 산화되었다. 불용성 산화전극에서는 화학반응이 일어나지 않았다. 전원이 공급되지 않는 폐쇄 회로에서는 불용성 산화전극과 환원전극에서 갈바닉 상반변화 반응(galvanic disproportionation reaction)에 의해 산화전극에서 일가 구리 이온이 형성되기 때문에 동일한 속도로 분해되었다. 전류가 흐르는 전기 분해 조건에서는 환원액 속에 있는 SPS가 일가 구리 이온과 용존 산소에 의해 형성되는 활성 라디칼에 소비되는 것뿐만 아니라 혼입반응(incorporation)에 의해서도 분해되는 반면, 산화액에서는 화학반응과 비교하여 훨씬 빠른 전기화학 반응을 통해 더 빨리 분해되었다.

구리 전해 도금 공정에서 억제제인 PEG의 분해 메커니즘은 각각 산화, 환원액에서 세 가지 조건 아래에서 순환 전류 탈착(CVS)과 말디토프 질량 분광(MALDI-TOF) 분석 방법을 이용하여 조사되었다. 개방 회로 조건 하에서 PEG 분해는 구리 일가 이온의 영향으로 인해 환원전극에서만 발생하였다. 전원이 공급되지 않는 폐쇄 회로에서는 PEG가 갈바닉 상반변화 반응을 통해 두 전극에서 분해되었으며, 이는 산화전극에서도 닫힌 회로에서 전류가 흐르면서 구리 일가 이온이 형성되었기 때문이다.

전기 분해 조건 하에서 PEG는 두 전극 모두에서 분해되었지만, 48시간 분해된 용액의 평균 분자량을 측정한 값이 다르게 관찰되었다. 이는 환원전극에서는 PEG의 분해가 구리 일가 이온과 관련되는 반면, 산화전극에서는 물 분해 반응에 의해 형성되는 활성 라디칼이 원인이 되어 발생했다. 놀랍게도, 전기 분해 조건 하에서 PEG의 분해 속도는 폐쇄 회로 조건에서의 분해 속도보다 더 느리게 측정되었는데, 이는 용액 내의 활성 라디칼의 형성이 더 적게 일어났다는 것을 나타낸다. 추가적으로, 구리 전해 도금 용액 내에서 용존 산소가 없는 경우에는 구리 일가 이온의 촉매 반응이 일어났다. 따라서 PEG의 분해는 직접적인 전기 화학적 반응이 아닌 라디칼에 유도된 화학반응과 구리 일가 이온의 직접적인 촉매 반응을 통해 진행된 것으로 판단된다.

SPS와 PEG의 분해 메커니즘 규명을 통해 분해 요인이 활성 라디칼, 구리 일가 이온, 그리고 용존 산소라는 것을 확인하였다. 따라서 분해 인자를 감소시키는 환원제의 효과를 SPS를 통해 조사하였다. 먼저 구리 전해 도금조에 환원제(하이포 포스파이트, 포름 알데하이드, 글라이옥살산, 하이드라진 및 옥살산)를 첨가한 후 용액 속 SPS의 전압 반응, 도금 조의 성능 및 안정성에 미치는 영향을 시험하였다. 이 중 하이드라진과 옥살산은 용액 내 침전물을 형성하여 정확한 분석을 할 수 없었다. 또한 하이포

포스파이트는 금속 인산염의 환원반응 때문에 환원반응 영역에서 전기 화학적인 활성을 보였으며, 이로 인해 CVS 분석에 오류가 발생했다. 따라서 포름 알데하이드와 글라이옥실산만이 구리 전해질에서 환원제로 사용할 수 있다는 것을 확인하였다. 포름 알데하이드는 SPS 분해 속도를 보다 효과적으로 감소시켰다. 포름 알데하이드의 유무에 따라서 도금 조의 수행 성능은 비아 채움(via-filling)을 통해 평가하였다. 결과적으로 포름 알데하이드가 존재하지 않는 경우에 SPS는 구리 일가 이온에 의해 급속하게 분해되어 3시간동안 열화 된 후 채움 성능이 나빠졌다. 반면, 포름 알데하이드가 존재할 때, 채움 성능은 최대 9시간 동안 유지되었으며 개방 회로 조건에서 SPS의 분해는 거의 일어나지 않았다. 이러한 결과는 포름 알데하이드가 용액 내 형성되는 활성 라디칼의 수를 감소시켜 화학적 산화를 감소시킨다는 것을 의미한다. 이를 통해 포름 알데하이드를 이용하여 첨가제의 분해를 억제할 수 있는 방법을 제시하였다.

주요어: 구리, 전해 도금, 분해, 첨가제, 비스-설퍼프로필 다이설파이드, 폴리에틸렌 글라이콜, 구리 일가 이온, 활성 라디칼, 환원제, 포름 알데하이드

학 번: 2015-22827

Appendix

Effect of electrolyte on Cu electrodeposition bath with additive

The influence of the electrolyte properties on additive in Cu electrodeposition was confirmed. Additives are decomposed by oxidant formed by chemical reactions in the solution. In CHAPTER III of this study, the decomposition factor was identified, and a method of control the decomposition factors formed in the electrolyte was examined by changing the concentration of Cu source and supporting electrolyte.

A.1. Introduction

Cu electrodeposition has been used as a basic technology for digital industry production, including interconnect metallization in semiconductor, printed circuit board, and Cu thin film in Li ion secondary batteries, because it offers excellent price competitiveness and productivity. In general, Cu electroplating carries out under the optimized CuSO_4 and a H_2SO_4 concentration with additives to, because low power

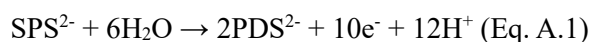
potential electroplating is required to productivity and thereby reduce processing costs.

¹ The basic requirements for economical and stable electrodeposition include an agitation system to aid in the mass transport of Cu^{2+} as well as the techniques to control the local coverage of additives, such as pulse-, pulse-reverse electrodeposition², step current electrodeposition.³⁻⁵

The representative accelerator is bis-(3-sulfopropyl) disulfide (SPS) with disulfide- and mercapto- functional groups, which increases the Cu electroplating rate. The suppressor is mainly used such as polyethylene glycol (PEG), polypropylene glycol (PPG), which form a $\text{PEG-Cu}^+\text{-Cl}$ complex attached to the electrode surface with Cl^- ion, inhibiting with electroplating and decrease the plating speed. The leveler serves to reduce the difference in height of the surface by attaching it to the convex region of the surface. Cu electroplating has demanded a variety of mechanical properties and features, the synthesis and combination of organic additives has diversified. As the conditions for Cu electrodeposition are becoming more and more difficult, degradation of organic additives in electrolyte during the electroplating has emerged as an important problem. By-products are generated and additives optimized concentration are changed due to decomposition of additives, which makes it impossible to obtain the desired mechanical properties or filling performance. Degradation of SPS chemically occurs through the

process of active radical ($\cdot\text{OH}$) formation due to the reaction of Cu^+ ion with dissolved O_2 in Cu electrodeposition bath. In addition, SPS electrochemically degraded at anode with electron in electrolysis condition.⁶ PEG is decomposed only through chemical reactions by directly Cu^+ ion catalytic reaction and active radical ($\cdot\text{OH}$) by Cu^+ ions with O_2 in the solution.⁷

Therefore, by controlling the decomposition factors, decomposition of the additives can be prevented. However, it is difficult to perfectly control the decomposition factor in industry. In particular, it is economically difficult to remove dissolved O_2 from the solution. First, as shown in the Eq. A.1, the SPS degradation by electrochemical reaction, where occurs rapidly at the anode, is controlled using an ionic-conductive membrane like Nafion for inhibition direct adsorption to electrode surface.



In addition, Kim et al. proposed a method of suppressing decomposition of additives by adding a reducing agent to prevent the active radical ($\cdot\text{OH}$) formed by successive chemical reactions from reacting with SPS in the Cu electrodeposition bath.⁸

In this study, the electrolyte pH with the additives were controlled through the

concentration of sulfuric acid (0.001~1 M H₂SO₄) to exam the deposited Cu properties and electrochemical results. In addition, the effect on the degradation of SPS and PEG depending on the Cu electroplating solution properties change was identified electrochemically by CVS measurement of the SPS concentration (C_{SPS}) and average molecular weight of PEG (MW_{PEG}).

A.2. Experimental

A.2.1. Electrochemical effect on electrolyte pH change experiment

The electrolytes consisted of 0.25 M CuSO₄, x M H₂SO₄ (x=0.001, 0.01, 0.1, and 1 M), 1.0 mM NaCl with 25 μM SPS or 300 ppm PEG-3350. The trench patterned wafer (bottom: 50 nm Cu/30 nm Ta, sidewall: 15 nm Cu/15 nm Ta/SiO₂, active surface area: 1 cm²) with an aspect ratio of 2 was used to test the filling performance under no agitation condition. Prior to electrodeposition, the patterned wafer was immersed into an etching solution (0.02 M citric acid and 0.03 M KOH) for 2 minutes to remove the native oxide.

Linear sweep voltammetry (LSV) was carried out in a three-electrode system at 25 °C with a scan rate of 10 mV/sec. Electrochemical impedance spectroscopy (EIS) was conducted with an open circuit potential in the frequency range from 0.01 Hz to 100 kHz with an AC voltage amplitude of 10 mV. A Cu rotating disk electrode (RDE, active area: 0.1257 cm², rotating speed: 300 rpm) was used as the working electrode, and a Cu rod (99.9%) and Ag/AgCl (sat. KCl) were used as counter and reference electrodes, respectively. Trench filling experiments were carried out at 10~50 mA/cm² with a fixed deposition amount of 700 mC/cm². The Cu wafer, Cu rod, and Ag/AgCl were used as

the working, counter, and reference electrodes, respectively. The distance between working and reference electrodes was 1.5 cm². An electrochemical analysis and trench filling were performed with a Parstat 2273 potentiostat (EG&G Princeton Applied Research Corporation). The field emission scanning electron microscope (FESEM; Hitachi) were used to observe the deposit surface and structure.

A.2.2. Effect on the additives decomposition experiment

The degradation experiments were carried out in a two-electrode system under open-circuit condition. The Cu plate (99.9%, active area: 25 cm²) was used as a deterioration factor in the Cu electrodeposition bath. The bath initially consisted of 0.25 CuSO₄, y M H₂SO₄, 1 mM NaCl with 50 μM SPS or 300 ppm PEG-3350. The temperature of the electrolyte was precisely controlled to be within 23~25°C, while a stirring bar was rotated at 300 rpm. The solutions were sampled between 0 to 10 h in SPS and 0 to 48 h in PEG.

The concentration of SPS (C_{SPS}) and the average molecular weight of PEG (MW_{PEG}) was measured by cyclic voltammetry stripping (CVS, 797 VA Computrace, Metrohm) for the degradation of additives. A CVS three-electrode system consisted of Pt rotating

disk electrode (Pt RDE, 0.0314 cm²), Pt rod, and Ag/AgCl (3 M KCl), which used as the working (WE), counter (CE), and reference electrode (RE), respectively. The potential ranged from 1.575 to -0.25 V in C_{SPS} and 1.575 to -0.45 V in MW_{PEG}, with a scan rate of 100 mV/sec. During analysis, the working electrode rotated at 2000 rpm, and the temperature of the bath was kept at 30°C using a thermostat. In first, C_{SPS} was measured by dividing into two conditions: as sampled and after 3 days using the pH titration. As a virgin make-up solution of C_{SPS} analyzing (VMS-A, Cu plating solution with excessive suppressor) consisted of 0.125 M CuSO₄, 0.5 M H₂SO₄, 0.86 M NaOH, 1 mM NaCl, and 1.4 mM PEG-3350 was used. MW_{PEG} was determined from the maximum hysteresis area (given as Q_b-Q_f where Q_b is the charge density in the backward scan and Q_f in the forward scan) at the cathodic region in the voltammogram. As a virgin make-up solution of MW_{PEG} analyzing (VMS-B) was composed of 0.25 M CuSO₄, 1 M H₂SO₄, 1 mM NaCl was applied.

A.3. Results and Discussion

A.3.1. Electrochemical effect on electrolyte pH change

When the composition of the electrolyte was changed, the various concentration of H_2SO_4 was applied to confirm the effect on the Cu electroplating bath, and electrochemical analysis and deposited Cu were confirmed by voltammogram and filling performance. Through this, the effect of the control the electrolyte pH on the Cu electrodeposition in the actual process was firstly checked.

Figs. A.1(a)-(d) show a cross-sectional image of the trenches after electrodeposition at 10~50 mA/cm^2 under pH 0~3. At pH 0, the superfilled feature was formed only at a low current density ($\leq 20 \text{ mA}/\text{cm}^2$) (**Fig. A.1(a)**). The bump began to disappear at 30 mA/cm^2 , and at over 40 mA/cm^2 , the dendrite growth of the Cu was observed. The chronopotentiometry (CP) results show that, at a high current density ($\geq 30 \text{ mA}/\text{cm}^2$), the potential abruptly moved in the negative direction because the Cu depletion at the electrode surface (**Fig. A.2(a)**). Due to the depletion of Cu at the electrode surface, the dendrite structure was formed at 40 and 50 mA/cm^2 as shown in **Fig. A.1(a)**.^{9, 10} As the pH increased, however, the current density enabling successful filling was gradually

extended toward a higher value. Eventually, at pH 3, void-free filling was accomplished at 50 mA/cm² without abrupt changes in the potential during CP. These results showed that a higher pH led to better mass-transfer, and consequently allowed to apply high-speed Cu superfilling.

An analysis with a rotating-speed of 300 rpm was carried out in various solution pHs to examine the effects of the pH on the additive behavior (**Fig. A.3**). In a standard acidic condition (pH 0), PEG suppressed the Cu reduction in the kinetic-controlled region (approximately 0 ~ -0.4 V), while SPS partially dismissed the suppression by displacing PEG (**Fig. A.3(a)**).¹¹ In a weakly acidic condition (pH 3), the behavior of the SPS and PEG were similar to those at pH 0, but the current density was lower than that at pH 0 irrespective of the additive chemistry (**Fig. A.3(d)**). This was because the solution resistance for the weakly acidic bath (6.35 Ω·cm²) was 15.5 times higher than that of a standard bath (0.41 Ω·cm²). To examine the effects of the pH on the mass transport of Cu²⁺, LSV experiments were carried out in an extended potential range and a lower rotating-speed of 100 rpm. As shown in **Fig. A.4(a)**, the limiting current densities were measured to be 69, 84, 95, and 107 mA/cm² at pH 0, 1, 2, and 3, respectively, indicating that the higher solution pH resulted in better mass-transfer. The limiting current density is determined by the rates of diffusion, convection, and migration, as given in Eqs. A.1

and A.2.

$$i_{\text{lim}} = i_{\text{Levich}} + i_{\text{m}} \text{ (Eq. A.1)}$$

$$i_{\text{Levich}} = 0.62 \times n F A D_0^{2/3} \nu^{-1/6} C \omega^{1/2} \text{ (Eq. A.2)}$$

where i_{Levich} is the current flowing by diffusion and convection, i_{m} is the current flowing by migration, n is the number of electrons, F is the Faradaic constant, A is the geometric area, C is the Cu^{2+} concentration, ν is the kinematic viscosity, ω is the rotating-speed and D_0 is the diffusion coefficient. To determine i_{m} , we assumed that the movement of Cu^{2+} ions at the diffusion layer is approximately equal to that at the bulk electrolyte, as shown in Eq. A.3.

$$i_{\text{m}} = t_{\text{Cu}} \times i \text{ (Eq. A.3)}$$

The transport numbers (t_i) for each of the ions at various pH values were calculated using Eq. A.4, based on the ion concentration data presented by J. M. Casas et al. experimental data (**Fig. A.4(b)**).¹²

$$t_i = |Z_i|FC_iu_i / \sum_j |Z_j|FC_ju_j \text{ (Eq. A.4)}$$

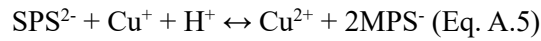
Where Z_i is the charge number and u_i is the mobility of the ion. As shown in **Fig. A.4(b)**, increasing the pH resulted in a higher transport number of the Cu^{2+} ions. Using Eq. 1-4, the fractions of i_{Levich} and i_m in i_{lim} were determined at various pH values (**Fig. A.4(c)**). The increase in pH led to a high i_m while i_{Levich} was almost constant, indicating the the improvement in filling capability at pH 3 came from a high i_m . Using equation, the diffusion coefficients of Cu^{2+} at pH 0~3 were determined to be between $4.5\sim 5.5 \times 10^{-6} \text{ cm}^2/\text{sec}$ (**Table A.1**), which are close to former reference paper ($4.9\sim 5.9 \times 10^{-6} \text{ cm}^2/\text{sec}$)¹³, demonstrating the validity of our approximation. Based on this result, increasing the pH value by lowering H_2SO_4 was confirmed to be a good approach to increase the migration rate of Cu^{2+} , which enables high-speed electrodeposition without the use of an agitation system.

A.3.2. Effect on the additives decomposition

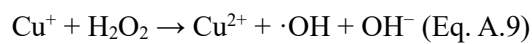
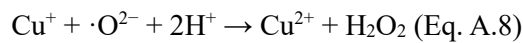
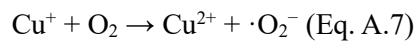
By changing the Cu electrolyte property, the effect on the additive was confirmed. First, the decomposition of SPS and PEG was confirmed by pH control. After that, the effect on the additive degradation was investigated.

In first, it was measured by CVS that the C_{SPS} and decomposition rate of SPS was changed under open-circuit condition according to the electrolyte pHs. In first, as shown in the **Fig. A.5**, the concentration of SPS as sampled condition was decreased in aging process. The degradation rate of SPS was calculated at 4.72 $\mu\text{M/h}$ in the pH 0. At pH 1 solution, SPS decomposed in the highest rate at 7.63 $\mu\text{M/h}$, and the rate decreased more and more as the electrolyte pH increasing 4.99 and 4.08 $\mu\text{M/h}$, respectively. On the other hand, **Fig. A.6**, sampling after 3 days' later condition, it was confirmed that the SPS decomposition rate was measured at 9.01 $\mu\text{M/h}$ in pH 0 electrolyte. As the pH increased, the rate of SPS degradation decreased to 8.33, 5.13, and 4.02, respectively. Under the pH 0 solution, the decomposition rate of SPS after 3 days' condition was 1.91 times higher than that of as sampled condition. This is because the Cu(I)MPS^- complex formed in the Cu electrodeposition bath could be stably presented in the solution as the pH was lowered. In a solution with high acidity, the concentration of MPS^- increased in the SPS

and MPS interconversion reaction (Eq. A.5) due to the high H⁺ ion concentration. Subsequently, when the concentration of MPS⁻ is high by the Cu(I)MPS⁻ formation reaction (Eq. A.6), the concentration of Cu(I)MPS⁻ increases. Therefore, Cu⁺ ion and MPS⁻ in the electrolyte could exist more stably for a long time.



On the other hand, in low acidity solution, since MPS⁻ did not exist for a long time because backward reaction of Eq. A.5 is accelerated by low H⁺ concentration. Since Cu⁺ ion could not exist as a Cu(I)MPS⁻ complex in the solution, Cu⁺ ion was quickly oxidized by oxygen. Therefore, active radical is formed by successive reactions (Eq. A.7~A.9), and SPS was decomposed by active radical.



Secondly, the degradation of PEG in various pH solution was confirmed as the average molecular weight of PEG (MW_{PEG}) under open-circuit condition by CVS analysis. As shown in the **Fig. A.7**, MW_{PEG} was similarly degraded under the condition of pH 0, pH 1, and pH 2, among which the most rapidly decomposed in the pH 1 solution. On the other hand, it was checked that less decomposition of PEG occurred in the pH 3 condition. Looking at the MW_{PEG} after 48 hours condition, it was measured as 862.4 Da (pH 0), 753.9 Da (pH 1), 913.3 (pH 2), and 2090.3 Da (pH 3), respectively.

It was found that the decomposition of SPS and PEG differed as the pH of the electrolyte changed, indicating that the decomposition factors of SPS; Cu^+ ion, dissolved oxygen, and active radicals was affected by the change of H^+ ion concentration. Therefore, further studies on the concentration of decomposition factors like Cu^+ ion, active radical were necessary to understand the SPS decomposition mechanism by thermodynamics and kinematics.

Table A.1. i_{Levich} , i_m , and the Diffusion Coefficient of Cu^{2+} in Mass Transport-limited Region at Various pHs

pH	Limiting current (mA)	Diffusion coefficient ($\times 10\text{cm}^2\text{sec}^{-1}$)
0	8.72	6.13
1	10.5	8.13
2	11.9	9.82
3	13.4	11.8

Table A.2. Transport Numbers for Various Ions in the 0~3 pH Solutions

Ion		Cu²⁺	SO₄²⁻	HSO₄⁻	H⁺	Cl⁻	Na⁺
Ionic conductivity(λ_j) (cm ² · Ω ⁻¹ ·equiv ⁻¹)		107.20	159.60	38.86	349.82	76.34	50.11
Mobility (u_i) (cm ² ·sec ⁻¹ ·V ^{-1b})		1.11 E-03	1.65 E-03	4.03 E-04	3.63 E-03	7.91 E-04	5.19 E-04
Charge number (z_j)		2	2	1	1	1	1
pH 0	Concentration (C_j) (M)	0.2325	0.4325	0.8	1	0.001	0.001
	κ (ion conductivity)	49.848	138.054	31.088	349.820	0.076	0.050
	t_i (Transport #)	0.0876	0.2427	0.0546	0.6149	0.0001	0.0001
pH 1	Concentration (C_j) (M)	0.1813	0.2063	0.075	0.1	0.001	0.001
	κ (ion conductivity)	38.860	65.835	2.915	34.982	0.076	0.050
	t_i (Transport #)	0.2723	0.4613	0.0204	0.2451	0.0005	0.0004
pH 2	Concentration (C_j) (M)	0.175	0.181	0.004	0.01	0.001	0.001
	κ (conductivity)	37.520	57.775	0.155	3.498	0.076	0.050
	t_i (Transport #)	0.3787	0.5831	0.0016	0.0353	0.0008	0.0005
pH 3	Concentration (C_j) (M)	0.175	0.1759	0.0001	0.001	0.001	0.001
	κ (ion conductivity)	37.520	56.147	0.004	0.350	0.076	0.050
	t_i (Transport #)	0.3985	0.5964	0.0000	0.0037	0.0008	0.0005

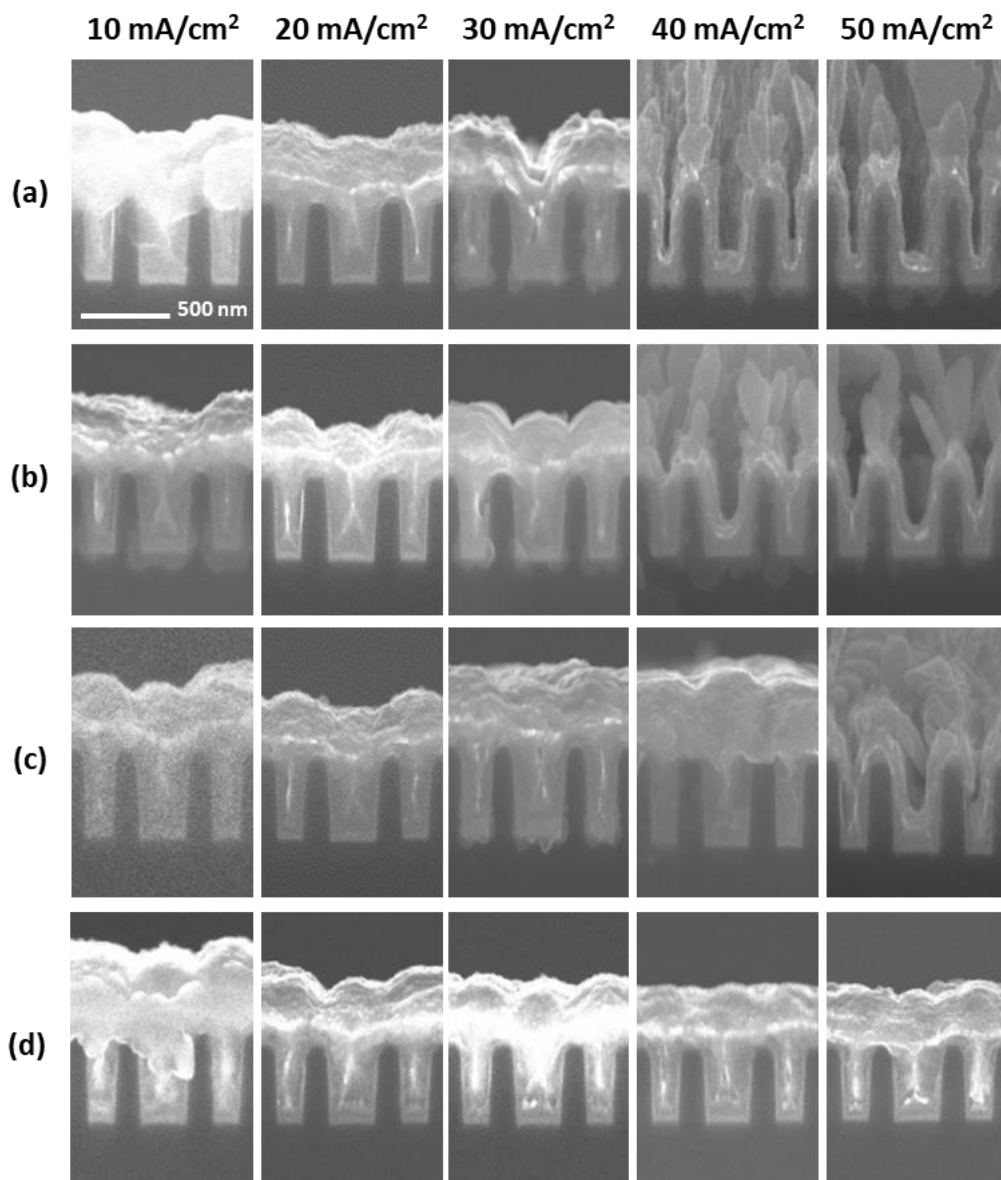


Fig. A.1. Cross-sectional SEM views of trench after Cu electrodeposition at 10 – 50 mA/cm² under (a) pH 0, (b) pH 1, (c) pH 2, and (d) pH 3 solutions.

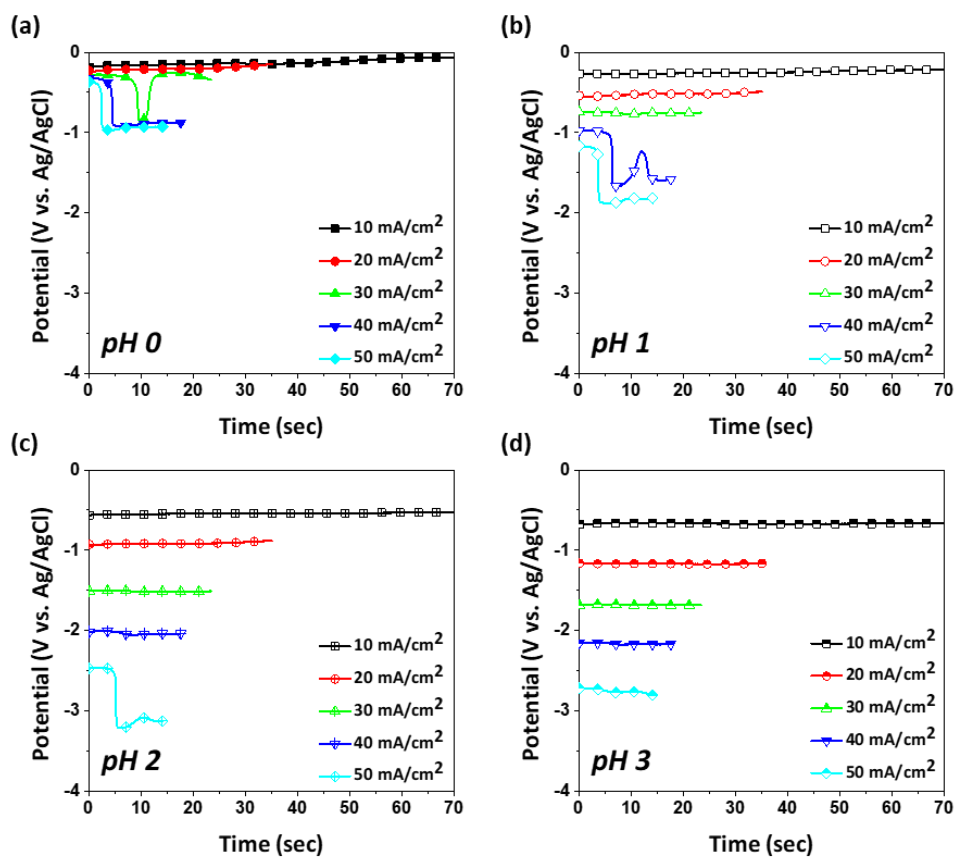


Fig. A.2. Chronopotentiometry profiles during trench filling at (a) pH 0, (b) pH 1, (c) pH 2, and (d) pH 3 solutions at 10 – 50 mA/cm².

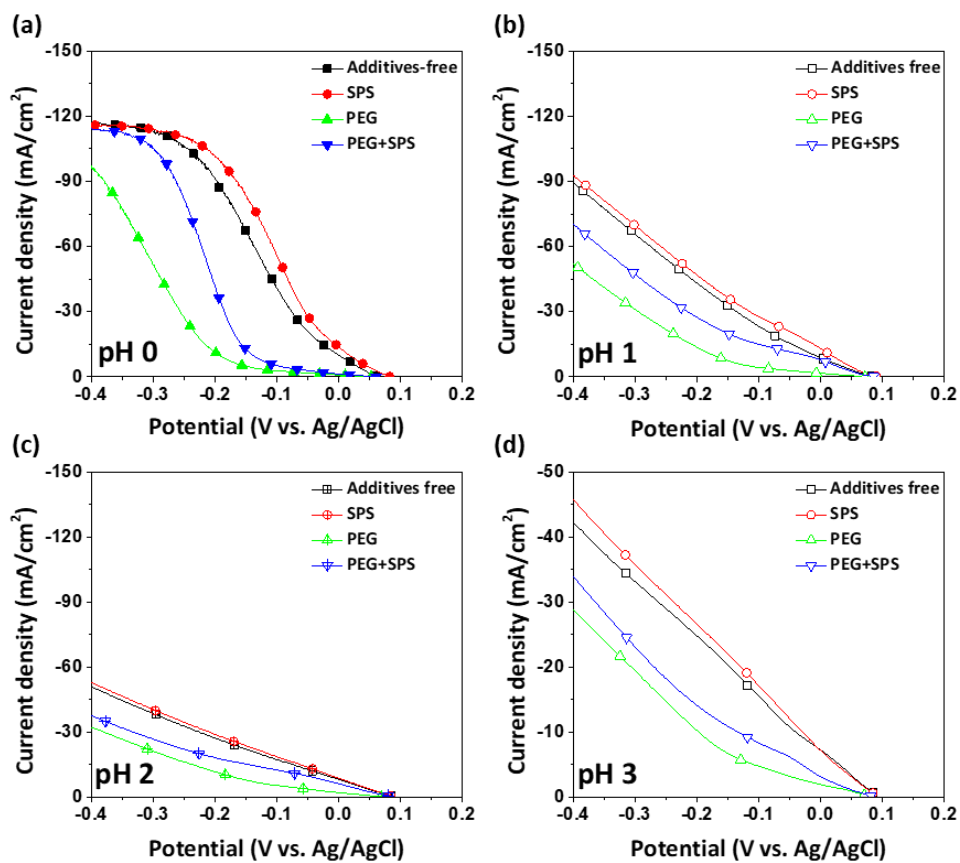


Fig. A.3. LSV results with rotating-speed of 300 rpm for Cu bath containing various organic additives (25 μ M SPS, 300 ppm PEG-3350) at (a) pH 0, (b) pH 1, (c) pH 2, and (d) pH 3.

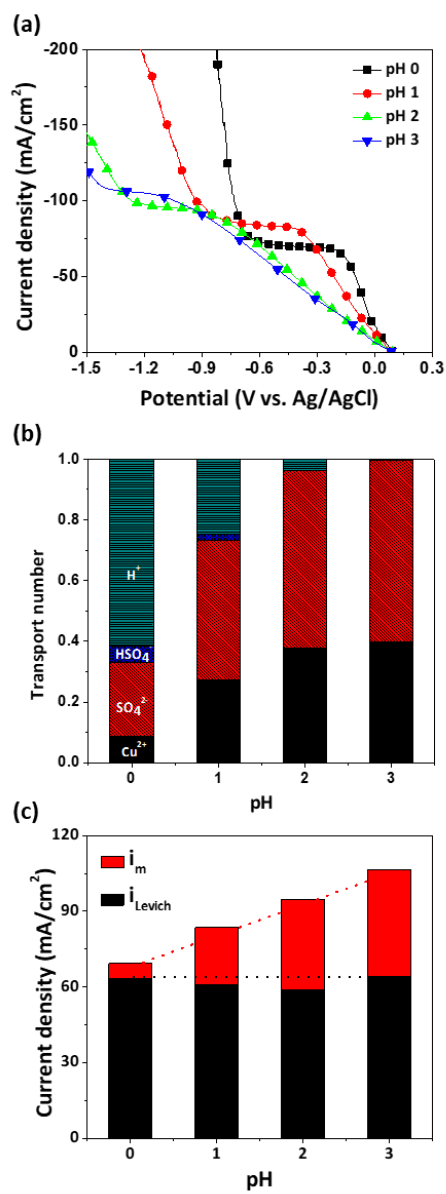


Fig. A.4. (a) LSV profiles for additive-free bathes with rotating-speed of 100 rpm, (b) transport numbers for various ions, and (c) the values of i_{Levich} and i_m in mass transport-limited region at pH 0 – 3.

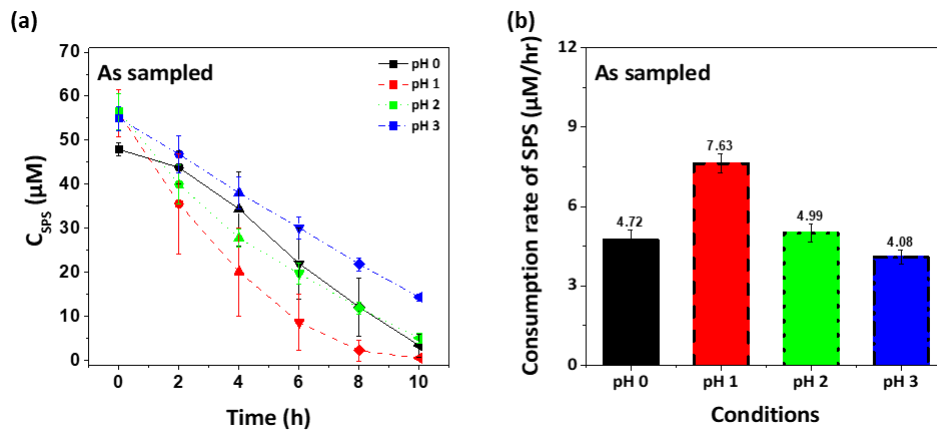


Fig. A.5. The SPS decomposition as sampled condition of various pH (a) C_{SPS} for 10 hours, (b) SPS consumption rate.

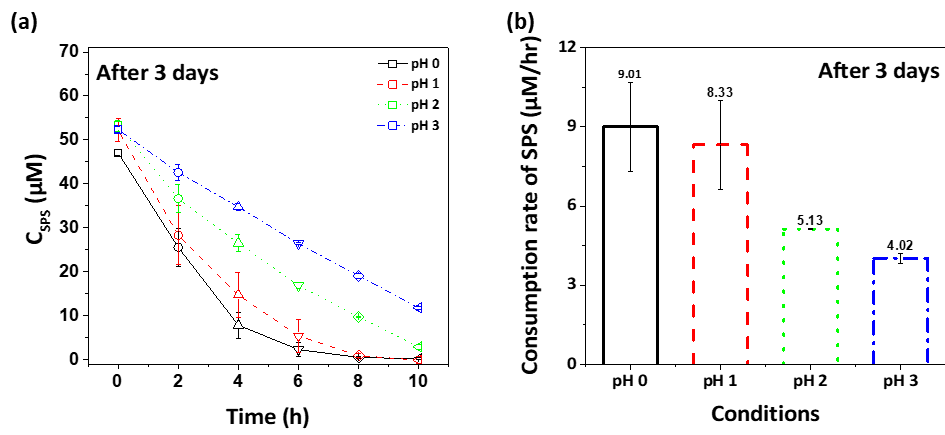


Fig. A.6. The SPS decomposition after 3 days condition of various pH (a) C_{SPS} for 10 hours, (b) SPS consumption rate.

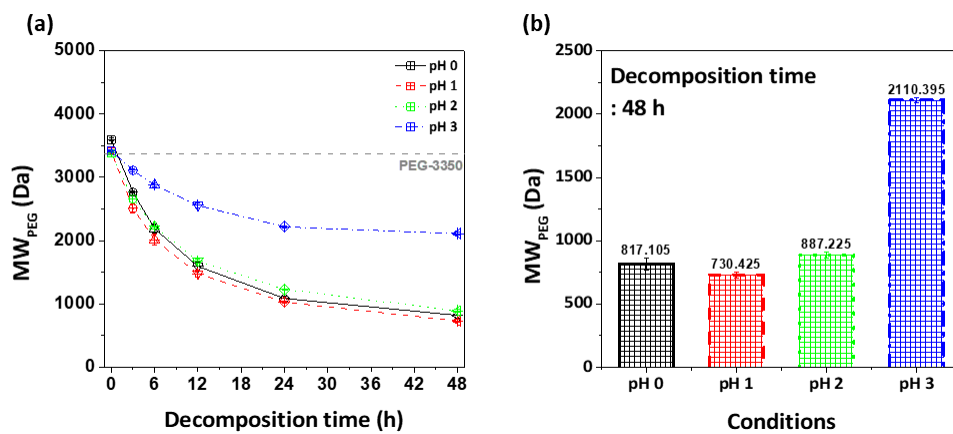


Fig. A.7. The PEG decomposition of various pH (a) MW_{PEG} , (b) MW_{PEG} in 48 hours.

A.4. Conclusion

Increasing the solution pH to 3 by lowering the H₂SO₄ content enables high-speed superfilling at up to 50 mA/cm² without the aid of an agitation system. At an elevated pH, the mass transport rate of Cu²⁺ ion increased while the organic additives behave similarly. The improved mass transport is ascribed to the rapid migration of Cu²⁺ ions at the diffusion layer, resulting from the high transport number.

When the pH of the solution was changed, it was confirmed that the decomposition of additives was changed under the open-circuit condition. In the case of SPS, it was confirmed that when all of Cu(I)MPS⁻ was oxidized in the solution after 3 days, decomposition of SPS was inhibited when the solution pH 0 was increased. In the case of PEG, degradation was fastest at pH 1, and degradation was inhibited at pH 3. This is predicted to be due to the thermodynamics and kinetics effect of Cu⁺ ion and active radical (\cdot OH), which are the decomposition factors of the additive in the Cu electrodeposition solution.

A.5. Reference

1. T. Elshenawy, S. Soliman and A. Hawwas, *Def Technol*, **13**, 439 (2017).
2. S. C. Hong, W. G. Lee, W. J. Kim, J. H. Kim and J. P. Jung, *Microelectron Reliab*, **51**, 2228 (2011).
3. H. C. Kim, M. J. Kim, Y. Seo, Y. Lee, S. Choe, Y. G. Kim, S. K. Cho and J. J. Kim, *Ecs Electrochem Lett*, **4**, D31 (2015).
4. K. Kondo, Y. Suzuki, T. Saito, N. Okamoto and M. Takauchi, *Electrochem Solid St*, **13**, D26 (2010).
5. T. Hayashi, K. Kondo, T. Saito, M. Takeuchi and N. Okamoto, *J Electrochem Soc*, **158**, D715 (2011).
6. T. Y. Kim, M. Sung, Y. Yoon, K. H. Lee, S. Choe and J. J. Kim, *J Electrochem Soc*, **166**, G61 (2019).
7. T. Y. Kim, S. Choe and J. J. Kim, *Electrochim Acta*, **357**, 136803 (2020).
8. T. Y. Kim, M. H. Lee, J. Byun, H. Jeon, S. Choe and J. J. Kim, *J Electrochem Soc*, **168** (2021).
9. M. Georgiadou, D. Veyret, R. L. Sani and R. C. Alkire, *J Electrochem Soc*, **148**, C54 (2001).
10. N. D. Nikolic, K. I. Popov, L. J. Pavlovic and M. G. Pavlovic, *J Electroanal Chem*, **588**, 88 (2006).
11. T. P. Moffat, D. Wheeler and D. Josell, *J Electrochem Soc*, **151**, C262 (2004).
12. J. M. Casas, F. Alvarez and L. Cifuentes, *Chem Eng Sci*, **55**, 6223 (2000).

13. J. T. Hinatsu and F. R. Foulkes, *J Electrochem Soc*, **136**, 125 (1989).

감사의 글

먼저, COVID-19로 인해 어려운 시기에도 제가 졸업할 수 있도록 도와주신 김재정 교수님께 감사드립니다. 교수님께서 다방면으로 가르침을 주신 덕분에 많은 것을 얻을 수 있었고, 발전시킬 수 있었습니다.

2015년도부터 2021년까지 6년 동안 소자 공정 연구실에서 동료들과 함께 많은 경험과 추억을 만들었습니다. 처음 연구실에 들어올 때 같이 있었던 동료들이 한 학기 한 학기 시간이 지나면서 졸업도 하고, 새로운 동료가 입학도 하면서 드디어 제가 졸업을 합니다. 명준이 형, 승희 형, 광환이 형, 성경이 형, 회철이 형, 혜자, 명호 형, 옥환이 형, 유석이 형, 오성이, 승연이, 민재, 안나 누나, 배기호 선배, 진욱이 형, 명현이 형, 정규 형, 진우가 순서대로 졸업을 했고, 송이 누나도 중간에 출산하면서 나가셨네요. 이제는 저랑 영이가 졸업을 하게 되면서 영근이, 병근이, 현수, 경규, 현우 형, 희주, 수웅이가 실험실에 남아서 실험실을 운영하겠네요. 실험실 동료들과 매 주마다 하는 실험실 세미나와 미팅, 단체 운동을 했던 기억들이 아직도 머리 속에 남아있습니다. 또한, 매 년마다 가는 학회와 방학 기간에 다녔던 실험실 MT도 즐거운 기억입니다. 같이 동고동락했던 사람들 덕분에 즐겁고 행복하게 실험실 생활할 수 있었습니다. 앞으로도 각자의 생활 환경에서 건강하고 열심히 살면서 연락하고 지낼 수 있었으면 좋겠습니다.

제가 대학원생으로 생활하면서 건강하게 졸업할 수 있었던 이유는 저를 항상 물심양면으로 도와주시는 가족 덕분인 것 같습니다. 항상 아들이 최고라고 말씀하시며 믿어주시고 모든걸 지지해주시는 어머니, 아버지 감사합니다. 또한 저보다 항상 많은 것을 알고 도와주는 누나 고마워. 저는 운이 좋게도 졸업하기 전에 2020년 12월 결혼식을 올려 한 가정을 꾸릴 수 있게 되었습니다. 먼저 와이프를 만날 수 있도록 도와주신 매형 감사합니다. 또한 부족한 제게 딸을 내주신 장인 어른과 장모님께 감사드립니다. 그리고 나를 항상 배려해주고 이해해주는 보은아 사랑하고 고마워. 덕분에 박사 졸업할 수 있었어. 앞으로 나운이랑 같이 더 행복하고, 좋은 일들 만들어 가자. 마지막으로 나운아 사랑해.

2021년 8월

김 태 영